TU Clausthal

Influence of Temperature on Light Scattering of poly-*N*-isopropylacrylamide Hydrogels Synthesized by Two Different Cross-Linking Methods

Doctoral Thesis

Saadet Dogu

Influence of Temperature on Light Scattering of poly-*N*-isopropylacrylamide Hydrogels Synthesized by Two Different Cross-Linking Methods

Doctoral Thesis

(Dissertation)

to be awarded the degree of

Doctor rerum naturalium (Dr. rer. nat.)

submitted by

Saadet Dogu

from Üsküdar / Istanbul

approved by the Faculty of Natural and Materials Sciences

Clausthal University of Technology

Date of Oral Examination

18.06.2013

Chair Person of the Board of Examiners:	Prof. Dr. D. E. Kaufmann
Chief Reviewer:	Prof. Dr. W. Oppermann
Reviewer:	PD Dr. J. Adams

Name, Vorname: **Datum:**

Dogu, Saadet **14.03.2013**

EIDESSTATTLICHE ERKLÄRUNG

Hiermit erkläre ich an Eides Statt, dass ich die bei der Fakultät für Natur- und Materialwissenschaften der Technischen Universität Clausthal eingereichte Dissertation selbständig und ohne unerlaubte Hilfe verfasst und die benutzten Hilfsmittel vollständig angegeben habe.

_____

Unterschrift

Part of this thesis was published in:

Dogu, S., Oppermann, W.:

Influence of observation temperature on light scattering of poly-*N*-isopropylacrylamide hydrogels, *Soft Matter*, 2012, 8, 2705-2713.

FOREWORD

I would first like to express my deepest gratitude to my supervisor, Prof. W. Oppermann, for his precious guidance and support in every aspect of my studies at TU-Clausthal. I also thank to PD Dr. J. Adams for reviewing my thesis, his helps and nice advices during my study.

I am grateful to Dr. A. Langhoff for his excellent and endless help and patience in this work. I thank to the secretary, Andrea Kornhardt, for her willingness to help at all the times. Further I would like to thank to former and current people at the Institute of Physical Chemistry at Clausthal University of Technology for the cheerful atmosphere.

I want to thank to Dr. S. Grube, Dr. M. Susoff, Dr. A. Langhoff and Volkan Can for proofreading of this manuscript.

I am deeply grateful to Volkan Can for his willingness to provide help, support, interesting discussions and friendship during the study.

I appreciate the encouragements and strong friendship from Ayse Ertekin during my study. I also thank to all my friends that support me during this study.

Special thanks go to Dr. M. Susoff who has always been with me during my Ph.D. study. His endless support, advice, help and encouragement were always with me to overcome the difficulties during the study.

I gratefully acknowledge financial support received from the German Research Foundation (DFG) through my Ph.D. study.

Finally I would like to express my appreciation to my family for their love, endless support and patience in every stage of my life.

TABLE OF CONTENTS

1 Introduction

Polymer gels are cross-linked systems composed of polymer networks and solvent. Since they have many practical applications such as in contact lenses, super absorbents, tissue engineering, drug delivery systems, sensors and actuators etc. many research groups concentrate on characterizing them and improving their properties.

It is well established that polymer gels generally possess some kind of structure on length scales larger than the mesh size of the network. This is due to an uneven topological or spatial distribution of cross-links and, accordingly, polymer concentration, commonly referred to as spatial gel inhomogeneity and can be caused by cyclization reactions, micro-gel formation during preparation, differences between the reactivities of functional groups, and diffusion controlled reactions [1,2]. Although it is of considerable interest and attempts to attain detailed insight have been ongoing for decades, it is still not fully understood. Light scattering and neutron scattering techniques are most frequently applied to investigate the structure and, in particular, the spatial inhomogeneities in gels. In the light scattering regime (low q-range, $q << 0.1$ nm^{-1}), the scattering intensity from gels is generally markedly larger than that from a corresponding polymer solution, while the differences between gel and solution diminish significantly in the higher q-range ($q >> 0.1$ nm^{-1}) covered by small angle neutron scattering. The excess scattering is related to spatial inhomogeneity, and a number of theoretical approaches or models have been proposed for its interpretation [3-11]. Another manifestation of the inhomogeneity is the appearance of a speckle pattern when a gel is illuminated with coherent light. In dynamic light scattering experiments, it is then observed that different locations within a gel scatter differently [12-16]. Procedures to divide the total scattering intensity into two parts originating from thermal concentration fluctuations and from spatial network heterogeneity were developed in the early 90s [15,17].

Poly-*N*-isopropylacrylamide (PNIPA) is a well-suited model substance to form polymer gels, in which heterogeneity can easily be influenced. PNIPA in water forms a temperature sensitive polymer-solvent system with a lower critical solution temperature (LCST) around 33 °C. It is the prime example of a stimuli-responsive polymer, and an extensive literature exists covering studies of, e.g., its phase behavior, [18-20] its potential in creating ‘‘intelligent’’ materials or devices, [21-23] etc. Likewise, investigations on PNIPA gels by scattering methods are numerous. SHIBAYAMA et al. demonstrated that the spatial inhomogeneities increased with raising cross-link concentration and with raising preparation

temperature of the gels [24]. They also showed that the ensemble-average light scattering intensity increased when the gels were swollen, while the fluctuating part of the scattering intensity seemed to decrease upon swelling [25]. The same group studied the effect of pressure at gel preparation, [26,27] and they explored the influence of weak ionization of the polymer on the structure factor [28-30]. WU et al. studied the properties of PNIPA hybrid gels formed when a sufficiently concentrated dispersion of micro-gels was cooled from temperatures above the LCST to below the LCST [31,32]. Their light scattering investigations showed that the static scattering component of the macroscopic gel attained by close-packing of the swollen micro-gel particles was due to large voids. These could be avoided when the temperature change occurred very slowly [31].

Although there have been many studies about PNIPA gels, researchs focusing on a detailed inspection of the dependence of scattering behavior on the observation temperature in the one-phase region, below the LCST, are rather scarce. The main emphasis was focused on a study of the critical behavior and the collapse. Already in 1994, TANAKA et al. pointed out that the static spatial fluctuations reversibly increased with raising temperature and diverged at the spinodal line [13]. This statement was applied to measurements close to the LCST (T > 25 °C), while data at lower temperatures were somewhat ambiguous. Later, SHIBAYAMA et al. confirmed the observation that the static (frozen-in) and the fluctuating (thermal) part of light scattering intensity, as well as the cooperative diffusion coefficient, are strongly dependent on the observation temperature [14]. While this was expected for the latter two quantities, the authors concluded that there must be a strong coupling between static and fluctuating components. KOIZUMI et al. deduced from neutron scattering and spin echo data that, as the temperature was raised towards the LCST, the static scattering intensity increased more rapidly than the thermal component [33]. They explained this behavior via the excluded volume parameter in the PANYUKOV RABIN theory, even though the theory was derived for gels made by instantaneous cross-linking of semi-dilute polymer solutions, which does not apply to the PNIPA gels studied.

The first part of the present study aims at a careful inspection of the influence of temperature on the static and thermal scattering components of PNIPA gels synthesized by free radical cross-linking copolymerization, FRC, in the range 10-27.5 °C, i.e. below LCST by means of static and dynamic light scattering methods. It is expected to obtain PNIPA gels which are reversible with the temperature changes. Specifically, for a gel synthesized at 25 °C, light scattering measurements were performed at 25, 20, 15, 10, 12.5, 17.5, and 27.5 °C (in that

sequence) in order to verify that the scattering properties are fully reversible with regard to a temperature variation within the range studied. Obviously, the thermal scattering should raise when the LCST is approached from lower temperatures. The dependence of the static scattering on temperature is not so clear and the few literature data diverge to some extent. In order to extract the excess part from dynamic light scattering experiments, the non-ergodic [15-17] and partial heterodyne [34-38] approaches were applied, thus separating the contributions of the dynamic or thermal concentration fluctuations and of the static inhomogeneities to the total scattering intensity. The much simpler approach based on static scattering is also used for comparison. It will be shown that both dynamic light scattering (DLS) and static light scattering (SLS) methods agree very well and that the static scattering varies with temperature to the same degree or slightly stronger than the thermal scattering.

Many studies have shown that structures of networks obtained by FRC generally seem to be inhomogeneous in the q-range << 0.1 nm^{-1}. An alternative approach to obtain homogeneous gels is UV induced photo cross-linking polymerization, PC. Cross-links are expected to be introduced randomly in space for photo cross-linked gels.

The purpose of the second part of this study is to compare network structures i.e. inhomogeneity, of the free radical cross-linking PNIPA gels (FRC gels) prepared at 25 °C to photo gels (PC gels) synthesized by photo cross-linking polymerization of (*N*-isopropylacrylamid)-2-(dimethylmaleimido)-*N*-ethyl-acrylamide, poly(NIPA-co-DMMIAAm) at observation temperatures 25, 20, 15, 10, 30 °C (in that sequence). It is expected that photo gels starting from semi-dilute polymer solution are more homogenous than free radical gels prepared by free radical cross-linking copolymerization starting from monomers and cross-linkers.

2 Theoretical Background

2.1 Polymer Solutions

For a given polymer, there are solvents that dissolve the polymer and solvents that do not dissolve the polymer. The former solvents are called "good solvents" and the latter "non-solvent". Monomer-monomer interactions are replaced by monomer-solvent interactions in a situation that polymer dissolves in a good solvent. As a result, the polymer coils swell and large excluded volume appears. By contrast, poor solvents cause coil-shrinkage leading to phase separation in order to enhance monomer-monomer interactions. The theta (θ) conditions occur at a particular temperature known as the theta or FLORY temperature $T = \theta$. Under theta conditions the dilute solution behaves as an ideal solution and the polymer coil has its ideal unperturbed conformation. A solvent that gives the theta condition of a given polymer is called a theta solvent, e.g., PNIPA in water at LCST (33 °C). Coils at θ-conditions exhibit their ideal unperturbed random conformations, and θ-solvents stay in a transition region between good and poor solvents.

There are several characteristic measures for the coil dimensions in solution, e.g., the hydrodynamic radius, R_H, the end to end distance, $< r^2 >^{0.5}$, or the radius of gyration, R_G, as shown in Figure 1. FLORY–HUGGINS interaction parameters [39,40] and the HILDEBRAND solubility parameters [41] are among the most common parameters that give the effective interaction potentials between solvents and polymer chains.

Polymer solutions can be divided into three different regimes according to their concentration: the dilute, the semi-dilute and the concentrated solutions [42]. A schematic illustration of the state of polymer molecules in the solutions with different polymer concentrations is given in Figure 1. At low concentrations, $c < c^*$, the polymer coils are separated from each other and behave more or less independently. The solution is called dilute. The polymer chains occupy a certain amount of space in the solution. If the concentration of polymer coils increases to a critical concentration they fill the whole volume and start to interpenetrate each other. This concentration is called the critical overlap concentration, c^* (Fig. 1, $c \cong c^*$). At this overlap threshold the coils begin to be densely packed. The properties of the polymer solution change at concentrations above c^*. The solution in this regime is called semi-dilute. At this concentration, chains are overlapped and entangled. Their mobility is greatly reduced compared to dilute solutions.

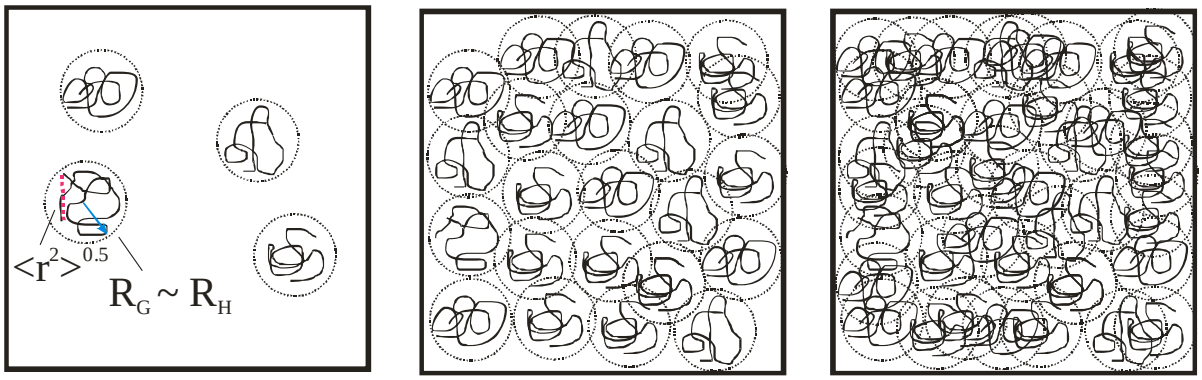

Figure 1 Concentration regimes for solutions of linear flexible polymers: dilute solution, $c < c^*$; solution at the overlap concentration $c \cong c^*$; semi-dilute solution $c > c^*$. Adapted from [42].

There are several descriptions that have been reported for the overlap threshold, c^* [43,44], e.g.

$$c^* = \frac{3M_w}{4\pi R_G^3 N_A} \tag{1}$$

and

$$c^* = \frac{1}{[\eta]} \tag{2}$$

where M_w is the weight average molecular weight, R_G the radius of gyration, N_A the Avogadro number, and $[\eta]$ the intrinsic viscosity, which is explained below.

The intrinsic viscosity, $[\eta]$, is a quantity that is characteristic of polymers. It represents an increase in the solution viscosity when the concentration is raised to a certain level. It is expressed by the MARK–HOUWINK–SAKURADA equation.

$$[\eta] = KM^{\alpha} \tag{3}$$

The parameter K is a constant and α is the so-called MARK–HOUWINK–SAKURADA exponent. The exponents are different from polymer to polymer and depend on the solvents as well. They are tabulated for many pairs of polymers and solvents [45]. The value of α is around 0.7-0.8 for flexible chains in a good solvent and exceeds unity for rigid chains. In the theta solvent, the flexible chain has $\alpha = 0.5$.

2.1.1 The semi-dilute regime

In semi-dilute solutions, the chains are congested and highly overlapping with other chains as shown in Figure 1. The blob model is widely used to predict various properties of semi-dilute solutions and to find out how these properties depend on the concentration and molar mass of polymers. In dilute solutions, the single chain dynamics which involve all the interactions, such as excluded volume and hydrodynamic interactions, are referred to all monomers in the same chain. However, in semi-dilute solutions, interactions between monomers of different chains come into effect. In semi-dilute polymer solutions, the intermolecularly and intramolecularly coupled many chain dynamics can be renormalized into independent motions. These independent motions are described by so-called blobs depicted in Figure 2b.

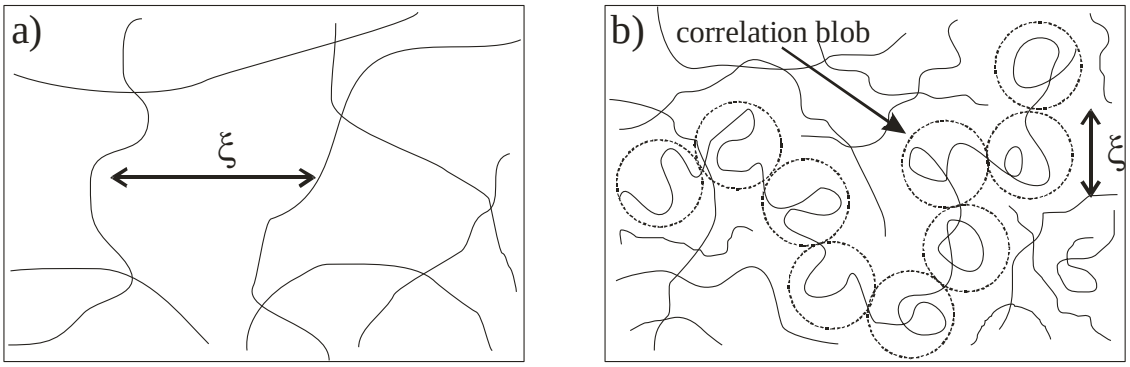

Figure 2 a) the average mesh size, ξ, in an entangled semi-dilute solution, b) a polymer chain with so-called blobs, being the correlation length. Adapted from [42].

Physically, the blobs can be treated as spheres of size of the correlation length, ξ, as shown in Figure 2b. Inside the blob, dynamic behavior resembles the single chain dynamics. The sites of interactions between different chains are called the entanglement points. There is only a small chance for monomers of other chains to sneak in. In this way, the entire solution can be regarded as to be filled up with blobs.

A characteristic parameter for the average mesh size in an entangled semi-dilute solution is the correlation length, ξ, (Fig. 2a). DE GENNES and EDWARDS have shown that in semi-dilute solutions, the correlation length, ξ, scales as the average distance between interchain contacts (Fig. 2a) [42,46]. If cross-linking occurs in these interchain contacts to form a gel, ξ also describes the mesh size of the gel network. At the overlap concentration, ($c \approx c^*$), coils have contact but not strongly interpenetrate each other. At this regime ξ can be compared to the

size of one coil as measured by the radius of gyration, R_G. The correlation length in a semi-dilute solution ($c > c^*$) decreases with increasing amount of coil overlap as given by eq. 4 [42]

$$\xi \propto \phi^{\frac{-\nu}{3\nu-1}} \tag{4}$$

ϕ is the volume fraction of the polymer and ν is the FLORY exponent [40]. The scaling assumption suggests that the functional dependence of correlation length, ξ, on concentration, c, is universal if c is properly scaled to a fundamental scale which is assumed to be the overlap concentration, c^*. Consider that ξ approaches R_G at c^*, therefore

$$\xi \approx R_G (c^*/c)^{\gamma} \tag{5}$$

where $\gamma = -0.75$, $\nu = 0.6$ in a good solvent, and $\gamma = -1$, $\nu = 0.5$ in θ-solvents.

The scaling theory clearly shows that the blob size is closely related to the correlation length ξ.

2.1.2 Thermodynamics of Polymer Solutions [47]

Mixtures are systems that are formed by two or more different chemical species. Binary mixtures consist of only two different species. If the mixture is uniform and all components are mixed on a molecular scale, the mixture is called homogeneous. If the mixture has different phases, it is called heterogeneous. Both types of mixtures in the equilibrium state have a dependency on entropy and energy changes during mixing. While entropy always favours mixing, energetic interactions between species can either promote or inhibit mixing. In general, two species will mix if the GIBBS energy, G, is decreased.

$$\Delta G_{mix} = \Delta H_{mix} - T\Delta S_{mix} \tag{6}$$

ΔH_{mix} is the enthalpy of mixing and ΔS_{mix} is the entropy of mixing. If $\Delta G_{\text{mix}} < 0$ the polymer will dissolve in the solvent and form a solution. As in most experimental situations the pressure is constant, the energy of binary mixing is described by using the enthalpic interactions. In the FLORY-HUGGINS theory it is assumed that there is no volume change on mixing, hence instead of analyzing the enthalpic interactions, the energy of interactions are used to describe the energy of mixing by the change of the Helmholtz free energy of mixing ΔF.

$$\Delta F_{\text{mix}} = \Delta U_{\text{mix}} - T\Delta S_{\text{mix}} \tag{7}$$

Volume V_A of species A is mixed with volume V_B of species B to make a mixture of volume V_A+V_B. The volume fractions of the two components in the binary mixture are ϕ_A and ϕ_B

$$\phi_A = \frac{V_A}{V_A+V_B} \quad , \quad \phi_B = \frac{V_B}{V_A+V_B} = 1-\phi_A \tag{8}$$

The entropy, S, can be calculated from the BOLTZMANN equation

$$S = k_B \ln \Omega \tag{9}$$

k_B is the BOLTZMANN constant with natural logarithm of the number of possibilities Ω to arrange molecules on the lattice (FLORY–HUGGINS theory).

For the polymer solution entropy is given as

$$\Delta S_{\text{mix}} = -k\left[\frac{\phi_{\text{A}}}{N}\ln\phi_{\text{A}} + \phi_{\text{B}}\ln\phi_{\text{B}}\right] \tag{10}$$

with N the degree of polymerization.

The FLORY interaction parameter χ is defined to characterize the difference of interaction energies in the mixture (eq. 11).

$$\chi \equiv \frac{z}{2}\frac{\left(2u_{\text{AB}} - u_{\text{AA}} - u_{\text{BB}}\right)}{kT} \tag{11}$$

u_{AA}, u_{BB}, u_{AB} are the interaction energies between adjacent lattice sites occupied by the two species, z is the coordination number, the number of nearest neighbors for a lattice site, each one occupied by one chain segment or a solvent molecule. χ is a dimensionless measure of the differences in the strength of pairwise interaction energies between species in a mixture. Thus the energy of mixing is given by eq. 12.

$$\Delta U_{\text{mix}} = \chi\phi(1-\phi)kT \tag{12}$$

Combining the entropy of mixing (eq.10) with the energy of mixing (eq.12), HELMHOLTZ free energy of mixing is obtained for polymer solutions (eq. 13).

$$\begin{aligned}\Delta F_{\text{mix}} &= \Delta U_{\text{mix}} - T\Delta S_{\text{mix}} \\ &= kT\left[\frac{\phi}{N}\ln\phi + (1-\phi)\ln(1-\phi) + \chi\phi(1-\phi)\right]\end{aligned} \tag{13}$$

This equation is called the FLORY–HUGGINS equation. The interaction parameter χ is used to indicate whether a solvent is good or poor for the polymer. A good solvent has a low value of

$\chi < 0.5$ while a poor solvent has a high value of $\chi > 0.5$. Since theta solvents lie in the transition region between good and poor solvents, the interaction parameter $\chi = 0.5$. In good solvents, the polymer network chains are in the extended conformation due to the strong molecular interaction between polymer and the solvent. A positive χ denotes that the polymer-solvent contacts are less favored compared to the polymer-polymer and the solvent-solvent contacts. A negative χ means that polymer-solvent contacts are preferred, promoting solvation of the polymer.

2.1.2.1 PNIPA as Thermo-Responsive Polymer

Thermo-responsive polymers are the most common smart polymers applied to responsive systems like actuators and valves in vitro as well as in vivo in biomedical applications. Thermo-responsive polymers in solution possess a unique critical solution temperature. If a thermo-responsive polymer solution is miscible below the critical temperature and is phase-separated above the critical temperature, the critical temperature is called a lower critical solution temperature (LCST) of the polymer. On the other hand, if a miscible solution exists above the critical temperature and the solution is phase-separated below the critical temperature, it is an upper critical solution temperature (UCST) [48].

Since PNIPA was first synthesized in the 1950s, it has been studied and utilized as the most common intelligent polymer. PNIPA exhibits a volume phase transition at the LCST around 33 °C [49-54]. Below its LCST, this thermo-responsive polymer is hydrated and represents a swollen coil-like conformation. Above the LCST, it becomes dehydrated and adopts a folded structure. The structure of PNIPA is shown in Figure 3. Its thermo-responsiveness is thought to be resulting from the presence of the hydrophobic carbon backbone, a hydrophobic isopropyl group and a hydrophilic amide group along the side chain in each monomer unit.

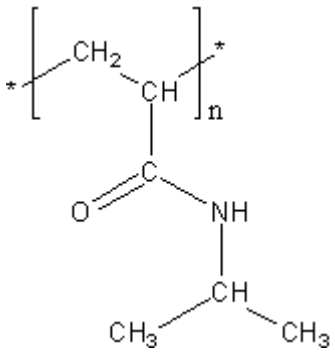

Figure 3 Chemical structure of Poly-*N*-isopropylacrylamide, PNIPA.

The research on temperature dependent interactions between PNIPA and water revealed the possible mechanisms for the PNIPA's LCST phase transition or the hydrophobic-hydrophilic transition. It is generally thought that entropy is the driving force for the LCST phase transition in aqueous solution [55-61]. When temperature is below its LCST, the enthalpic contribution including hydrogen-bonding interactions between the amide groups on PNIPA and water dominates so that PNIPA possesses a hydrophilic coil-like conformation. However, when the temperature is above its LCST, the solvation entropy of the hydrophobic isopropyl groups and the carbon backbone dominates and PNIPA exhibits a hydrophobic folded structure.

2.2 Polymer Gels

2.2.1 Fundamentals

Gels are three-dimensional macroscopic polymer networks that are swollen in a solvent. They are formed by linear polymer strands which are flexibly connected by cross-linking points. A gel cannot dissolve in a solvent, but swell in it. Gels have the ability to reversibly swell or shrink (up to a factor 1000 in volume) because of small changes in their environment (pH, temperature, electric field). Due to these properties they are used in particular as superabsorbents, sensors and actuators. In contrast to liquids, gels possess a non-zero shear modulus that means, they are not able to flow. The mechanical properties of gels correspond to those of solids although they have a disordered structure, and usually a large amount of solvent. They can be described by the theory of rubber elasticity [47,62].

According to the nature of the cross-links connecting the network strands, gels are divided into two classes; chemical and physical gels. Different types of gelation are gathered in Figure 4.

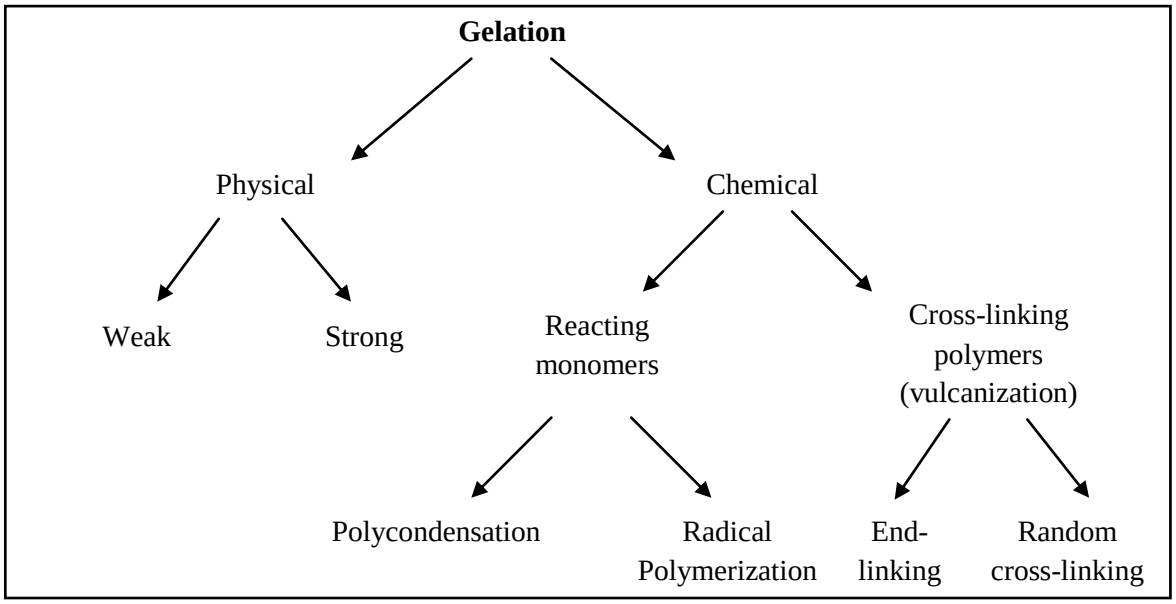

Figure 4 Scheme for the classification of gelation transitions. – Adapted from RUBINSTEIN [47].

Gels from physical networks have only intramolecular covalent bonds. Since the intermolecular bond is not covalent they can break or re-bond by changes in thermodynamic parameters. It is useful to distinguish between strong and weak physical gels. Strong physical gels that are effectively permanent can be formed if the polymer chains partially crystallize

[63,64], form micelles [65,66] or helical structures [67,68]. They are analogous to chemical gels, e.g., thermoplastic elastomers, e.g., thermoplastic polyurethanes. In contrast weak physical gelation arises due to the hydrogen bonding, formation of block copolymer micelles above their glass transition temperature, and ionic associations which have finite lifetimes, breaking and reforming continuously. Whether a physical gel is strong or weak depends only on the observation time [47,62].

Chemical gels are created when monomers form permanent covalent bonds which irreversibly connect the network chains. They always result in a strong gel. There are three main chemical gelation processes:

- condensation; by step growth polymerization of multifunctional monomers,
- vulcanization; by cross-linking of long linear chains,
- addition polymerization; by free radical cross-linking chain reactions.

In this study addition polymerization and vulcanization are employed for cross-linking. Figure 5 shows a type of vulcanization (random cross-linking) and addition polymerization.

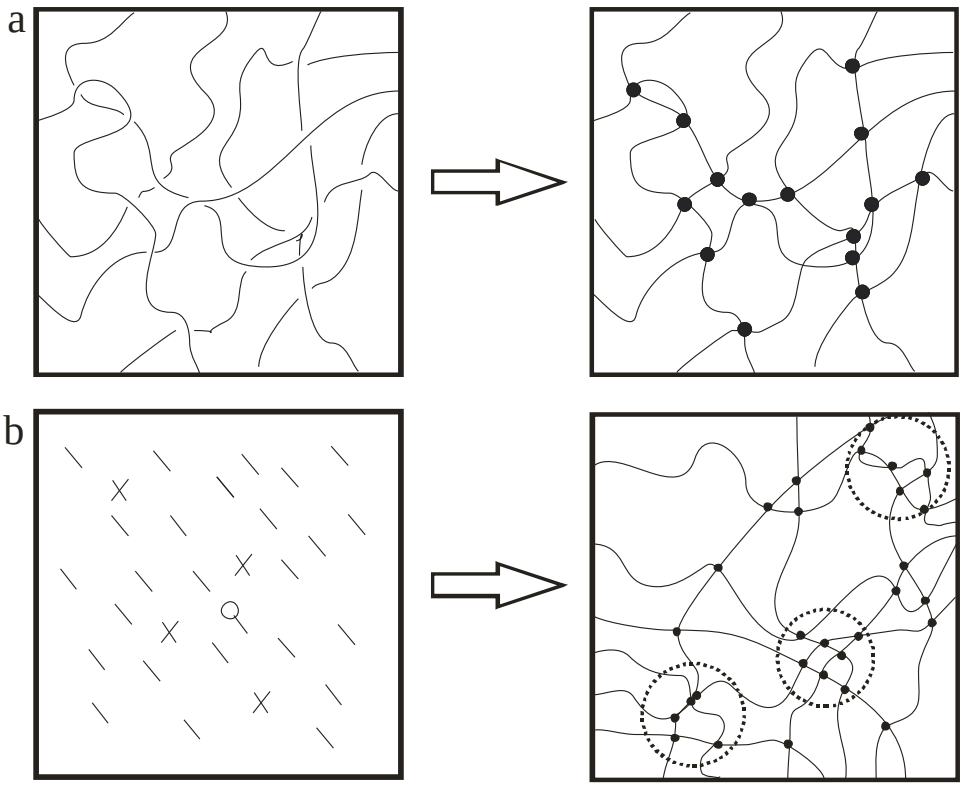

Figure 5 Vulcanization of polymers (a) and addition polymerization (b); X shows cross-linker, \ shows monomer and shows initiator.

2.2.2 Theory of Gelation

To describe the sol-gel transition, some models have been developed such as mean field gelation, critical percolation theory and scaling model theory. All theories are well described in the literature [47]. The sol-gel transition is described here by the critical percolation model since the reacting structures are just at overlap.

At the percolation threshold or gel point, p_c, the system undergoes a connectivity transition. Shortly before the gel point, the system is a polydisperse mixture of branched polymers. Shortly after reaching the gel point, the system still has a large proportion of polydisperse branched polymers, but one structure percolates through the entire system thus forming a coherent structure. This is the initial gel fraction in which an infinite cluster of bonded monomers is formed and spans the whole lattice from side to side. Since bonds are randomly formed between monomers, intramolecular bonding is allowed. The gel fraction can be regarded as an order parameter for the entire gelation process. The growth of the gel fraction is accompanied by a simultaneous decay of the sol fraction, beyond the gel point, p_c. The sol-gel transition is very similar to a continuous phase transition. While the bond formation is continous, the macroscopic properties, e.g., the rheological behavior, change in an abrupt manner. This gelation process is described by the percolation theory [47,62].

The classical theory from FLORY and STOCKMAYER assumes a mean-field approach of the gelation process. The whole gelation is seen as a branching process of multifunctional monomers. It is assumed that this branching takes place on an infinite Bethe lattice with monomers possessing a functionality of f. This lattice is also called "CAYLEY tree". In this classical model, loops that are formed by intramolecular cross-linking are not considered. The gel point is reached in this model at a critical conversion, p_c. The prediction for the gel point is [47,62] given by eq. 14.

$$p_C = \frac{1}{f - 1} \tag{14}$$

This equation is applicable to step-growth polymerization. If one assumes the functionality of the cross-linker, f = 4, the gelation point, p_c, is reached at a conversion 0.33%. While the number average molecular weight does not diverge at the critical conversion, p_c, the weight average molecular weight goes infinity.

In the cross-linking of long linear polymer chains with the degree of polymerization, N_0, a very high number of cross-linkable group functionality f can be set equal with the degree of polymerization. This applies for example to the vulcanization process of rubber with sulphur according to GOODYEAR's famous process which can be described by mean-field theory. It is applied to the gel point in the following relationship

$$p_C = \frac{1}{f-1} \approx \frac{1}{N_0} \qquad N_0 >> 1 \tag{15}$$

The gel point corresponds to an average of one cross-link per chain.

2.2.3 Theory of Rubber Elasticity

Rubbers are cross-linked networks whose glass transition and melting temperature are below room temperature. They have a lot of applications like rubber bands, adhesives and tires. Their outstanding properties are due to the entropic nature of rubber elasticity [47,62]. The macroscopic mechanical properties of those rubbers are described by the theory of rubber elasticity. There exist two fundamental network models based on mean-field approaches relating the molecular and macroscopic strain-stress behavior: a) the affine network model, b) the phantom network model. These models use the analogy between the elastic properties of an ideal GAUSSIAN chain and a classical elastic spring to calculate the overall network free energy F.

The main assumption of the affine network theory is that the cross-link junction points move affinely with macroscopic deformation. The fluctuation of the junction points about their mean positions is restricted by the neighboring chains sharing the same region of space. Summing up the entropy changes of all network strands during deformation yields the overall entropy change of the entire network. This entropy change is calculated as follows

$$\Delta S = -\frac{nk_B}{2}(\lambda^2{}_x + \lambda^2{}_y + \lambda^2{}_z - 3) \tag{16}$$

with λ_x, λ_y and λ_z the relative deformations in x-, y-, and z-direction, and k_B the BOLTZMANN constant, n the number of elastically effective network strands.

In the case of an uniaxial deformation in *x*-direction the entropy change is calculated with the following equation (eq. 17).

$$\Delta S = -\frac{nk_B}{2}(\lambda^2 + \frac{2}{\lambda} - 3) \tag{17}$$

As the main contribution to the free energy is due to entropic changes, the enthalpic contributions can be ignored. The change in free energy, ΔF, due to a uniaxial deformation is thus calculated by

$$\Delta F = -T\Delta S = \frac{nk_BT}{2}(\lambda^2 + \frac{2}{\lambda} - 3) \tag{18}$$

From the stress, σ, defined as the ratio of force and cross-sectional area, and deformation, γ, the shear modulus, G, is obtained. It follows the important relation [47,62]

$$G = \frac{\sigma}{\gamma} = \frac{nk_BT}{V} = \nu k_BT = \frac{\rho RT}{M_S} \tag{19}$$

with ν number of network strands per unit volume, M_s the average molecular weight of the strands, ρ the network density (mass per unit volume) and R the gas constant. It can be seen that the shear modulus depends on temperature and the number of network chains. The modulus G equals k_BT per network strand. This equation relates the elastic property of each network chain to the macroscopic mechanical behavior of the whole network.

Another model in the field of rubber elasticity is the phantom network theory. In contrast to the affine network model, the phantom network theory allows fluctuations of the junction points around their mean position due to Brownian motion. The cross-links can move freely and the chains can pass through each other. Hence, the phantom network model is a more realistic approach than the affine network model. The fluctuations of the junction points lead to a net decrease of the free energy of the system by reducing the cumulative stretching of the network. The shear modulus for the phantom network model is calculated from the equation

of the affine network model by adding a factor that contains the functionality *f* of the cross-linking points

$$G = \nu k_B T \frac{f-2}{f} = \frac{\rho RT}{M_S}\left(1-\frac{2}{f}\right) \tag{20}$$

So, the enabling of fluctuations of the junction points lead to a lowered shear modulus of the gel by a factor of (1-2/*f*). Compared to the affine network model, gels described by the phantom network model are softer because of a lower *G*. If the functionality *f* is increasing or even goes to infinity, the prediction of the affine network model is reached.

For real networks, the shear modulus is normally higher than that predicted by the phantom and the affine network model. In these classical models, the monomers other than chain ends do not feel any restriction potential. However, real networks show that the network chains impose topological constraints because they cannot penetrate each other. These topological constraints are called entanglements implemented by EDWARDS using the tube model as the essence of those entanglements. The modulus of the entangled polymer network is calculated by summing the contributions arising from the cross-links, G_x, and the contributions arising from the entanglements, G_e, [47].

$$G \cong G_x + G_e \approx \rho RT\left(\frac{1}{M_x}+\frac{1}{M_e}\right) \tag{21}$$

with M_x the molecular mass between cross-links and M_e the molecular mass between entanglements. In the case of networks with very short chains ($M_x < M_e$), *G* is dominated by permanent cross-links. But it is almost independent of the molecular mass of the network strands between cross-links in the case of high molecular mass strands between cross-links in the limit of very long strands ($M_x > M_e$).

2.2.4 Structural Inhomogeneity

In the phantom network and the affine network models only network chains that run between cross-linking points are considered as elastically active and therefore they can change their conformation by the outer dimensions of the network. Chain segments which are connected to only one point of the network are considered as inactive network chains. They are called network malfunctions. These topological network defects include loops and dangling chains as shown in Figure 6.

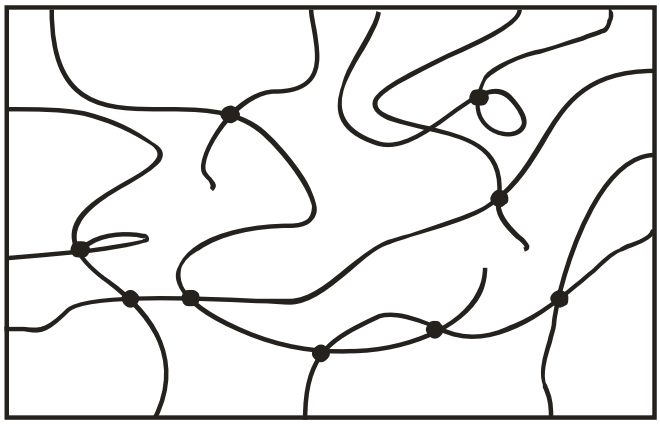

Figure 6 Network (f = 4) with topological network defects (loops and dangling chains).

Polymer gels are generally spatially inhomogenous, as well [69]. In these cases the concentrations of network chains and junctions points are non-uniform. They exhibit an inhomogeneous cross-link density distribution known as spatial gel inhomogeneity [3,69]. Figure 7 shows a schematic representation of an ideal gel and a spatially inhomogeneous real gel. In ideal gels, the length of network chains between the cross-links is constant and all the cross-linker molecules are consumed by effective cross-linking reactions. However, real gels exhibit a wide distribution of chain lengths between the network junction points. There are areas that possess a very high chain density, other areas that possess low network chain density. The areas that have a high network chain density are quite stiff and therefore exhibit a higher shear modulus and a lower degree of swelling compared to ideal gels [5]. They can resist relatively high stresses under deformation. The regions that have low network chain density are much less stiff and highly swellable. They are not strong enough to resist high stresses under deformation. Hence, regarding deformation, these sections are weak points of

spatially inhomogeneous gels [70]. As a result concerning application, it may be therefore desirable to obtain a gel that is as homogenous as possible.

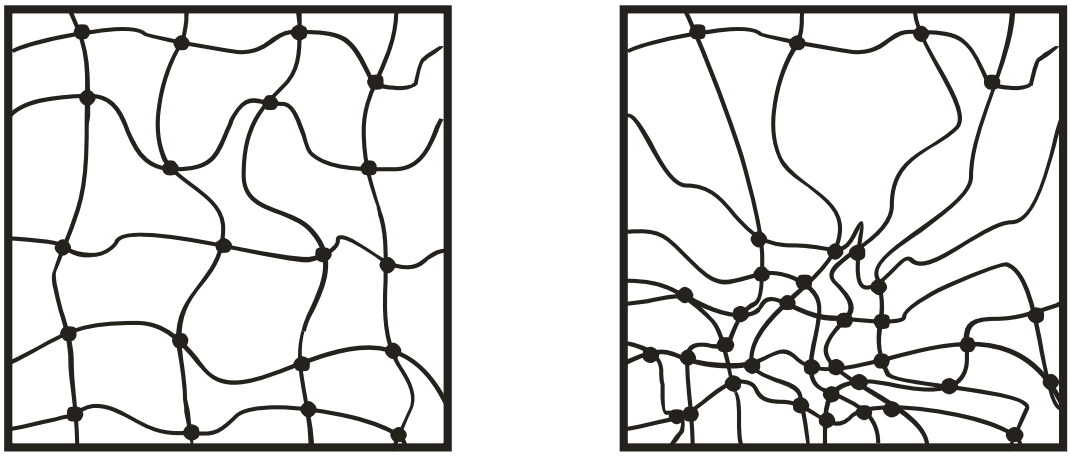

Figure 7 Schematic representation of a homogenous ideal gel (left hand side) and a spatially inhomogenous real gel (right hand side).

The spatial inhomogeneity is widely investigated through a number of modern analytical techniques such as small angle neutron scattering (SANS), small angle X-ray scattering (SAXS), nuclear magnetic resonance (NMR), dynamic light scattering (DLS) and static light scattering (SLS) [3,5,69,71-73]. In this study, DLS and SLS are used to analyze the structure of hydrogels (chapter 3.1).

2.2.4.1 Spatial Inhomogeneity in Free Radical Cross-linking Gels

The existence of spatial inhomogeneities on sub-micrometer scales in hydrogels is mainly a result of the gel formation mechanism by free radical cross-linking copolymerization, FRC, i.e. a monovinyl monomer (repeating unit) with a divinyl monomer (cross-linker). The different reactivities of the functional groups lead to different morphologies of the networks. If the reactivity of cross-linker is greater than that of monomer, the reaction of the vinyl groups of the cross-linker is preferred. Additionally, the probability of the reaction with the cross-linker is higher due to the fact that every cross-linker molecule carries at least two vinyl groups. Thus the growing chains in the pre-gel stage are rich in cross-linker units. As a consequence of this unequal vinyl group reactivity, the cross-link density of gels fluctuates. The computer simulations made by SCHRÖDER and OPPERMANN also showed that there is an influence of the cross-linker reactivity on the extent of the concentration fluctuations in gels [74].

During the FRC, cyclization reactions occur when the macroradical attacks the pendant vinyl groups in the same kinetic chain. The cyclization reactions, which predominate in the early stage of polymerization, increase as the dilution increases or as the cross-linker concentration increases. The cycles formed due to the cyclization are elastically ineffective intramolecular links and therefore, they reduce the effective cross-link density of gels [1,75,76].

The solvent quality also affects the spatial inhomogeneity. The spatial inhomogeneity of a gel increases as the solvent quality decreases. If the polymer-solvent interaction is good during cross-linking, pendant vinyl groups will be found more difficult by radicals due to the thermodynamic excluded volume effect. Thus, the presence of larger coils in the polymerization system will reduce the cross-linking and multiple cross-linking reactions. If the polymer-solvent interaction is poor, the chains will coil more than stretch out, and the probability of cross-linking and multiple cross-linking is greater due to increased proximity of the pendant double bonds. As a result, a decrease of the solvent quality during the formation increases both the elastic and the spatial inhomogeneity of gels [77, 78].

2.2.4.2 Photo Cross-linking Polymerization to Obtain More Homogeneous Gels [163]

In this study, gels were also synthesized by the photo cross-linking polymerization, PC, as an alternative method to the free radical cross-linking copolymerization, FRC. PC gels are formed by using functionalized linear polymers, i.e. *N*-(*N'*-Acryloyl-2-aminoethyl)-dimethyl maleimide (DMMIAAm). In this method cross-linking occurs gradually so that a higher control of reaction can be achieved. This method is called "random cross-linking" and has the following advantages compared to the free radical cross-linking copolymerization:

- improved control of critical conversion and gelation time.
- adjusting a desired viscosity of the system before cross-linking reaction.
- easy to introduce certain functionalites into the network.
- Spatially more homogeneous gels are formed in the case of random cross-linking when compared to free radical cross-linking copolymerization [81,82].

Photo chemical cross-linking reactions represent a perceptive method to obtain polymer gels. There are several examples in the literature about photo chemically synthesized gels and networks. Cinnamates were employed by PROCTOR et al. [83]. JONES et al. carried out

photochemical cross-linking by the dimerization reaction of anthracene units of copolymers consisting of poly(ethylene terephthalate) and 2,6-anthracenedicarbocxlate [84]. WOLFF and SCHINNER used photo chemical dimerization of indenes [85-87]. KUZNETSOVA et al. and NGAI et al. synthesized polymeric precursors with coumarins for photo cross-linking [88,89]. SUSOFF employed sensitized photo cross-linking for functionalized poly(styrene-co-aminomethyl styrene) gels which resulted in highly homogenous gels [90].

ZWEIFEL, KUCKLING, GANSEL and SEIFFERT describe the [2+2] cycloaddition of dimethyl maleimide to form permanent network knots [91-96]. The photo chemical cross-linking of functionalized PNIPA using [2+2] cycloaddition of dimethyl maleimide such as Poly(*N*-isopropylacrylamide-co-dimethylmaleimido acrylamide) poly(NIPA-co-DMMIAAm) is used in this study to generate PNIPA gels. The synthesis of PNIPA gels by means of photo cross-linking is described in the literature [97].

In this work, the photo cross-linking of poly(NIPA-co-DMMIAAm) is used in the presence of thioxanthone in water to gradually synthesize PNIPA gels (chapter 4.2.2).

2.2.5 Photo Cross-linkable Matrix [98]

Under exposure to UV light, olefins are able to undergo various types of photo chemical transformations from their excited singlet or triplet states. One important example of such a process is the so called [2+2]-cycloaddition, a reaction yielding cyclobutane derivatives as illustrated in Figure 8.

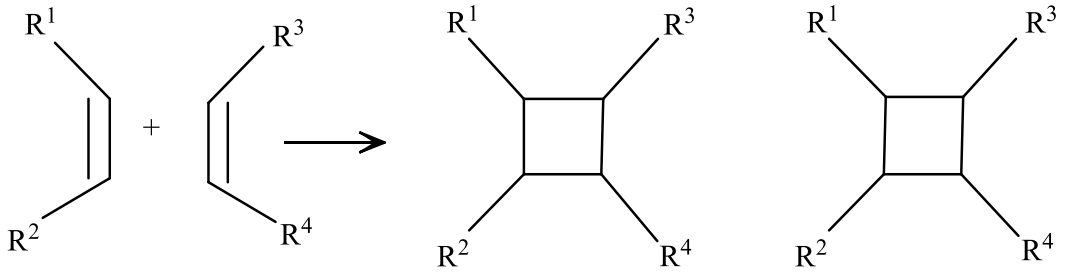

Figure 8 Two new σ bonds are formed at the expense of two π bonds, which is in principle possible between differently as well as identically substituted olefins.

Suitable groups which undergo photo dimerization and can therefore be used for photo cross-linking of accordingly functionalized polymers, e.g., comprising cinnamate (and related) moieties [99-105], coumarins [106-109], and maleic acid derivatives like dimethyl maleimide (DMMI) [110-115]. One of the major drawbacks of cinnamates, besides advantageous features such as controlled reversibility of the dimerization [104], is the photo chemically induced cis / trans isomerization resulting in a noticeable decrease of the quantum yield of photo cross-linking [111]. A second shortcoming is their sensitivity to radical reactions, which prevents them from being used in radical copolymerisations. Coumarins and DMMIs do not show these disadvantages.

For the present work, the DMMI functionality was chosen to be employed because of the higher polarity and water solubility of this group, and because of favorable spectroscopic and electronic properties in comparison to coumarins.

2.2.5.1 Photo Chemical [2+2]-Cycloaddition

Photo chemical [2+2]-cycloaddition reactions can basically start from both the excited singlet (S_1) and triplet (T_1) state of one of the two molecules eventually forming a dimer. In the first case, the reaction occurs in a concerted action and yields cyclo-dimers in the stereospecific cis form, whereas the reaction from the T_1 state proceeds in a stepwise manner, and dimeric products thus obtained are a mixture of cis and (favored) trans isomers.

The energy of the excited singlet state of DMMI is considerably higher than that of the triplet state. Direct excitation of DMMI requires short-wavelength UV light which might as well cause unwanted degradation of the polymer chains. It is therefore advantageous to proceed from the T1 state, which can be reached by energy transfer from an excited, suitably chosen sensitizer [116-120]. The S_1 and T_1 states of the sensitizer molecule have to be closer together with their energies between those of the S_1 and the T_1 states of DMMI. Figure 9 shows a scheme of such a sensitized process. After excitation of the sensitizer to its S_1 state by comparatively long-wave UV light, it can undergo intersystem crossing to its slightly lower T_1 state and subsequently transfer the triplet energy to the substrate (DMMI), from which the dimerization reactions proceed. This way of effectively achieving a high population of the T_1 state as a starting point for photochemical reactions was described by HAMMOND et al. [116-120]. Suitable sensitizer molecules are aromatic ketones since they generally show a combination of strong spin-orbit coupling, leading to high quantum yield of intersystem

crossing, and small energy gaps between the S_1 and the T_1 states. In addition, their nπ* or ππ* triplet states provide sufficiently high energy levels and lifetimes [121] to enable effective energy transfer to a substrate.

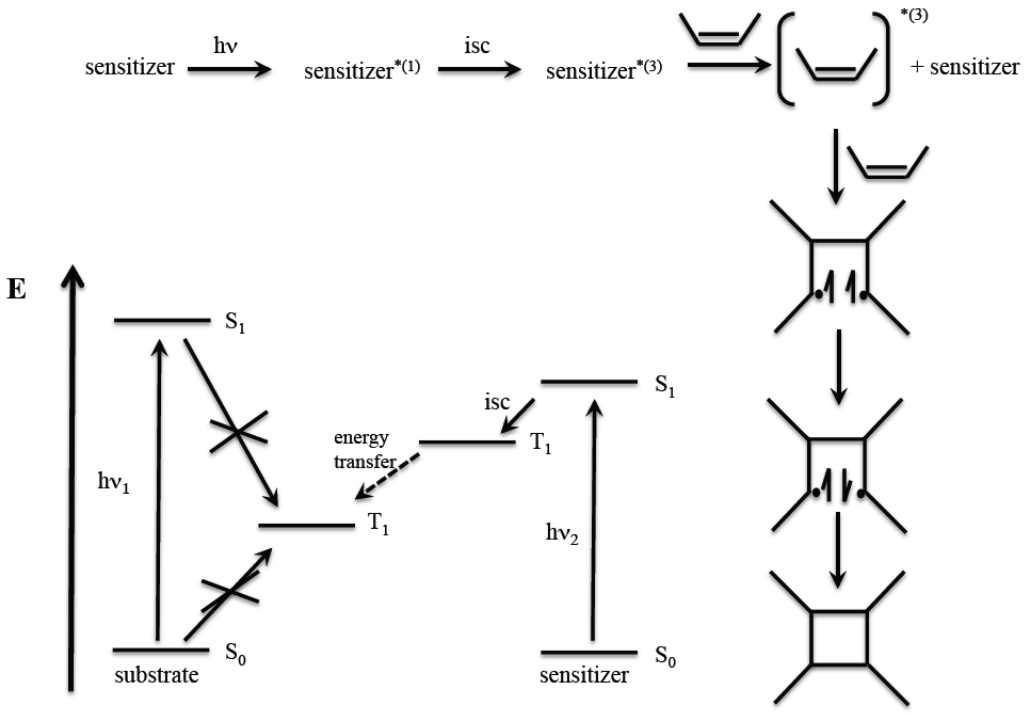

Figure 9 Mechanism of sensitized [2+2]-cyclodimerization according to HAMMOND et al. [116-120].

The majority of aromatic ketones possesses nπ* triplet states. These molecules can undergo various types of side reactions such as hydrogen abstractions or PATERNO–BUCHI additions [122,123]. Molecules with ππ* triplet states are therefore preferred as sensitizers, because unwanted reactions can be largely excluded. There have been several studies showing that the T_1 state of thioxanthones in polar media corresponds to a ππ* transition [124,125]. Thioxanthones have been widely used for photo sensitization and initiation purposes [126]. The energy of their T_1 state is relatively high [117,127] and only marginally less than that of S_1. Intersystem crossing occurs with high quantum yield [127,128], and they show adequately long triplet lifetimes [124]. In the present work, the sodium salt of thioxanthone disulfonate is employed. The sulfonate groups only act in terms of increasing the water solubility without affecting the spectral properties significantly [124,129].

3 Methods

3.1 Light Scattering

Light scattering is a process which covers a wide range of interactions of electromagnetic radiation with particles. Therefore, the analysis of the scattered radiation arising from these interactions is an important physical method. Light scattering can be classified as elastic (no absorption) and inelastic (absorption, e.g., fluorescence, phosphorescence) light scattering. Light scattering normally refers to light scattering of nonabsorbing macromolecules or colloidal particles. When monochromatic light is incident onto a dilute macromolecule solution, due to the difference in refractive index of solvent and solute, the incident light is scattered by the illuminated macromolecule into all directions [130,131]. This scattered light contains information of the macromolecule or particles in solution, such as the size, the molar mass, and the conformation of the macromolecules or particles.

The extent of light scattered by a polymer network strongly depends on its structure. Liquids and gases scatter light to a small extent caused by density fluctuations due to thermal motion of the particles. In a solution, e.g., of a polymer in a good solvent, there are additional concentration fluctuations of the diffusing polymer coils that exceed the density fluctuations of the solvent itself and yield a much stronger scattering. If the coils can diffuse freely this is called an ergodic system. In an ergodic system the time-average of the scattered light intensity is the same as the ensemble-average.

A polymer gel is obtained by fixing the polymer coils by introducing cross-links in a polymer solution. In this case, the concentration fluctuations within the solution become frozen-in. Hence, polymer coils cannot move freely, resulting in a non-ergodic system. In polymer gels, there are parts exhibiting high polymer concentrations and low polymer concentrations. This concentration difference leads to a spatially inhomogeneous structure. Intensity of light scattered from polymer gels is stronger than scattering of corresponding uncross-linked polymer solutions [77,81,132-136].

In the present work only the elastic light scattering is employed. Light scattering can be classified as dynamic light scattering (DLS) and static light scattering (SLS). The light scattering intensity can be monitored either in the microsecond or in the second time range domain. This is the main difference between SLS and DLS. The fluctuations of the intensity

of the light scattered by a small volume of a solution in the microsecond time range are directly related to the Brownian motion of the sample. The fluctuation rate can be related to different kinds of relaxation process such as diffusion and internal motions of the macromolecules. Static light scattering measures the time-average scattered intensity, whereas the dynamic light scattering measures the intensity fluctuations. In dynamic light scattering, the frequency broadening ($\approx 10^5$-10^7 Hz) is quite small in comparison with the incident light frequency ($\approx 10^{15}$ Hz), so the detection of DLS in frequency domain is very difficult. But it can be effectively recorded in the time domain through a time correlation function. That is why DLS is sometimes called photon correlation spectroscopy (PCS).

In static light scattering the time-average scattered intensities are measured at different angles and concentrations, from which three parameters of macromolecules for dilute polymer solutions, namely the weight-average molecular weight, M_w, the *z*-average root-mean-square radius of gyration ,$<R_G^2>^{0.5}$, simply R_G, and the second osmotic virial coefficient, A_2, can be obtained. On the other hand, dynamic light scattering is designed to measure the fluctuation of scattered intensity. Relaxation rate, Γ can be obtained from dynamic light scattering. Translational diffusion coefficient, D_{trans}, and hydrodynamic radius, R_H, can be calculated with the appropriate equations related with the relaxation rate.

3.1.1 Static Light Scattering

Scattering intensities obtained by SLS are usually reported in relative ratio as RAYLEIGH ratios, $R(q)$. Here

$$q = \left(\frac{4\pi n}{\lambda_0} \right) \sin \frac{\theta}{2} \tag{22}$$

is the amplitude of the scattering vector with θ being the scattering angle, λ_0 the wavelength of the incident light in vacuum and n the refractive index of the medium, respectively. Figure 10 schematically shows a typical light scattering set up.

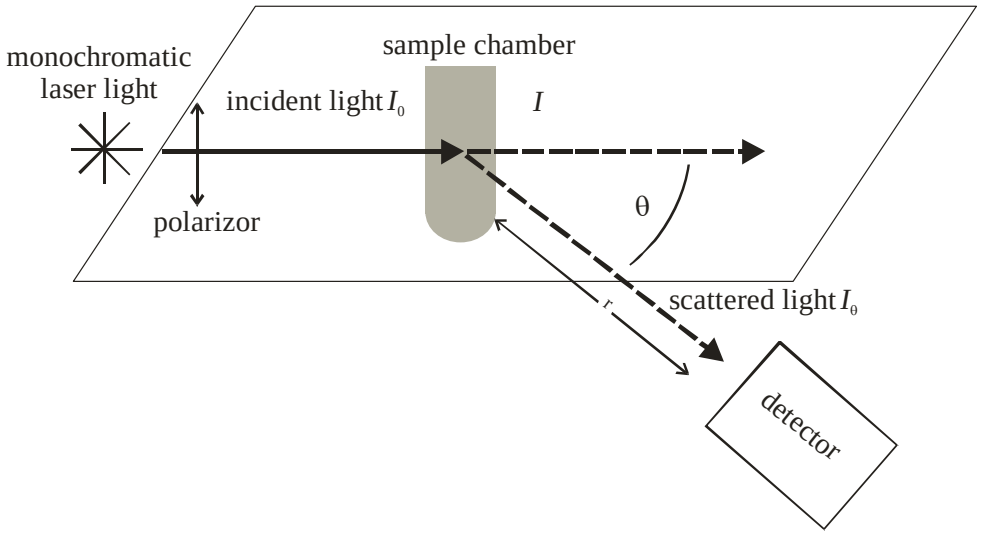

Figure 10 Schematic illustration of light scattering. I_0 is the intensity of the incident light, I_θ is the intensity of the scattered light measured at the angle θ and I is the intensity of light that passes through the sample without any scattering.

For gels [5-11]

$$R(q) = R_{\mathrm{F}}(q) + R_{\mathrm{C}}(q) \tag{23}$$

where the total scattering intensity, $R(q)$, has been split into two contributions: $R_{\mathrm{F}}(q)$, termed the dynamic or fluctuating part, is due to thermal concentration fluctuations and $R_{\mathrm{C}}(q)$, termed the static (frozen-in) part, is due to spatial inhomogeneities possibly resulting from the cross-linking process. The latter is the quantity of interest to characterize the microstructure of the gels. In a common SLS device, the detector has a wide aperture or slit, collecting the scattered light in a rather large solid angle Ω (typically of the order of 10^{-3}). This results in a correspondingly small coherence area of order λ^2/Ω, [137] which is much smaller than the cross-section of the scattering volume. As a consequence, SLS measurements automatically report the scattering intensity as an ensemble-average over the scattering volume. This comes usually pretty close to the macroscopic ensemble. Therefore, all quantities in eq. 23 represent ensemble-averages.

In an experimental approach to determine $R_{\mathrm{C}}(q)$ from SLS measurements, one often presumes that the thermal fluctuations in a gel are practically identical with those in a solution of the linear polymer,[6] hence $R_{\mathrm{F}}(q) \approx R_{\mathrm{SOL}}(q)$, and $R_{\mathrm{C}}(q) \approx R(q) - R_{\mathrm{SOL}}(q)$. $R_{\mathrm{SOL}}(q)$ becomes available by separately measuring the scattering intensity of a (semi-dilute or concentrated)

solution of the uncross-linked polymer under conditions equivalent to those in the gel. Although this seems to be a plausible assumption, it is not generally valid. GEISSLER et al. showed by a series of carefully devised experiments based on a thorough theoretical treatment that $R_F(q)$ is generally some 30% larger than $R_{SOL}(q)$ [138-140]. In many cases, however, the static scattering intensity is so much larger than the dynamic scattering that the appreciable error in $R_F(q)$ becomes irrelevant or is plainly accepted. On the other hand, it is frequently difficult or even impossible to prepare a solution of the linear polymer. Either a polymer of exactly the same composition as that in the gel is not available, or the preparation of a homogeneous solution proves impractical because the viscosity becomes too high.

By determining the static scattering, $R_C(q)$, one can directly draw conclusions on the inhomogeneities which were formed during gelation. These spatial inhomogeneities typically occur on a length scale on the order of 10-100 nm [30,35,141]. A good overview of the formation of inhomogeneities in gels is given by SHIBAYAMA [35]. According to DEBYE–BUECHE theory $R_C(q)$ provides a statement about the mean square fluctuation of refractive index, $<\eta^2>$, and a static correlation length, ξ [4,6,81]. The static scattering is given by DEBYE–BUECHE theory

$$R_C(q) = \frac{8\pi K \xi^3 \langle \eta^2 \rangle}{\left(1 + q^2 \xi^2\right)^2} \tag{24}$$

K is a constant in which n is the refractive index of the medium and λ_0 the wavelength of the incident radiation in vacuum

$$K = \frac{4\pi^2 n^2}{\lambda_0^4} \tag{25}$$

3.1.2 Dynamic Light Scattering

Unlike static light scattering which measures the time-averaged scattered intensity, dynamic light scattering measures the fluctuation of the scattered intensity with time. These fluctuations arise from the fact that the particles undergo random thermal (Brownian) motion. Therefore, the distance between them is continuously varying. The fluctuation of the intensity of scattered light at the detector is due to the constructive and destructive interference of light scattered by the randomly moving particles within the illuminated sample volume. The time dependent changes of the intensity contain information about this Brownian motion. DLS measures the temporal correlations of these statistical fluctuations of the scattered intensity. The light scattering set up was already shown in Figure 8. In order to perform dynamic light scattering experiments, additionally a correlator is used to analyze the intensity fluctuations that are monitored by the detector.

In DLS, the detection optics is designed to achieve a large coherence factor. Modern instruments employ single-mode or few-mode light guides for this purpose [142,143]. As a consequence, minor changes in the position or orientation of a gel sample produce marked variations of the measured scattering intensity, forming a so-called speckle pattern. This behavior is typical of non-ergodic samples such as gels or disordered solids, it does not appear in fluids.

It is common in the literature on DLS to denote the scattering intensity by $I(q)$. This custom is important for this study, these intensities will be reported in absolute units to enable direct comparison with data measured by SLS. Hence, $I(q)$ and $R(q)$ are equal quantities, the different letters just refer to distinct measuring methods. Since it is the major purpose of DLS to measure intensities on the scale of microseconds and to analyze temporal intensity fluctuations, time average is explicitly indicated here by $\langle ... \rangle_T$.

As stated above, the time-averaged scattering intensity, $\langle I(q) \rangle_T$, measured on a gel sample varies markedly with sample position or orientation. $\langle I(q) \rangle_T$ has two contributions which can be written as [15, 17, 35]

$$\left\langle I(q) \right\rangle_T = \left\langle I_F(q) \right\rangle_T + I_C(q) \tag{26}$$

Eq. 26 looks very similar to eq. 23, but there is a significant difference. Whereas eq. 23 applies to the sample as a whole because the intensities are ensemble averages, eq. 26 applies only to one particular speckle, i.e. a definite location in the sample observed under a definite scattering vector. $\langle I_F(q)\rangle_T$ is the time-average of the fluctuating component arising from dynamic, liquid-like concentration fluctuations. Because this contribution is ergodic, $\langle I_F(q)\rangle_T = R_F(q)$. On the other hand, the static component of the scattering intensity, $I_C(q)$, is independent of time, but depends on the position [144]. That is why generally $I_C(q) \neq R_C(q)$ and $\langle I(q)\rangle_T \neq R(q)$. The remainder of this section is therefore concerned with determining the ensemble-averages $\langle I(q)\rangle_E$ or $\langle I_C(q)\rangle_E$, respectively.

$\langle I(q)\rangle_E$ can of course be obtained by taking measurements of the scattering intensity on a sufficiently large number of positions and subsequent averaging, or by rotating the sample while the measurement is running. But these procedures alone do not allow for a separation of the different contributions i.e. fluctuating part and static (frozen-in) part. For that purpose, it is necessary to make use of the intensity correlation functions.

The normalized time-average intensity correlation function (ICF), $g_T^{(2)}(q,\tau)$, of the scattered intensity determined from a single DLS experiment is given as

$$g_T^{(2)}(q,\tau) = \frac{\langle I(q,0)I(q,\tau)\rangle_T}{\langle I(q,0)\rangle_T^2} \tag{27}$$

where τ denotes the time, I the the scattered intensity. The scattered intensity is the square of the absolute value of the electric field of the scattered light at the detection (eq. 28).

$$I(q,t) = |E(q,t)|^2 \tag{28}$$

The square of the electric field, E, of the light scattered is proportional to the corresponding scattered intensity. For an ergodic system, the scattered intensity contains only a fluctuating component, i.e. $\langle I(q,t)\rangle_T = \langle I_F(q,t)\rangle_T = \langle |E_F(q,t)|^2\rangle_T$, where $E_F(q,t)$ is a zero-mean complex GAUSSIAN variable in the time domain and independent of position. $g_T^{(2)}(q,\tau)$ is then equivalent to an ensemble-averaged ICF, $g_E^{(2)}(q,\tau)$, and can be related to the normalized

scattering function or the scattering field time correlation function $g_T^{(1)}(q,\tau)$ via the SIEGERT relation [131].

$$g_T^{(2)}(q,\tau) = g_E^{(2)}(q,\tau) = \frac{\langle I(q,0)I(q,\tau)\rangle_E}{\langle I(q,0)\rangle_E^2} = 1 + \beta\left|g_T^{(1)}(q,\tau)\right|^2 \tag{29}$$

where β is the coherence factor of the instrument and $\langle ... \rangle_E$ indicates an ensemble-average over all possible configurations of the medium.

The scattering field time correlation function, $g_T^{(1)}(q,\tau)$, can be approximated by a single rexponential decaying function

$$g_T^{(1)}(q,\tau) = \exp(-\Gamma\tau) \tag{30}$$

Γ^{-1} is a characteristic decay time

$$\Gamma = D_{trans}\, q^2 = \frac{1}{\tau} \tag{31}$$

where D_{trans} is a translational diffusion coefficient and q is the scattering vector (eq. 22).

Dynamic light scattering mainly is a convenient method to detect the hydrodynamic radii of polymer coils or other particles in dilute solution. The size of a particle or hydrodynamic radius, R_H, is calculated from the translational diffusion coefficient, D_{trans}, which describes the center of mass movement of the whole coil by using the STOKES–EINSTEIN equation (eq. 32), with η the viscosity of the solvent, k_B BOLTZMAN's constant, T absolute temperature [47].

$$R_H = \frac{k_B T}{6\pi\eta D_{trans}} \tag{32}$$

For a non-ergodic system containing an infinite network or having a "frozen-in" structure, the scattered intensity also contains another contribution, i.e. the frozen-in (or static) component, $\langle I(q,t)\rangle_T = \langle I_F(q,t)\rangle_T + I_C(q)$ (eq. 26) and $I_C(q) = |E_C(q)|^2$. The frozen-in component, $I_C(q)$, is independent of time but depends on the position of the scattering volume within the sample.

Different regions in one sample scatter differently, a fact leading to the so-called "speckle pattern" in DLS measurements. In this case, the SIEGERT relation (eq. 29) does not hold. There are basically two different approaches to analyze the fluctuating part, $\langle I_F(q)\rangle_T$, and the static part, $I_C(q)$, of polymer gels in the literature. In the following two chapters these two methods will be explained.

3.1.2.1 Non-Ergodic Method

Polymer gels generally have more or less inhomogenous structures. Inside the gel there are two different behaviors. One of them arises from liquid-like structures while the other one comes from solid-like structures. The fluctuating part, $\langle I_F(q)\rangle_T$, corresponds to liquid-like concentration fluctuations, thus being ergodic [144]. On the other hand, the static part of the scattered intensity, $I_C(q)$, arises from spatial inhomogeneities resulting from the cross-linking process. The total ensemble average scattering intensity, $\langle I(q)\rangle_E$, is the sum of these two contributions. If $\langle I_F(q)\rangle_T = \langle I(q)\rangle_E$ the gel doesn't exhibit static scattering from spatial inhomogeneities. Hence, the gel is seemingly ergodic and exhibits no static fluctuations. Since in polymer solutions $\langle I_F(q)\rangle_T = \langle I(q)\rangle_E$, they are called ergodic. The non-ergodic method proposed by PUSEY and VAN MEGEN [17] stresses the importance to take the ensemble-average of the scattered intensity, $\langle I(q)\rangle_E$, by measuring scattered intensities at a large number of sample positions from which the degree of inhomogeneity and the diffusion coefficient can be evaluated. $\langle I(q)\rangle_E$ can be obtained by taking measurements of scattering intensity by rotating the sample while the measurement is running. Figure 11 describes here how an experiment according to non-ergodic method is run. Due to the non-ergodicity of the gels frozen-in inhomogeneities exist which are observed as a speckle pattern. Thus, at different sample positions different time-average scattering intensities, $\langle I(q)\rangle_T$, are measured. Measurements were usually done at $\theta = 90°$ because average of the particle sizes is observed better at this angle.

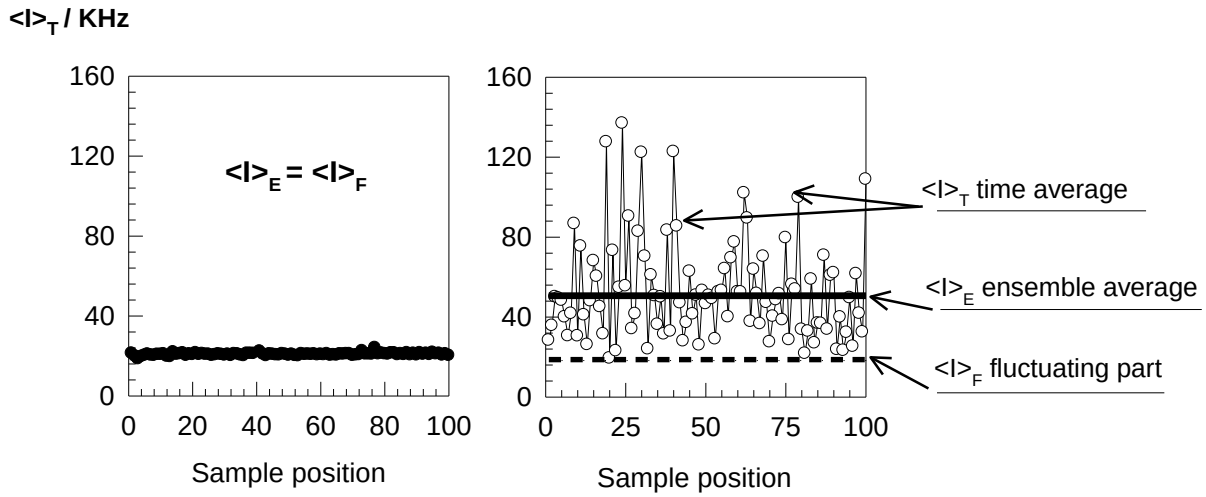

Figure 11 Time-average scattering intensity, $\langle I \rangle_T$, ensemble-average scattering intensity, $\langle I \rangle_E$, and intensity of fluctuating part, $\langle I_F \rangle_T$, can be determined through the non-ergodic method. Left hand side: solution without cross-linker, right hand side: gel structure; $\theta = 90°$.

According to PUSEY and VAN MEGEN [17] (non-ergodic method), the intensity of the fluctuating part, $\langle I_F(q) \rangle_T$, is related to time-average scattering intensity, $\langle I(q) \rangle_T$, via

$$\left\langle I_F(q) \right\rangle_T = \left\langle I_F(q) \right\rangle_E = \left\langle I(q) \right\rangle_E \left[1 - f(q,\infty)\right] \tag{33}$$

$f(q,\tau)$ is the normalized intermediate ensemble-averaged scattering function (the letter f is used to clearly distinguish the intermediate scattering function of non-ergodic medium from the field correlation function, $g_T^{(1)}$, of ergodic meduim) and $f(q,\infty)$ its asymptotic value at $\tau \rightarrow \infty$ which shows the static scattering fraction. $f(q,\tau)$ can in turn be calculated from the time-averaged intensity correlation function measured at a particular position, $g_T^{(2)}$

$$f(q,\tau) = 1 + \frac{\left\langle I(q) \right\rangle_T}{\left\langle I(q) \right\rangle_E} \left[\sqrt{\frac{g_T^{(2)}(q,\tau) - 1 - \sigma^2}{\beta}} + 1 - 1 \right] \tag{34}$$

with $\sigma^2 = g_T^{(2)}(q,0) - 1$, the initial amplitude of the time-averaged intensity correlation function. By converting the time-averaged intensity correlation function, $g_T^{(2)}$, into the normalized intermediate ensemble-averaged scattering function, $f(q,\tau)$, it is "shifted" up to a ordinate intercept with the value of one resulting in an offset, $f(q,\infty)$, different from zero (Figure 12).

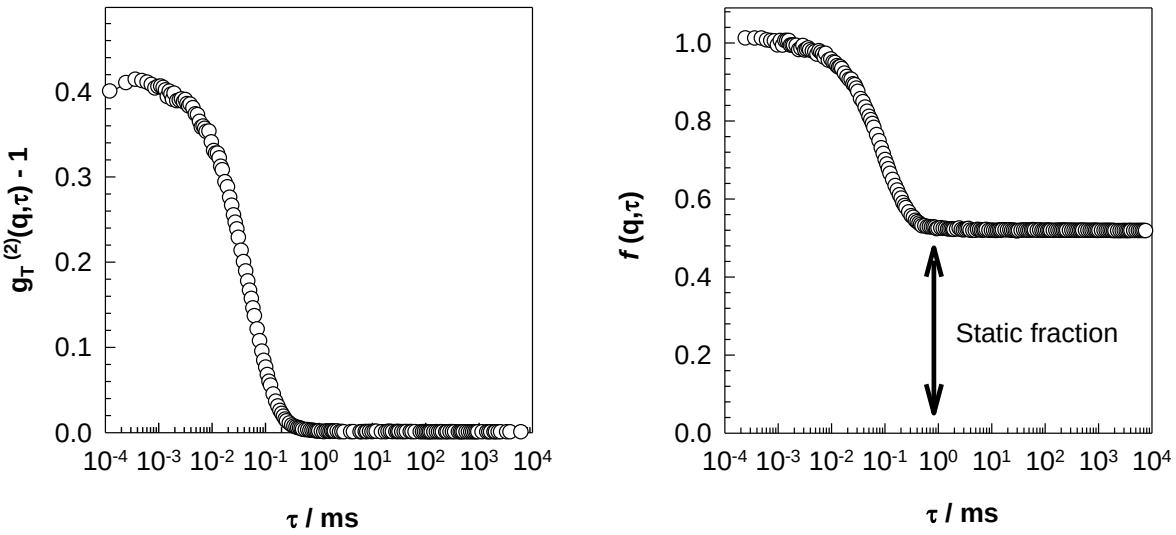

Figure 12 In order to obtain $f(q,\tau)$ by the non-ergodic method $g_T^{(2)}(q,\tau) - 1$ is shifted to a ordinate intercept of 1 according to eq. 33.

From the fitted curve the asymptotic value, $f(q,\infty)$, and the correlation time, τ, is calculated according to eq. 35. The amplitude $A = 1 - f(q,\infty)$.

$$f(q,\tau) = f(q,\infty) + A\exp(-\frac{t}{\tau}) \tag{35}$$

While the asymptotic value, $f(q,\infty)$, indicates the static fraction of the polymer gel, ($\langle I_C(q)\rangle_T$), the amplitude, A, of the curve corresponds the fluctuating part, ($\langle I_F(q)\rangle_T$). The lower the asymptotic value, the more homogenous is the polymer gel. In the non-ergodic method the aim is to separate the static and fluctuating part of the investigated polymer gel as percentages. The accuracy of this method, often termed the *non-ergodic approach* (NE), has also been assessed [145].

In addition, it is possible to obtain the dynamic correlation length, ξ, by means of the cooperative diffusion coefficient, D, which defines the relaxation of network chain segments according to eq. 36. This equation is partially different from the STOKES–EINSTEIN equation (eq. 32). The correlation length shows the distance between cross-links that are connected by network chains and the cooperative diffusion coefficient is used instead of the translational diffusion coefficient.

$$\xi = \frac{kT}{6\pi\eta D} \tag{36}$$

3.1.2.2 Partial Heterodyne Method

The alternative method, the *partial heterodyne method* (PH) proposed by JOOSTEN et al. [15] is applicable if intensity correlation functions have been determined on a (large) number of positions. It is assumed that the scattered intensity for a non-ergodic medium can be given by the sum of fluctuating and static intensity components and ergodicity can be applied to the fluctuating part. Apparent diffusion coefficients, D_A, can be estimated according to

$$D_A = -\frac{1}{2q^2}\lim_{\tau\to 0}\frac{\partial}{\partial\tau}\ln\left(g_T{}^{(2)}(q,\tau)-1\right) \tag{37}$$

For different sample positions, different values of D_A are obtained, and these come along with different local scattering intensities, $\langle I(q)\rangle_T$. A fully fluctuating, ergodic and thus homogeneous and homodyne system ($\langle I_F(q)\rangle_T = \langle I(q)\rangle_T$) yields $D = D_A$. In a predominantly static, non-ergodic, inhomogeneous and heterodyne system ($\langle I_F(q)\rangle_T << \langle I(q)\rangle_T$) it is $D = 2D_A$. A relationship between D_A and the cooperative diffusion coefficient, D, has been derived:

$$D = \left(2 - \frac{\langle I_F(q)\rangle_T}{\langle I(q)\rangle_T}\right) D_A \tag{38}$$

Eq. 38 applies to each sample position. For different sample positions, different values of D_A and $\langle I(q)\rangle_T$ are obtained. According to the eq. 38a, which is simply a rearrangement of eq. 38, a plot of $\langle I(q)\rangle_T / D_A$ versus $\langle I(q)\rangle_T$ should yield a straight line, from the slope and intercept of which the fluctuating component of the scattering intensity, $\langle I_F(q)\rangle_T$, and D can be obtained. A sufficiently large number of data points are needed in order to define the straight line with adequate accuracy.

$$\frac{< I(q) >_T}{D_A} = 2\frac{< I(q) >_T}{D} - \frac{< I_F(q) >_T}{D} \tag{38a}$$

Figure 13 shows the typical decomposition plots for the gel samples. For each system 100 data points are plotted. From the linear regression cooperative diffusion coefficient, D, as well as the fluctuating component, $\langle I_F(q)\rangle_T$, are evaluated.

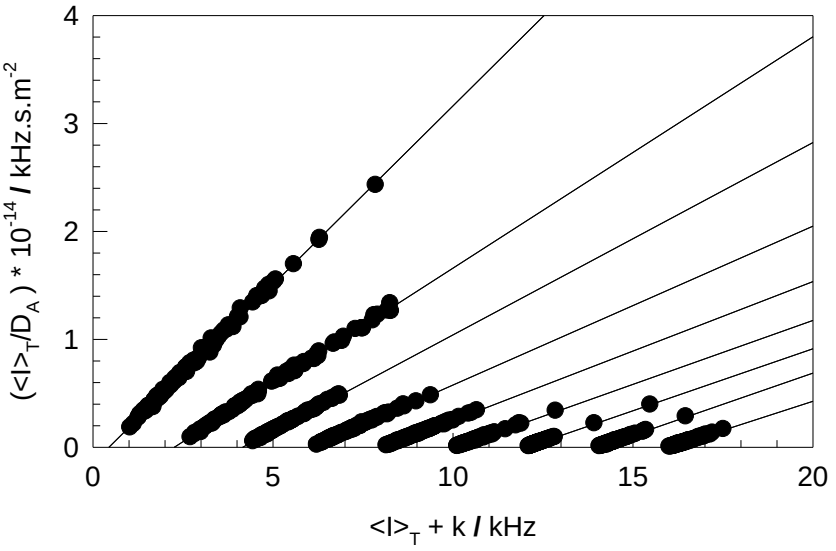

Figure 13 Decomposition plots according to eq. 38a for different gel samples. k is an arbitrarily chosen additive constant for each gel in order to separate the corresponding plots.

Both approaches described allow separation of the ensemble-averaged scattering intensity, $\langle I(q)\rangle_E$, into its components, $\langle I_F(q)\rangle_E$ and $\langle I_C(q)\rangle_E$.

3.2 Rheology

3.2.1 Introduction

While the microstructure of the gels is analyzed using light scattering methods, the characterization of the polymeric matrix, in which the diffusion takes place, is done by means of rheometry.

Rheology is defined as the science of flow and deformation matter. It investigates the relationship between force, deformation and time. The material that is investigated in rheology can be everything from an elastic solid to a viscous liquid. This material property is known as viscoelasticity. The rheology is therefore a suitable method to determine the macroscopic properties of gels [47,146-148].

3.2.2 Viscoelastic Behavior of Polymer Gels

Polymers are viscoelastic materials, since they show strongly viscous and elastic behavior at the same time. Viscoelastic behavior accordingly consists of a combination of the laws of NEWTON and HOOKE The relationship between stress and strain is called constitutive equation. The simplest constitutive equation which describes the elastic behavior of an ideal solid, is HOOKE's law. According to HOOKE's law the stress is proportional to the deformation.

$$\sigma = G \cdot \gamma \tag{39}$$

σ is the force per unit area or stress, γ is the relative length change or stress. The proportionality factor, G is the shear modulus which shows the resistance of a material against deformation.

On the other hand, for liquids the constitutive equation is NEWTONS's law of viscosity which states that the shear stress, σ, is no longer proportional to the deformation, but proportional to the rate of deformation. The ratio of stress and deformation rate is referred to as viscosity, or resistance to flow η. It is NEWTON's law

$$\sigma = \eta \cdot \dot{\gamma} \tag{40}$$

Liquids that follow this law are referred to as Newtonian fluids.

These constitutive equations do not hold for viscoelastic materials. Oscillatory measurements are ideal to investigate viscoelastic behavior. The principal advantage is that the viscoelastic response of any material can be measured directly on different time scales while the angular frequency, ω, is varied. For purely Hookean solid the shear stress is "in-phase" with applied strain. For ideal elastic solids, the following equation gives the relation between stress and deformation

$$\sigma(t)=G\cdot\gamma(t) \tag{41}$$

with *G* the elastic shear modulus. For a harmonic periodic, the time-dependent deformation can be expressed as

$$\gamma(t)=\gamma_A\cdot\sin(\omega t) \tag{42}$$

γ_A is the deformation amplitude and ω is the angular frequency. For elastic materials the shear stress and shear deformation curve are "in-phase" and correspond to a sinusoidal curve.

On the other hand, for ideal viscous liquids according to NEWTON,

$$\sigma(t)=\eta\cdot\dot{\gamma}(t) \tag{43}$$

The shear stress in a Newtonian liquid still oscillates with the same angular frequency, but is out-of-phase with the strain by π/2. The course of deformation is shown as a sinus curve, resulting for the shear stress and the deformation speed a cosinusoidal course.

More generally, the linear response of a viscoelastic material always shows the stress leading the strain by a phase angle δ

$$\sigma(t)=\sigma_0\cdot\sin(\omega t+\delta) \tag{44}$$

where the phase angle, δ, is frequency dependent and can take values between 0 and π/2. For solids that obey to HOOKE's law δ = 0 and for a Newtonian fluid δ = π/2 at all frequencies. By separation of the resulting shear stress into two mutually orthogonal functions which oscillate with the same frequency, one in-phase with the strain and the other out-of-phase with the strain by π/2

$$\sigma(t)=\gamma_A\left[G'(\omega)\sin(\omega t)+G''(\omega)\cos(\omega t)\right] \tag{45}$$

the shear modulus is separated into two values, G' being elastic the modulus and G'' the viscous modulus. G' is also called the storage modulus which is a measure for the deformation energy stored during the shear process. G'' is the loss modulus characterizing the energy dissipated by deformation. They can be regarded as the real and the imaginary part, respectively, of a complex shear modulus, G^*

$$G^*(\omega)=G'(\omega)+\mathrm{i}G''(\omega) \tag{46}$$

The ratio of loss and storage modulus is the tangent of the phase angle, which is called loss tangent

$$\tan\delta=\frac{G''}{G'} \tag{47}$$

δ is also called loss angle or loss factor and can be used for characterization of solids and gels.

During the gelation process the gel point is reached when the weight average molar mass, M_w, diverges and thus goes to almost infinity [149]. In this gel point ($G'= G''$) the sample turns from liquid to solid behavior. CHAMBON and WINTER found out that G' and G'' are only equal if they both show an identical frequency dependence. An indication of the gel point in terms of rheology has been proposed with the formulation

$$G'(\omega)\sim G''(\omega)\sim\omega^n \tag{48}$$

n is called relaxation exponent and $0 < n < 1$ [150].

This relation does not mean that the gelation point is exactly the same as the intersection point $G' = G''$ [151,152]. However, the crossover point is a good estimate for the sol-gel transition. All of these considerations are only valid as long as the analyses are carried out in the so called linear viscoelastic regime. In this regime, the elastic and the loss modulus is independent of the applied deformation or shear stress.

The cross-linking reaction can be monitored in a time course experiment at constant frequency and strain. When *G*' and *G*" intersect the gelation threshold is reached (Figure 14). For liquid-like materials *G*" is much higher than *G*' and for solid-like material *G*' is much higher than *G*".

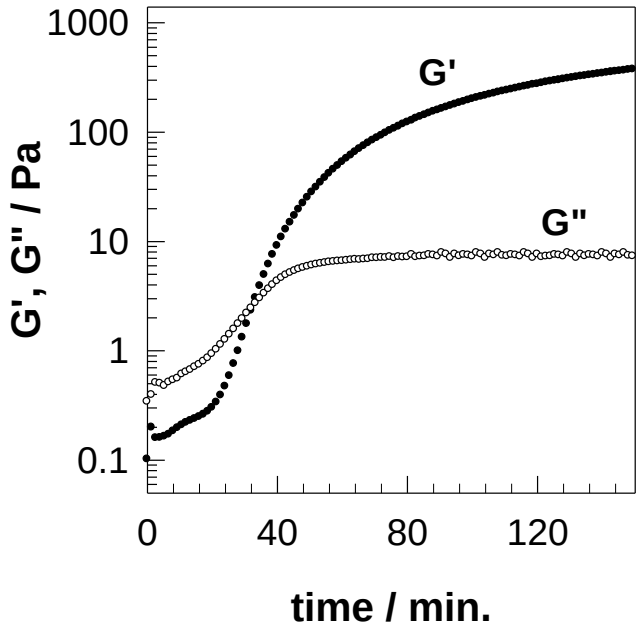

Figure 14 Elastic modulus, *G*', and viscous modulus, *G*", are plotted against reaction time of a cross-linking polymerization. The gel point is considered as intersection of the curves where the sample turns from solution to gel.

4 Experimental Section

4.1 Substances

4.1.1 Compounds used for Free Radical Cross-linking Copolymerization

N-isopropylacrylamide (NIPA, ACROS), *N*,*N'*-methylenebis(acrylamide) (MBA, Sigma), ammonium persulfate (APS, Sigma), and *N*,*N*,*N'*,*N'*-tetramethylethylenediamine (TEMED, Sigma) were used as received. PNIPA gels were prepared by free radical cross-linking copolymerization of NIPA and MBA in aqueous solution. NIPA is used as a monomer, MBA is used as a cross-linker.

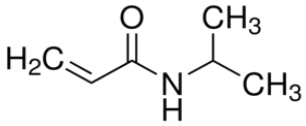

NIPA

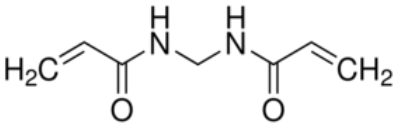

MBA

Figure 15 Monomers; left hand side: *N*-isopropylacrylamide; right hand side: *N*,*N'*-methylenebis(acrylamide).

Ammonium persulfate is used as an initiator and *N*,*N*,*N'*,*N'*-tetramethylethylenediamine is used as an accelerator in the polymerization reactions.

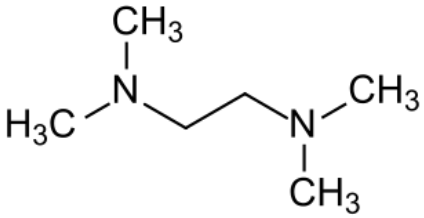

TEMED

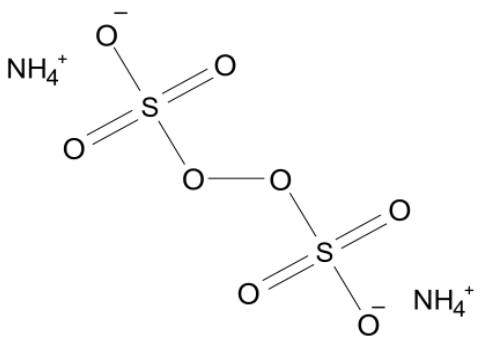

APS

Figure 16 Left hand side; *N*,*N*,*N'*,*N'*-tetramethylethylenediamine; right hand side: ammonium persulfate.

4.1.2 Compounds used for Photo Cross-linking Polymerization

NIPA was copolymerized with *N*-(*N'*-Acryloyl-2-aminoethyl)-dimethyl maleimide (DMMIAAm) by means of TEMED and APS.

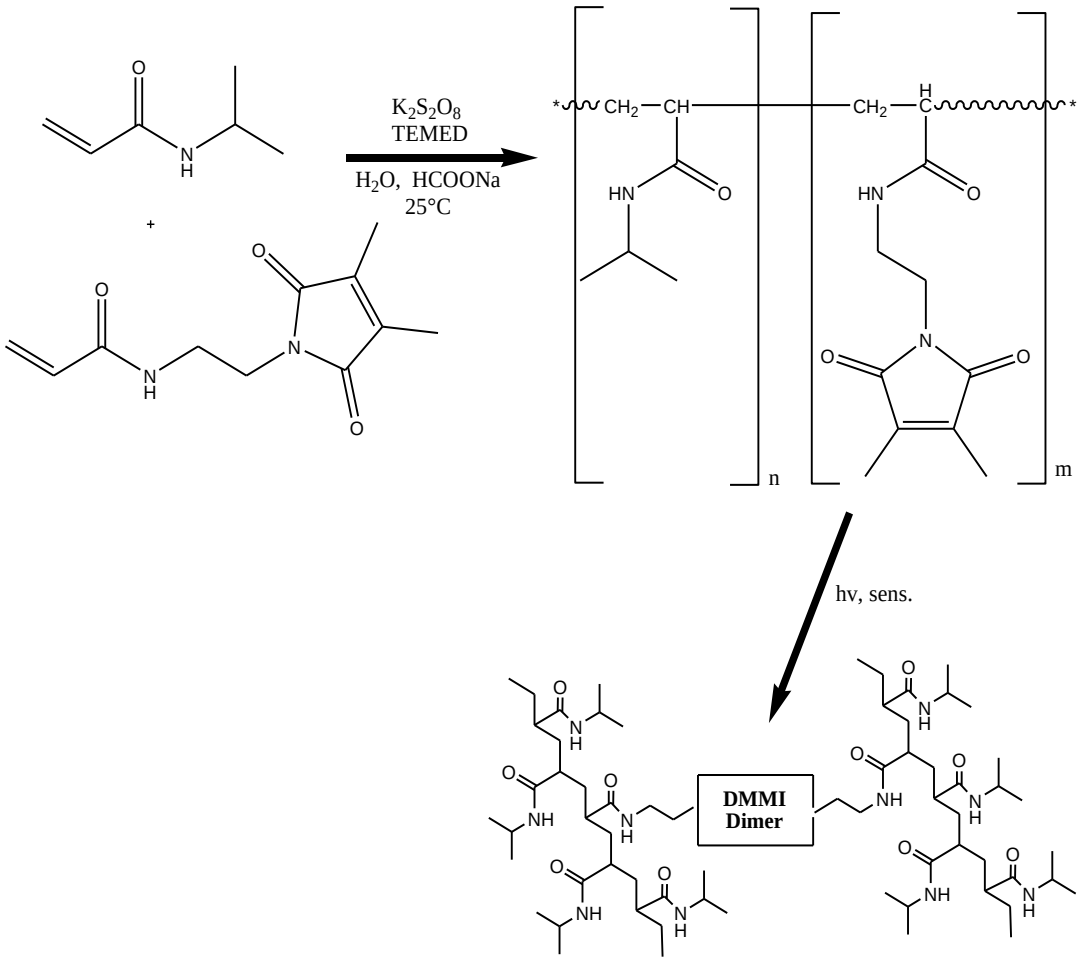

Figure 17 PNIPA functionalized with pendant DMMI-groups was synthesized by free radical copolymerization of NIPA and DMMIAAm according to Figure 17.

4.1.2.1 Synthesis of DMMIAAm

AAm was functionalized by DMMI (DMMIAAm) [153] according to [154]: one amine group of 2-diaminoethane was blocked with Boc (tert-Butyldicarbonat), the other one reacted with dimethylmaleic anhydride, and after removing the protecting group, the amine group reacted with acryloyl chloride. The reaction scheme and the detailed conditions are given in Figure 18.

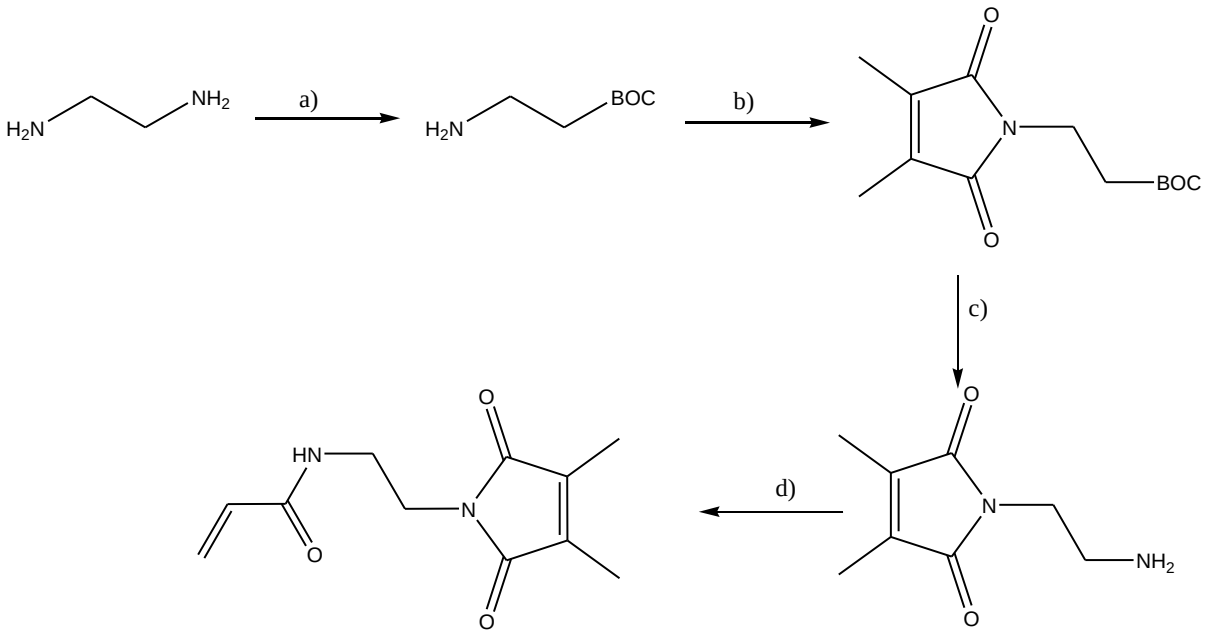

(a) $(Boc)_2O$/1,4-dioxane, 25 °C, 48 h

(b) Dimethylmaleic anhydride/toluene, 130 °C, 2.5 h

(c) CF_3COOH/CH_2Cl_2, RT, 1 h

(d) CH_2=CHCOCl, Na_2CO_3/CH_2Cl_2, 0-5 °C, 2 h

Figure 18 Synthesis of dimethylmaleimido acrylamide, DMMIAAm.

The following purification steps for the intermediate compounds and the final product were applied:

BocNH-$(CH_2)_2$-NH_2 was purified by vacuum distillation at 64 °C / 0.1 mbar, BocNH-$(CH_2)_2$-DMMI was re-crystallized from water/ethanol (1:1), H_2N-$(CH_2)_2$-DMMI was intensively washed with methylene chloride, and DMMIAAm was purified by re-crystallization from hexane/ethyl acetate (1:1).

4.1.2.2 Copolymerization of NIPA with DMMIAAm

Two copolymers of poly(NIPA-co-DMMIAAm), abbreviated here as PNIPA-DMMI, with different molecular weights and with 1 mol-% DMMI were prepared by free radical cross-linking copolymerization as shown in Figure 17 in the following manner adopted from SEIFFERT [97].

A total of 0.26 mol·L^{-1} of the monomers NIPA and DMMIAAm (herein after called "DMMI") as well as different amounts of sodium formate as chain transfer agent [97,155,156] were dissolved in an aqueous solution. After dissolving all the monomers, the solution was flushed with nitrogen for 15 min at room temperature. The polymerization was initiated by addition of 0.2 mol-% of APS and 0.5 mol-% TEMED (relating to the total amount of monomers) in concentrated aqueous solution. Having started the reaction, aliquots were withdrawn from reacting solutions and mixed with similar amount of methanol in order to check the precipitation. This was done every two seconds in the beginning and at longer intervals later. When a perceptible precipitation was noticed, the reaction was interrupted by adding an amount of methanol which equals the total volume of the mixture. The crude product was isolated by filtration. Then, the polymer was re-dissolved in water, purified by a ten days dialysis against water, and isolated by freeze drying. Viscosimetry was used to find the molecular weight, M_w, and UV-VIS spectrometry was used to find the composition of copolymers obtained. NMR measurement was also done but it was difficult to see the small amount of DMMI moieties with this method. The amounts of NIPA, DMMI and sodium formate, used to obtain the two different molecular weight polymers are given in Table 1.

Table 1 Amounts of reaction compounds for the synthesis of the copolymer in 500 ml pure water and the molecular weights were determined by viscosimetry (chapter 4.3.2). P1120 denotes the PNIPA-DMMI with M_w = 1.120.000 g/mol and P420 denotes the PNIPA-DMMI with M_w = 420.000 g/mol

Denotation	$\mathbf{n_{NIPA}}$ **mM**	$\mathbf{n_{DMMI}}$ **mM**	$\mathbf{n_{DMMI}}$ **mM**	$\mathbf{n_{HCOONa}}$ **mM**	$\mathbf{M_W}$ **g/mol**
		theoretical	**effective**		
P1120	250	2,50	1,40	29,80	1.120.000
P420	250	2,50	1,30	92,40	420.000

4.1.2.3 Sodium thioxanthone-2,7-disulfonate (TXS)

TXS which was introduced by GUPTA et al. [157] was used as water-soluble triplet sensitizer. KRONFELD and TIMPE [124] whose approach for synthesis and characterization was followed here, have studied the properties of TXS. The product was obtained as a mixture with Na_2SO_4 containing about 4 wt-% TXS (sodium salt).

4.2 Preparation of Hydrogels

4.2.1 Free Radical Cross-linking Copolymerization

Two series of PNIPA hydrogels were prepared. In the first series, the initial NIPA concentration C_0 was kept constant at 704.2 mmol·L^{-1} (80 g·L^{-1}) while the cross-linker concentration was varied between 2.81 mmol·L^{-1} (0.4 mol-% of monomer) and 10.0 mmol·L^{-1} (~1.5 mol-% of monomer). A corresponding solution of the linear polymer was prepared under identical conditions without addition of MBA. Redox initiation system consisting of 3.5 mmol·L^{-1} APS and 16.7 mmol·L^{-1} TEMED were used. Gels were prepared at T_{prep} = 10, 15, 20, and 25 °C. This thesis will focus on the gels made at 25 °C unless otherwise stated. The results obtained for gels made at the other preparation temperatures show essentially similar behavior.

Another series consisting of just four gels was prepared to allow for direct comparison with the photo cross-linked gels. It was intended to make gels by different synthetic route that were identical with regard to polymer concentration as well as to their macroscopic properties; i.e. same elastic modulus. In order to obtain the same elastic modulus, free radically cross-linked samples were prepared from solutions of NIPA and MBA (NIPA concentrations were 5 and 6.5 wt-% while MBA concentrations changed from 350 mmol·L^{-1} to 574 mmol·L^{-1}; ratios of NIPA and MBA as detailed in the Table 2) by adding 3.5 mmol·L^{-1} APS and 16.7 mmol·L^{-1} TEMED and polymerizing overnight at 25 °C.

Table 2 Concentrations of the monomers c_{NIPA} and c_{MBA} used in the second series of the FRC. FRC-5 and FRC-6.5 are the abbreviations of the free radical hydrogels which have 5 wt-% and 6.5 wt-% NIPA, respectively.

NIPA Concentration	**441 mM - (5 wt-%) (FRC-5)**	**574 mM - (6.5 wt-%) (FRC-6.5)**
C_{MBA} / mM	4.41 (1 mol-%)	3.50 (1.64 mol-%)
C_{MBA} / mM	5.74 (1 mol-%)	4.60 (1.25 mol-%)

NIPA, MBA and TEMED were dissolved in distilled water and then the solution was purged with nitrogen gas for 10 min. After addition of the required amount of an APS solution, one

part of the mixture was transferred between the plates of the rheometer maintained at the desired preparation temperature, T_{prep}, (10, 15, 20, or 25°C ± 0.2 °C), and the remaining part was filtered through Teflon membrane filters (pore size: 0.45 mm) directly into NMR tubes serving as light scattering vials. Polymerization took place in these tubes being submerged in a water bath kept at the particular T_{prep}. NMR tubes were chosen because of their small wall thickness of 0.6 mm, thus ensuring good heat transfer preventing a temperature rise due to the large negative enthalpy of polymerization.

The LCST was checked by visual inspection and UV-VIS spectrometry of several samples while slowly increasing their temperature in a water bath. The polymer solution became turbid at 33 °C with a sharp transition, while for the gels more gradual transitions were observed with the onset of barely visible turbidity at 29-30 °C followed by a noticeable increase of turbidity at 33.5 -34.5 °C.

In supplemental experiments**,** in the first part of this study weighed FRC gel samples were immersed in a large excess of water for 3 weeks to extract any soluble species. The water was replaced every second day. Eventually, the gels were dried in an oven at 55 °C and weighed again. The gel fraction was determined as final weight of the dry sample divided by the mass of monomer plus cross-linker in the initial gel sample. The gel fractions were found to be 90 ± 1 %.

4.2.2 Photo Cross-linking Polymerization

The two PNIPA-DMMI samples P1120 and P420 were cross-linked by UV irradiation. The concentrations of PNIPA-DMMI copolymers were 5 and 6.5 wt-% (441 mmol·L^{-1} and 574 mmol·L^{-1}) for each series of photo gels. PNIPA-DMMI was dissolved in water containing 10 μmol L^{-1} TXS (to ensure transmittance > 90 % at 380 nm) and stirred for 2 days until a clear solution was formed in the dark. One part of the reaction mixture was transferred between the plates of the rheometer maintained at the desired preparation temperature, around T_{prep}, 25 °C, and the remaining part was filtered through Teflon membrane filters (pore size: 0.45 mm) directly into NMR tubes serving as light scattering vials. To cross-link the precursor chains in the photo-gelling systems, all tubes containing the semi-dilute precursor solutions were exposed to UV light providing spatially homogeneous irradiation with a relatively broad spectrum in the range of 380 nm at around T_{prep} 25 °C. The copolymers that were employed in photo cross-linking systems are denoted as P1120-5, P1120-6.5, P420-5, P420-6.5.

Table 3 Photo gels and free radical gels, which have the same elastic modulus, are compared with each other. In the table the compared pairs are given.

Hydrogels made by	
Photo cross-linking	**Free radical cross-linking**
P1120-5	FRC-5_4.41mM
P1120-6.5	FRC-6.5_3.50mM
P420-5	FRC-5_5.74mM
P420-6.5	FRC-6.5_4.60mM

4.3 Characterization

4.3.1 UV-VIS Measurements

The UV-VIS measurements were performed on a Jasco V-550 spectrometer. The measurements were carried out to determine the light absorption of the reactants and conversion of DMMI moieties during the photo cross-linking polymerization. The progress of the cross-linking was observed from a semi-dilute solution of the sample PNIPA-DMMI (c = 20 g·L^{-1}) containing 10 μmol·L^{-1} TXS. Figure 19 shows the UV-VIS spectra recorded after several periods of irradiation. Pure PNIPA polymer solution that had the same polymer concentration as the PNIPA-DMMI solution was used as reference. In the spectra the consumption process of DMMI moieties is indicated during the cross-linking reaction. It is seen that the absorption peaks of DMMI moieties decrease with irradiation time at around 240 nm. The conversion $y(t)$ of the reaction can be obtained by

$$y(t) = \frac{A(t) - A(0)}{A(\infty) - A(0)} \tag{49}$$

Where $A(t)$ denotes the absorbance at time t, with $A(0)$ and $A(\infty)$ being the initial and final values. λ = 240 nm is used because the absorbance change is strongest at this wavelength.

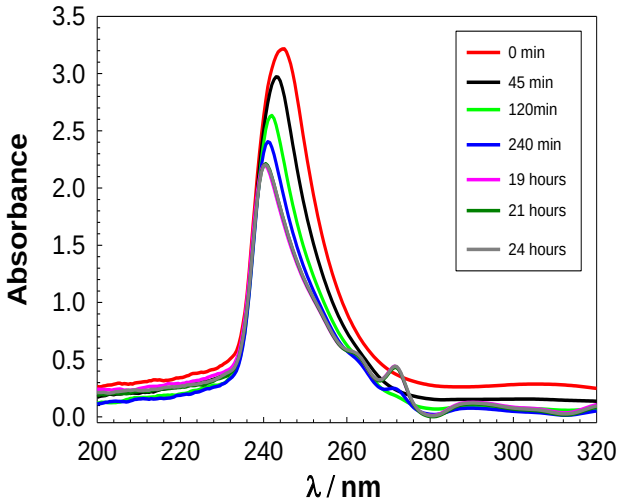

Figure 19 UV-VIS spectra recorded during cross-linking of a system of 20 g·L^{-1} PNIPA-DMMI in aqueous solution containing 10 μmol·L^{-1} TXS. PNIPA solution that has the same concentration as the PNIPA-DMMI solution is used as reference.

4.3.2 Viscosimetry Measurements

The viscosimetry method was used to find out the molecular weight of the synthesized polymers. Measurements of solution-viscosity were made on polymer solutions with concentrations of 0.5, 0.75, 1, 1.5 $g \cdot L^{-1}$ at 25 °C using an Ubbelohde-viscometer with a capillary diameter of 0.36 mm. Intrinsic viscosities were obtained with the help of HUGGINS plots. For calculation of the viscosity average molecular weight, MARK–HOUWINK–SAKURADA [158] parameters were used.

4.3.3 NMR Measurements

High-resolution ^1H spectra were recorded on a Bruker Avance 600 digital FT spectrometer at 400 MHz. After the DMMIAAm synthesis NMR spectrometry was used to characterize the polymer. NMR results agreed with data from the literature perfectly [159]. PNIPA-DMMI was also measured in NMR but it was hard to see the DMMI moieties since the concentration of DMMI was very low in PNIPA-DMMI.

NMR results:

^1H NMR (400 MHz, $CDCI_3$): δ (ppm) 1.92 (6H, $2CH_3$), 3.4 (2H, CH_2NH), 3.6 (2H, CH_2N), 5.52 (1H, CH_2=), 6.0 (1H, CH=), 6.15 (1H, CH_2=), 6.3 (1H, NH).

4.4 Light Scattering Measurements

SLS and DLS measurements were carried out for two types of gels (FRC and PC gels) at observation temperatures, $T_{obs.}$, between 10 °C and 30 °C. Specifically, in the first part of this study, the FRC gels were synthesized at T_{prep} = 25 °C, light scattering measurements were performed at 25, 20, 15, 10, 12.5, 17.5, 27.5, 30 °C (in that sequence). Similar experiments were performed on FRC gels synthesized at T_{prep} = 20 °C and 15 °C for. In the second part of the study PC gels and FRC gels were only synthesized at T_{prep} = 25 °C and measured at 25, 20, 15, 10 and 30 °C. Both light scattering apparatuses were equipped with a He-Ne laser operating at λ_0 = 633 nm and were calibrated against a toluene standard for absolute intensity. SLS was performed on a goniometer SLS-2 (Fica). For DLS, an ALV/CGS-3 compact goniometer (ALV, Langen, Germany) was used equipped with a cuvette rotation/translation unit (CRTU). A fiber optical detection unit based on three-mode detection was used, which includes an appropriate collimator/GRIN-lens fiber and the ALV/STATIC and DYNAMIC enhancer. Ideally, the three-mode detection unit gives an intercept in the time-averaged intensity autocorrelation function (ICF) $g_T^{(2)}(q,0) - 1$ of 0.33; i.e. β should be 0.33. An experimental check with a polystyrene latex suspension gave a coherence factor β of 0.36 ± 0.01, and this value was used for the evaluation of the DLS measurements. To protect the detector, the intensity of the incident light is automatically attenuated at each measurement by an eight-step automatic software-controlled attenuator and measured with a monitor diode. Thus, the intensity of incident light can be different within a series of measurements. When discussing scattering intensities, therefore the data that is used was rescaled to a preset value of the monitor diode assuming linear count rate dependence. Toluene was used as the index matching liquid. The temperature was controlled with an external thermostat. The time-averaged ICFs were acquired at 100 different sample positions selected by randomly moving the CRTU before each run. The acquisition time for each run was 30s. The ensemble-averaged scattering intensity, $\langle I(q)\rangle_E$, was determined by continuously moving the sample vial with the CRTU, and the acquisition time for $\langle I(q)\rangle_E$ was 2 min.

4.5 Rheological Measurements

In the first part of the study the shear modulus of the FRC gels were measured with a parallel-plate rheometer (CVO Rheometer, Bohlin Instruments) equipped with a Peltier device for temperature control. In the second part the shear modulus of the FRC and PC gels were measured again with plate-plate rheometer and a modified quartz glass bottom plate with a violet LED-lamp below it exhibiting a wavelength of ≅ 380 nm (Figure 20). Note that the UV-lamp was just switched on for PC gels. The plates (diameter 40 mm) were set to a distance of 500 μm before the onset of the reactions. During all rheological measurements, a solvent trap was used to minimize solvent evaporation. A frequency of 1 Hz and a deformation amplitude of $\gamma_0 = 0.01$ were selected to ensure that the oscillatory deformation was within the linear regime. The polymerization process was monitored in situ by measuring the storage modulus G' and loss modulus G'' as a function of time with the temperature being maintained at the desired T_{prep}. While both moduli for all FRC gels reached final constant values after a few hours, this time extended to 18 hours for PC gels indicating completion of the polymerization. In the first part of the study, the measurement temperature was changed during the rheology measurements of free radical samples in steps of 5 °C and the modulus was determined at temperatures different from T_{prep} to obtain data at 15, 20, and 25 °C.

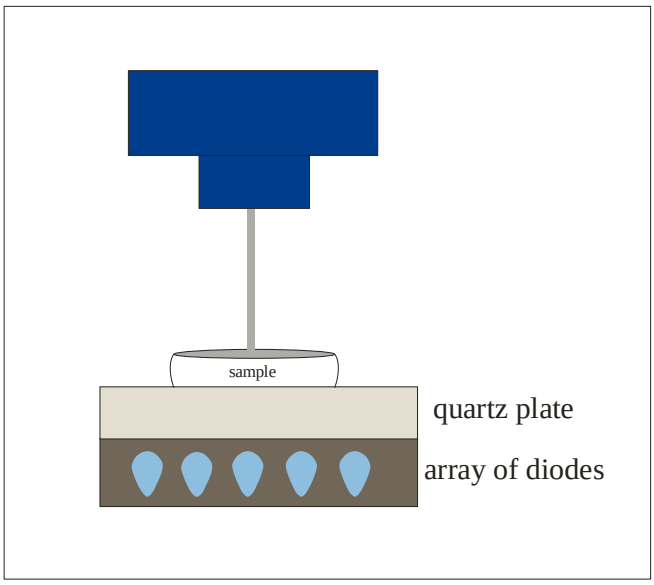

Figure 20 Schematic illustration of the rheometer with plate-plate geometry and irradiation apparatus for photo chemical cross-linking of the sample during the measurement.

5 Results and Discussion

In the first part of this study, the aim is to characterize the microstructure of gels i.e. inhomogeneity, synthesized by free radical cross-linking copolymerization of *N*-isopropylacrylamide (NIPA) by means of static and dynamic light scattering methods as well as macro-characterization by rheometry. Scattering behavior of FRC gels by changing observation temperature as well as preparation temperature below LCST were studied.

In the second part, the effect of the cross-linking method on the microstructure of the hydrogels has been investigated. For this purpose linear PNIPA-DMMI was synthesized in different M_w and cross-linked via a photo cross-linking reaction. The inhomogeneities of the resultant gels were compared to the analogous FRC gels that were synthesized by conventional free radical copolymerization of NIPA monomer with MBA as cross-linker.

5.1 Free Radical Cross-linking Hydrogels

5.1.1 Mechanical Properties

In order to have a general overview on the microstructure of the hydrogels some mechanical measurements have been performed to estimate the effective cross-link density and average chain length between the cross-link points. The hydrogels considered in the first part were synthesized via free radical copolymerization of NIPA and MBA in an aqueous solution. The initial NIPA concentration C_0 was kept constant at 704.2 mmol·L^{-1} (80 g·L^{-1}) while the cross-linker concentration was varied between 2.81 mmol·L^{-1} (0.4 mol-% of monomer) and 10.0 mmol·L^{-1} (~1.5 mol-% of monomer). Gels were prepared at T_{prep} = 10, 15, 20, and 25 °C. In the subsequent discussion, the gels made at 25 °C will be focused on unless otherwise stated. The results obtained for gels synthesized at the other preparation temperatures show essentially similar behavior.

The shear modulus was measured and evaluated according to rubber elasticity theory yielding an estimate of the effective network density, ν_{eff}, according to equation 49 [40,160]. For the case of thermo-responsive PNIPA gels, the elastic modulus is calculated by using a modified form of equation 20.

$$G' = \nu_{\text{eff}} \left(1 - \frac{2}{f}\right) RT \frac{< r^2 >}{< r^2 >_0} \qquad (50)$$

Here f is the functionality of the cross-links, hence for tetra-functional cross-links $1-2/f = 0.5$; R is the gas constant, and T the absolute temperature. $<r^2>$ is the mean-square end-to-end distance of network chains and $<r^2>_0$ the corresponding quantity for free chains. The calculation according to eq. 50 assumes that G', which is measured at 1 Hz, is identical to the equilibrium modulus within experimental error. This fact was substantiated by the finding that $G'' / G' \leq 0.01$ in each case. However, G' showed an unusually strong temperature dependence, decreasing about 12% when the measurement temperature was lowered from 25 °C to 15 °C. Similar dependencies were found for gels obtained at 15 and 20 °C. The change with temperature was fully reversible. Possibly, this is due to a decrease of $<r^2>_0$ when the temperature approaches the LCST from below. Formation of associations represents another possibility that cannot be excluded. (G' raises even stronger above the LCST.) To estimate ν_{eff}, G' measured at 25 °C is used and the ratio of $<r^2>$ / $<r^2>_0$ is assumed 1 at preparation conditions.

Table 4 contains a listing of the shear moduli of the gels prepared with different cross-linker concentrations and the quantities derived thereof. In addition to the effective network density, ν_{eff}, the average molar mass of the network chains, M_C, has been calculated according to $M_C = \rho/\nu_{\text{eff}}$, where ρ is the mass concentration. The large values obtained for M_C indicate that an effective network chain is likely to consist of branched and cycled structures.

It is useful to compare the effective network density, ν_{eff}, with the hypothetical network density, ν_{th}, of a network where all cross-links are perfectly interconnected by elastically effective network chains. This latter quantity was calculated from the molar concentration of the cross-linker in the system, C_{MBA}, by assuming that all cross-linker molecules have completely reacted as tetra-functional junction points: $\nu_{\text{th}} = 2C_{\text{MBA}}$. In fact, the cross-linkers may not have completely reacted and the real network may contain a variety of defects, a wide distribution of chain lengths between junction points, and inhomogeneities of cross-link density and connectivity. The ratio $\nu_{\text{eff}} / \nu_{\text{th}}$ (cross-linking efficiency) can serve as a measure for the extent of perfection. It is included in Table 4 as well. The values obtained are almost independent of cross-linker concentration. They are considerably smaller than 1 indicating a preponderance of network imperfections.

Table 4 Rheological data obtained on gels synthesized with different cross-linker concentrations. Monomer concentration C_{NIPA} = 704.2 mM corresponding to 7.15 vol-%.

C_{MBA} (mmol/L)	G'(25°C) (kPa)	ν_{eff} (mol/m^3)	M_C (g/mol)	ν_{eff}/ν_{th} (%)
2.81	0.93	0.75	100,000	13.2
4.69	1.80	1.44	55,000	15.4
7.04	2.37	1.91	42,000	13.5
8.80	2.94	2.36	34,000	13.4
10.0	3.25	2.60	31,000	13.1

5.1.2 Microstructure

An aqueous system containing linear PNIPA has a lower critical solution temperature (LCST) around 33 °C. Below the LCST, it forms a homogeneous solution. However, concentration fluctuations increase when the temperature gets closer to the miscibility gap. Stated otherwise, water is a good solvent for PNIPA at low temperature, but the solvent quality drops significantly with increasing temperature. This thermodynamic behavior gives rise to an increase of scattering intensities when the temperature approaches the LCST from below. The refractive index increment, dn / dc, measured for dilute PNIPA solutions, does not change perceptibly with temperature; it was found to be 0.181 mL·g^{-1} at 15 °C and 0.182 mL·g^{-1} at 25 °C. So the intensities are a good measure for concentration fluctuations. When PNIPA is cross-linked to form a gel, the determined LCST rises slightly and does not appear as sharp as in solution (cf. experimental section). In PNIPA gels, the thermodynamic fluctuations are superimposed by static concentration fluctuations that are independent of time, but depend on location. The influence of temperature on these static fluctuations is of particular interest in this first part of the study. Therefore the information obtained by light scattering on the microstructure of the hydrogels and the influence of temperature thereon will be discussed.

The length scale probed by light scattering is of the order of 1/q (cf. eq. 22), corresponding to 40-90 nm when the scattering angle is in the range 50°-140° at 630 nm. This length scale should be compared with the mean distance between cross-links, which is around 5-10 nm based on C_{MBA}. Hence structural characteristics appreciably larger than the mesh size of the network were investigated.

5.1.2.1 Static Light Scattering

As mentioned further above, SLS measurements, by the design of measurements, report the scattering intensity as an ensemble average over a large scattering volume, being close to a macroscopic ensemble. This was verified by repetition of the measurements after turning or shifting the sample and checking for reproducibility. Usually an average over five different positions was taken.

To investigate the influence of observation temperature on the microstructure of PNIPA hydrogels, static light scattering experiments were carried out in the range $10\ °C \leq T_{obs.} \leq 27.5\ °C$ on these gels as well as on the corresponding solution. The scattered light intensities, $R(q)$, were recorded at scattering angles from 50° to 140°, which corresponds to a scattering vector range of $q = 1.1 \cdot 10^5 - 2.5 \cdot 10^5\ cm^{-1}$.

Figure 21 shows the total scattering intensity $R(q) = R_C(q) + R_{SOL}(q)$ plotted against the square of the scattering vector, q^2, for the hydrogels prepared at 25 °C with various amounts of MBA at different observation temperatures. Increasing the MBA concentration and observation temperature increases the total scattering intensity, $R(q)$, of the hydrogels. The change with temperature is fully reversible. It should be mentioned that $R_{SOL}(q)$ raises from $1.02 \cdot 10^{-4}\ cm^{-1}$ at 15 °C to $1.82 \cdot 10^{-4} cm^{-1}$ at 25 °C. These results obviously show that the static portion of the scattered light from the PNIPA hydrogels is strongly temperature dependent. The angular dependence is too small to be exploited.

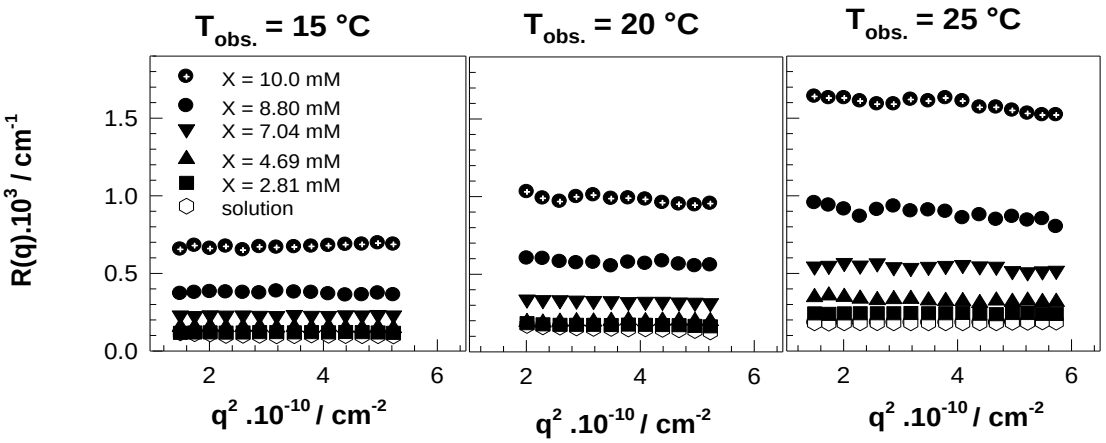

Figure 21 Total scattering intensity, $R(q)$, plotted versus the square of the scattering vector, q^2, for PNIPA hydrogels at different measurement temperatures, $T_{obs.}$, and MBA concentrations, X, as indicated. T_{prep} = 25 °C.

5.1.2.2 Dynamic Light Scattering

Figure 22 shows the results of DLS measurements made at $\theta = 90°$ on several gels having different cross-linker contents (b-d), and on a solution of the linear polymer (a). For each sample, 100 measurements were conducted at different sample positions. The observation temperature was 25 °C, identical to the preparation temperature. Fig. 23 clearly demonstrates that the gels exhibit the typical speckle pattern, becoming more pronounced when the cross-linker content was increased, while the scattering intensity observed on the solution is independent of position. This behavior is well known and has been reported repeatedly. Note that q is not given since the scattering angle that is used in measurements is 90°.

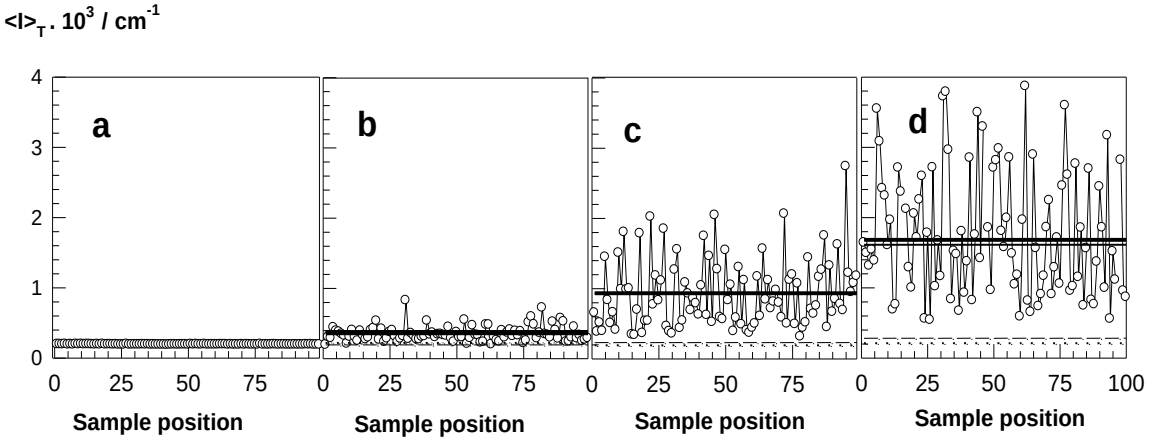

Figure 22.Variation of time-averaged scattering intensity, $\langle I \rangle_T$, with sample position for PNIPA hydrogels with (a) 0, (b) 4.69, (c) 8.80, and (d) 10.0 mM MBA concentration. The solid lines represent the ensemble-averaged scattered intensity, $\langle I \rangle_E$. The fluctuating components of the scattering intensity, $\langle I_F \rangle_T$, are represented by the dashed and dotted lines. $T_{obs.} = T_{prep} = 25$ °C; $\theta = 90°$

The solid horizontal lines represent the ensemble-average of scattered intensity, $\langle I \rangle_E$, obtained, on the one hand, by calculating the mean value of the data obtained at 100 positions (thin line), and, on the other hand, the value measured while the cuvette was steadily rotated (thick line). There is a slight difference between the two values reflecting experimental uncertainty. The dashed line indicates the fluctuating component of the scattered intensity, $\langle I_F \rangle_T$, estimated by the partial heterodyne method (based on 100 positions, eq. 37), while the dotted line gives the result for $\langle I_F \rangle_T$ when the non-ergodic method was applied on just 15 positions (eq. 32), with subsequent averaging. The essential features deduced from Fig. 23 are as follows: There is no appreciable discrepancy between the two methods of data evaluation (it will be elaborated on this point further below). While the ensemble-average scattered intensity, $\langle I \rangle_E$, increases significantly with rising cross-link density, the fluctuating component, $\langle I_F \rangle_T$, remains practically constant and is identical to the scattering intensity of a solution $1.8 \cdot 10^{-4}$ cm^{-1}.

To analyze the influence of observation temperature on the scattering behavior, the sample containing 8.8 $mmol \cdot L^{-1}$ MBA was focused on, shown in Fig. 22c. Fig. 23 shows the corresponding data measured at 10, 15, 20, and 25 °C at $\theta = 90°$. It is obvious that the spatial fluctuations of the time-average scattered intensity, $\langle I \rangle_T$, grow significantly with raising temperature, and so do the ensemble-averages, $\langle I \rangle_E$. The change with temperature is fully reversible.

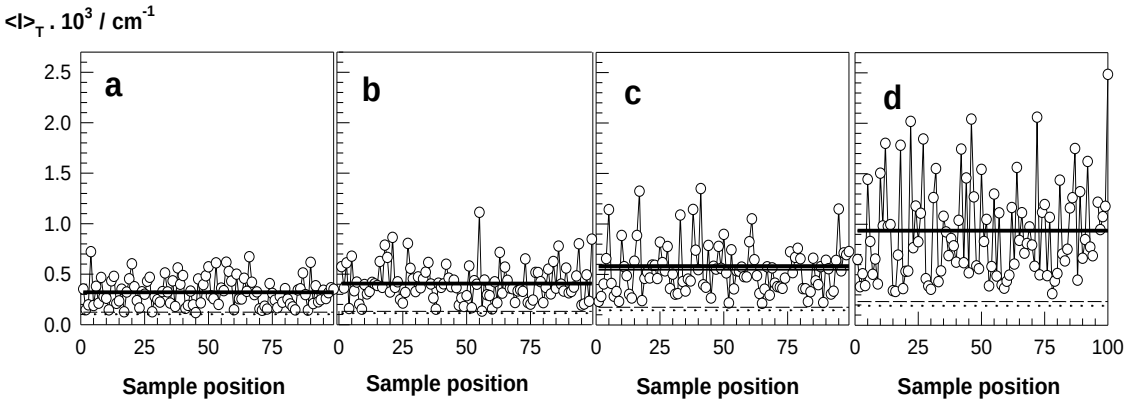

Figure 23 Variations of the time-averaged scattering intensity, $\langle I \rangle_T$, with sample position at 4 different observation temperatures, (a) 10, (b) 15, (c) 20, and (d) 25 °C, for a gel prepared at 25 °C with 8.8 mM MBA. The solid lines represent the ensemble-averaged scattered intensity, $\langle I \rangle_E$. The fluctuating components of the scattering intensity, $\langle I_F \rangle_T$, are represented by the dashed and dotted lines. $\theta = 90°$

Closer inspection shows that the fluctuating component, $\langle I_F \rangle_T$, also slightly raises with temperature. This is easier seen in a compilation of the data given in Table 5. Equation 50 is applied in order to convert the values obtained by DLS into the same order of SLS values. By this way, the ensemble average scattered light intensity, $\langle I \rangle_E$, was obtained as a Rayleigh ratio, $R(q)$, to compare them in the same scale.

$$R_{\text{sample}} = R_{\text{Tol}} \times \frac{I_E}{I_{\text{Tol}}} \tag{51}$$

R_{Tol} and I_{Tol} are the intensities of toluene from SLS and DLS, respectively.

Columns 2 and 3 represent the fluctuating part, $\langle I_F \rangle_T$, determined by the partial heterodyne method and the non-ergodic method, respectively. Columns 4 and 5 show, for comparison, the scattering intensity, of a PNIPA solution measured in the two apparatuses. All 4 values agree to within ± 20% at each temperature, while there is a distinct increase with raising temperature. This increase is expected, of course, because the thermal fluctuations become stronger when the LCST is approached.

The last three columns in Table 5 show the constant component of the static scattering intensity, I_C, obtained via the partial heterodyne method and the non-ergodic method, respectively, as well as R_C, obtained by SLS (eq. 23). Again, the data agree satisfactorily at each temperature. However, there is a marked increase with increasing temperature,

seemingly even stronger than that of the fluctuating component of the scattering intensity, $\langle I_F \rangle_T$. This observation requires further discussion.

Table 5 Intensity values (in 10^{-4} cm^{-1}) of the fluctuating (I_F) and frozen (I_C) part in dynamic and static light scattering at different observation temperatures. $\theta = 90°$, C_{MBA} = 8.80 mM, T_{prep} = 25 °C. PH: partial heterodyne method, NE: non-ergodic method.

$T_{obs.}$	I_F (PH)	I_F (NE)	$I_{F,SOL}$ (DLS)	$R_{F,SOL}$ (SLS)	I_C (PH)	I_C (NE)	R_C (SLS)
10 °C	1.23	1.03	1.04	0.76	1.95	2.17	1.92
15 °C	1.31	1.14	1.27	1.02	2.82	2.93	2.70
20 °C	1.74	1.46	1.71	1.50	3.73	4.36	4.24
25 °C	2.37	1.92	1.87	1.82	6.99	8.65	7.17

If one erroneously assumed that the static scattering was due to some permanently fixed, solid-like heterogeneity, there would be no influence of temperature on I_C. Obviously, this is not correct. In fact, the increase of the static scattering intensity, I_C, with increasing temperature for PNIPA gels below the LCST was already reported by Tanaka et al. [13] and SHIBAYAMA et al. [14,35] but without giving an in-depth explanation. They showed that above the LCST (36-50 °C) for weakly charged PNIPA gels, the static scattering intensity, I_C, raises markedly with increasing observation temperature due to the progressive formation of a two-phase structure, while the intensity of fluctuating part, $\langle I_F \rangle_T$, remains essentially constant [29].

Considering the scattering behavior in the homogeneous region below the LCST, it is proceeded from the notion that a given polymer network generally has an inhomogeneous distribution of cross-links. Hence, the local cross-link density (in an area defined by the static correlation length) is fixed through synthesis. This local cross-link density is controlling the local polymer concentration depending on thermodynamic conditions. It is predominantly the

polymer density correlation function that determines the scattering properties of the gel, not the (fixed!) cross-link density correlation function (unless the refractive index increment of the cross-linking moieties is by far greater than that of the polymer). The temperature dependence of the static scattering intensity, $I_C(q)$, therefore arises from the thermodynamics of variable local swelling.

The swelling pressure of a gel is given by the osmotic pressure of a semi-dilute solution of the uncross-linked polymer plus the negative pressure due to chain elasticity [47]. The osmotic pressure, as a crude approximation, changes in proportion with excluded volume, or $(1\text{-}2\chi)$, where χ is the Flory interaction parameter. For PNIPA, χ varies strongly with temperature and approaches 0.5 near the LCST. On the other hand, the pressure due to chain elasticity is nearly independent of solvent quality, but proportional to cross-link density. Now consider regions of high cross-link density in equilibrium with regions of lower cross-link density. At a given temperature, say 20 °C, this equilibrium results in distinct variations of local polymer concentration. As the temperature is increased, the osmotic part of the swelling pressure gets smaller while the elastic part becomes more dominant. This means that the more densely cross-linked regions deswell at the expense of the less densely cross-linked ones. The overall volume is kept constant, of course; the gel is not in macroscopic equilibrium with pure solvent. As a result, the characteristic length scales of the structure do not change, but the scattering contrast is enhanced, resulting in larger static scattering intensity.

By this argument, the temperature dependence of the static scattering intensity, $I_C(q)$, is traced back to the same origin as that of the fluctuating component of the scattering intensity, $\langle I_F(q)\rangle_T$, namely solvent quality. This does not necessarily mean, however, that the form of the dependence is similar. Thermal fluctuations, giving raise to $\langle I_F(q)\rangle_T$, are governed by the course of the spinodal, while the static concentration contrast, giving raise to $I_C(q)$, results from local swelling equilibrium.

In order to compare the temperature dependencies of the two components, it is worthwhile to look at the normalized intermediate scattering functions calculated from the measured $g_T^{(2)}(q,\tau)$ by eq. 34. Figure 24 shows the averaged $f(q,t)$-functions for $q = 1.9\cdot10^5$ cm^{-1} corresponding to a scattering angle of 90°. At long times they reach asymptotic plateau values that increase slightly with rising measuring temperature and are indicative of the frozen-in (static) inhomogeneity. According to the theory derived by PUSEY and VAN MEGEN, the $f(q, t)$-curves measured at one temperature on a given gel should be identical irrespective of sample position. Actually, there is quite some scatter in these plateau values. Table 6 therefore

shows a listing of the average values together with their standard deviations derived from measurements at 15 positions. They were obtained by fitting of the data to the expression

$$f(q,t) = f(q,\infty) + A\exp(-\frac{t}{\tau}) \tag{35}$$

using a nonlinear least-squares fitting procedure.

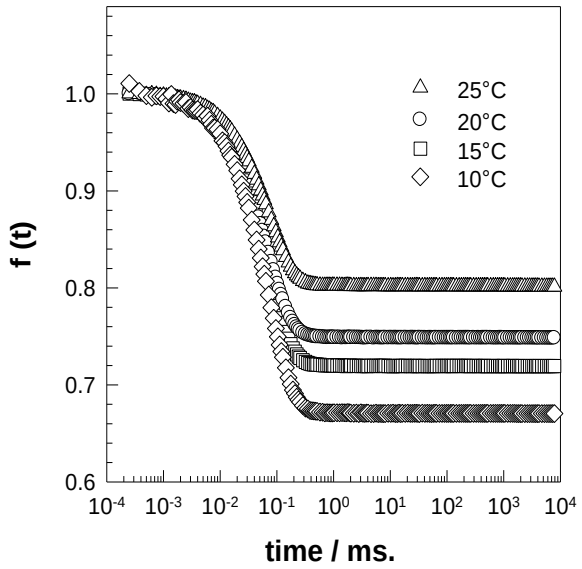

Figure 24 Normalized intermediate ensemble-averaged scattering functions, *f*(*t*), calculated from $g_T^2(\tau)$ values according the eq. 33 for different observation temperatures, T_{prep} = 25 °C.

f(*q*,∞), i.e. the (ensemble-averaged) fraction of scattered light which is due to static inhomogeneities, increases moderately from around 70% to around 80% when the measuring temperature is raised from 10 °C to 25 °C. This raise is clearly beyond experimental uncertainty and proves that the static scattering component is affected by temperature to a greater extent than the fluctuating component

Table 6 Listing of the average values of the ensemble-average fraction of the scattering intensity, $f(q,\infty)$, together with their standard deviations derived from measurements at 15 positions.

$T_{obs.}$	$f(q,\infty)$
10 °C	0.68 ± 0.057
15 °C	0.71 ± 0.047
20 °C	0.74 ± 0.035
25 °C	0.80 ± 0.036

The correlation time, τ, is around 70 µs corresponding to cooperative diffusion coefficients, D, between 35 and 43 $\mu m^2/s$. D raises moderately with increasing cross-link density, while the influence of temperature is amazingly small (less than 5% change when the observation temperature was increased from 10 to 25 °C, i.e. within experimental error). Since the viscosity of water and that of a PNIPA solution drops by 30% in that range, there is likely an opposing effect based on some structural rearrangement. The correlation lengths in the range 5-7 nm compare well with the mean distance between cross-links.

Figure 25 shows a side-by-side comparison of the temperature dependences of scattering intensity measured by SLS and DLS for a range of cross-link densities for gels prepared at 25, 20 and 15 °C. Note that $\langle I_F \rangle_T$ corresponds to R_F, and $\langle I \rangle_E$ corresponds to $R(q)$. The DLS and SLS graphs are closely identical for the all preparation temperatures. This is of course taken for granted as far as the ensemble-averaged total scattering intensities are concerned. In this case, the two methods just differ in the fact that the SLS apparatus yields the ensemble-average directly, while with the DLS apparatus, the averaging must be performed deliberately either by rotating the cuvette during the measurement or by taking the average over a sufficiently large number of measurements taken at different sample positions. The procedures applied to obtain the fluctuating components, however, are fundamentally different. In SLS, the polymerization was carried out without a cross-linker, and the scattering intensity of the resulting solution is *assumed* to represent the fluctuating component of

correspondingly synthesized gels. In DLS, the intensity correlation functions obtained on the gels were used to extract the fluctuating part. This could be done for each degree of cross-linking. Fig. 25 shows that the fluctuating component of the scattering intensity data, $\langle I_F \rangle_T$, of the studied gels coincide and form one single line (open symbols in Fig. 25a, 25c, 25e). These lines are pretty much the same as that of the solution (open symbols in Fig. 25b, 25d, 25f). These observations strongly support the notion that the two experimental approaches are equivalent. Fig. 25 further demonstrates that the discussion about the slightly different temperature dependences of $\langle I_F \rangle_T$ and I_C (or R_F and R_C) is a general phenomenon with PNIPA networks, irrespective of the degree of cross-linking.

It would be interesting to exploit the *q*-dependence of the static scattering component in order to obtain some information on the length scale of static inhomogeneities. As recognized from Fig. 21, the variation of scattering intensities in the experimentally accessible *q*-range is too small to be quantified with some confidence. The slope of the intensity vs. q^2-plot seems negative (as expected) in some instances, but positive slopes and slopes close to zero are also found. Similar behavior was found by DLS measurements (not shown). This means that the static correlation length does not exceed 10-15 nm, and light scattering experiments are not suited to obtain information at smaller scale.

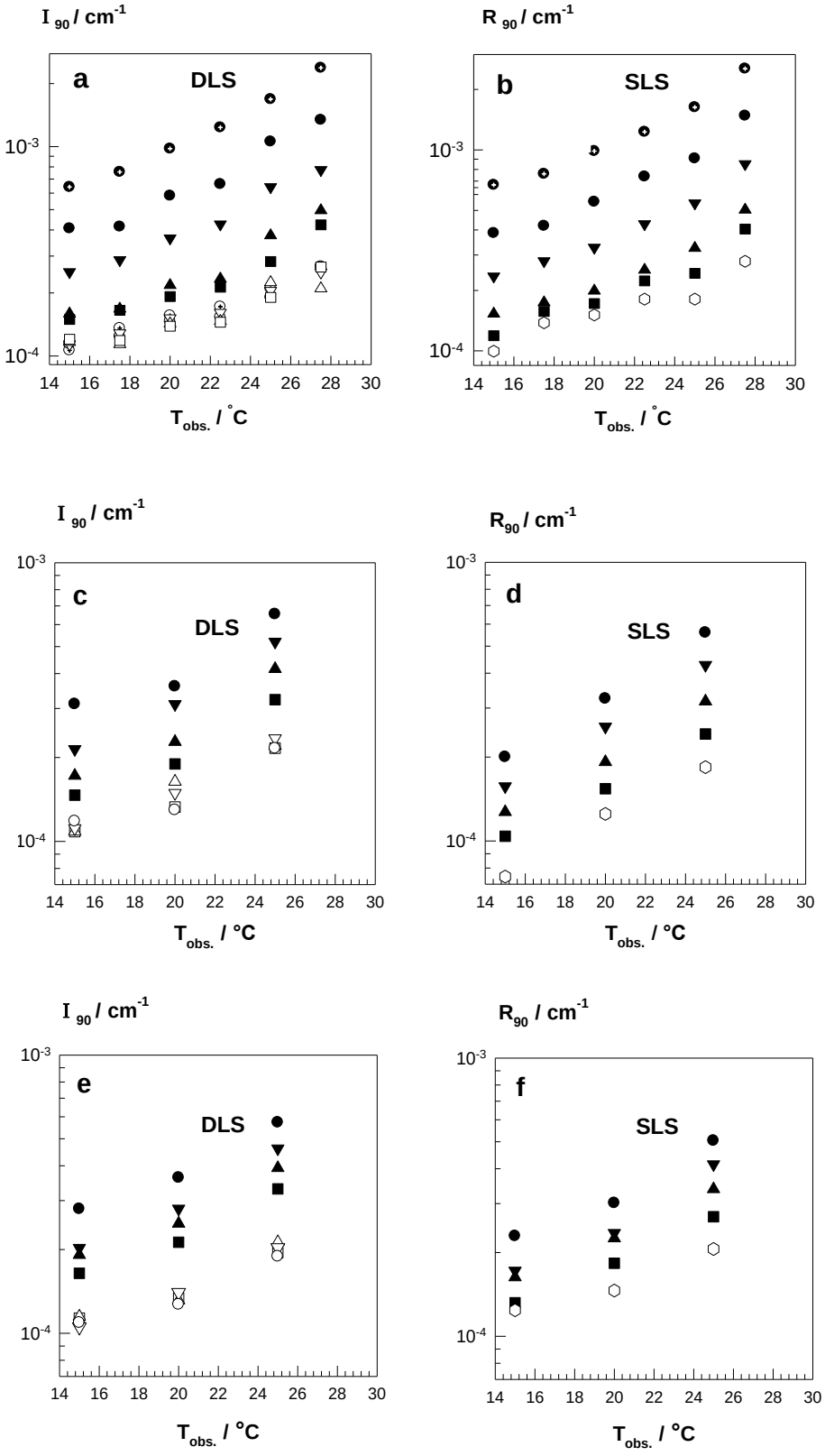

Figure 25 Comparison of the ensemble-average scattering intensities measured at 90° (a), (c), (e), by DLS (I_{90}) and (b), (d), (f) by SLS (R_{90}) as a function of observation temperature for gels prepared at 25; (a, b), 20; (c, d), 15; (e, f) °C. Cross-linker concentrations are: (❍) 10.0, (●) 8.8, (▼) 7.04, (▲) 4.69, and (■) 2.81 mM. Open symbols represent the fluctuating components for DLS or the solution scattering for SLS.

5.1.3 Summary

In the first part of this thesis static and dynamic light scattering measurements were performed on free radically cross-linked PNIPA hydrogels in order to carefully compare different methods of dividing the total scattering intensity into two parts: thermal scattering due to Brownian motion of the network chains and static scattering due to topological or spatial inhomogeneity. The major emphasis of the first part was on a detailed inspection of the dependence mainly on the observation temperature and partially on the preparation temperature of the thermal and static scattering components of a given gel. Earlier publications [13, 14, 35] showed that both parts seem to increase when the temperature was raised, but this became evident only in a rather narrow temperature range, from 30-33 °C, close to the LCST. The results presented here clearly show that both components also increase perceptibly in the range 10 °C ≤ $T_{obs.}$ ≤ 25 °C, much further away from the LCST of PNIPA in water. Comparison of dynamic and static light scattering methods was also done and consistent results were obtained.

5.2 Comparison of FRC Gels with PC Gels by Scattering Methods

In the second part of the study the network structure of hydrogels which are synthesized by free radical cross-linking copolymerization, FRC, are compared to networks that are formed by photo chemical cross-linking reaction. Photo chemical cross-linking, PC, provides the opportunity of controlling the rate and extent of the reaction at will. Cross-links are supposed to be introduced randomly in space for PC gels, whereas the distribution of cross-linking points of FRC gels are more inhomogeneous due to differences in the reactivity ratios of monomers and cross-linkers [161,162]. Therefore it is supposed that PC gels are more homogeneous from the microscopic point of view than FRC gels starting from monomers and cross-linkers.

Two kinds of PNIPA-DMMI copolymers that have different molecular weights for the PC were synthesized. One of them has an average molecular mass of M_w =1.120.000 g/mol (P1120) and the other one has a M_w = 420.000 g/mol (P420), both determined by viscosimetry. The concentration of photo cross-linkable groups is set to 1 mol-% for both PC copolymers. This means for the copolymers with molar masses of 420.000 and 1.200.00 there are theoretically approximately 37 and 98 cross-linkable groups available at one chain, respectively. The effective number of cross-linkable groups, shown in Table 1, is the half of the theoretical values. Having this concentration of DMMI group highly cross-linkable gels are obtainable. Since the cross-linking process starts from linear polymers in the semi-dilute regime, it is expected to obtain highly homogeneous structures of these in photo gels. In dilute solutions, it is known that polymers with high molecular weights show higher scattering intensities compared to solutions of low molecular weight chains. Theoretically this behavior is not true for semi-dilute solutions because the intensity of scattering should not depend on the molecular weight in this regime. However it is possible that other factors depending on the molecular weight like the dissolution or the aggregation behavior can influence the scattering properties of the polymer solutions. These effects should also be considered when comparing two PC gels starting from M_w = 420.000 and M_w = 1.200.000 g/mol. Additionally copolymers having different chemical sites can also show higher scattering because of incompatibility effects.

5.2.1 LCST of PNIPA solutions and PNIPA gels

Before starting the fundamental experiments, the LCST of PC and FRC gels were determined. The LCST of the P420 solution at 5 wt-% polymer concentration and its gel (P420-5), the analogous FRC solution and its gel at the same polymer concentration (FRC-5) were checked by the transmittance measurements carried out in UV-VIS spectrometry at 500 nm while slowly raising the temperature from 25 °C until the transition is observed (Figure 26). The transmittance of the both P420 and FRC solutions showed an abrupt decrease, becoming turbid at 33 °C with a sharp transition, while for both P420 and FRC gels more gradual transition was observed with the onset of barely visible turbidity at 29-30 °C followed by a noticeable increase of turbidity and decrease of transmittance at 34-34.5 °C.

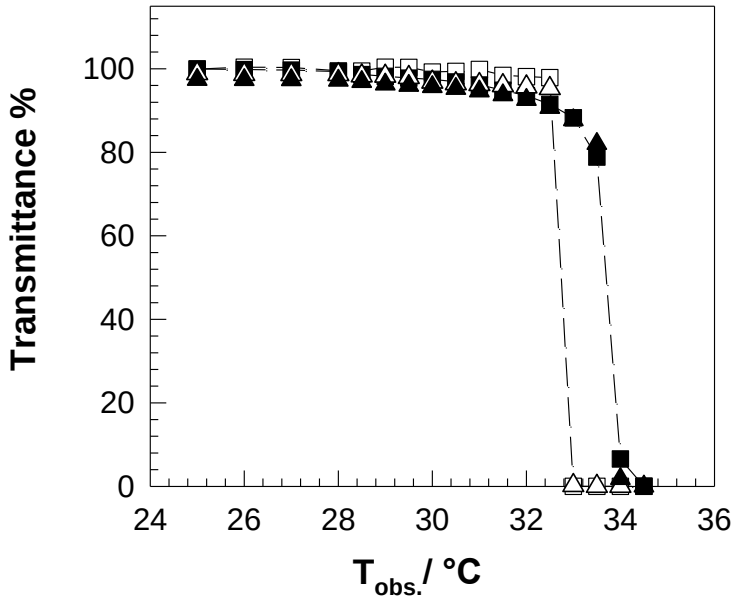

Figure 26 Transmittances of P420-5 sol and gel as well as analogous FRC-5 sol and gel are plotted against different observation temperatures, T_{obs}. (▲) P420-5 gel, (Δ) P420-5 sol, (■) FRC-5 gel, (□) FRC-5 sol.

It was shown that both types of gels and solutions have the same temperature dependent behavior showing similar LCST transitions. It can be concluded that the incorporation of DMMI-groups does not affect the typical thermo-responsive property of pure PNIPA.

5.2.2 Macroscopic Properties

In order to have a reliable comparison between the two network structures synthesized by two different methods, first it had to be ensured that both hydrogels have the same effective cross-link densities, i.e. the same elastic moduli. Gels that have the same elastic moduli show similar macroscopic behavior. As the elastic modulus originates from chemically effective network strands, the microstructures of the gels are responsible for the macroscopic properties. But different kinds of microstructure can lead to one and the same behavior as long as only the numbers of elastically active strands are the same. In this case that means a gel containing a high degree of inhomogeneity can show the same macroscopic behavior as a very homogenous gel, because the effective cross-link density is the same. In sum, adjusting elastic moduli to the same value is a reasonable starting point to compare the gels made by photo cross-linking and free radical cross-linking reactions. For this purpose, the elastic modulus of photo gel systems was investigated first and then the cross-linker (MBA) content of FRC gels was adjusted in the reaction mixture such to obtain the same elastic modulus as in the photo gel systems.

PNIPA hydrogels are obtained in an efficient and controlled manner by means of sensitized photo cross-linking of linear PNIPA chains which are functionalized with dimethylmaleimide (DMMI) groups. Concentration of PNIPA-DMMI polymers was 5 and 6.5 wt-% for both series of photo gels. The solutions prepared at concentrations higher than 6.5 wt -% were quiet viscous and filtration was quite difficult. Hence concentration of polymers was fixed at 5 and 6.5 wt-%. They were irradiated by a LED-lamp from below of the quartz glass bottom plate of rheometer at the room temperature around 25 °C. Thus the cross-linking process could proceed under rheological monitoring. The measurements lasted until the G' reached the plateau value.

The hydrogels made by free radical cross-linking were synthesized using initial NIPA concentrations of 5 and 6.5 wt-% while the cross-linker (MBA) content varied in order to obtain the same elastic modulus with the described photo gels above (Table 2). The reaction mixture was transferred between the plates of the rheometer maintained at the desired preparation temperature, T_{prep} = 25 °C ± 0.2 °C. Reaction proceeded without irradiation by the LED-lamp, accelerated by the redox initiation system.

Figure 27 shows the course of the elastic and viscous modulus during the reaction time of photo cross-linked systems with an initial molecular weight of 420.000 g/mol linear polymer

at the concentrations of 5 and 6.5 wt-% and of analogous free radical cross-linked systems with 5 and 6.5 wt-% as well, synthesized by different amounts of MBA. The differences between the progress of the elastic modulus of PC gels and analogous FRC gels are seen in the graphs. Note that the scale of the abscissa is different for both graphs.

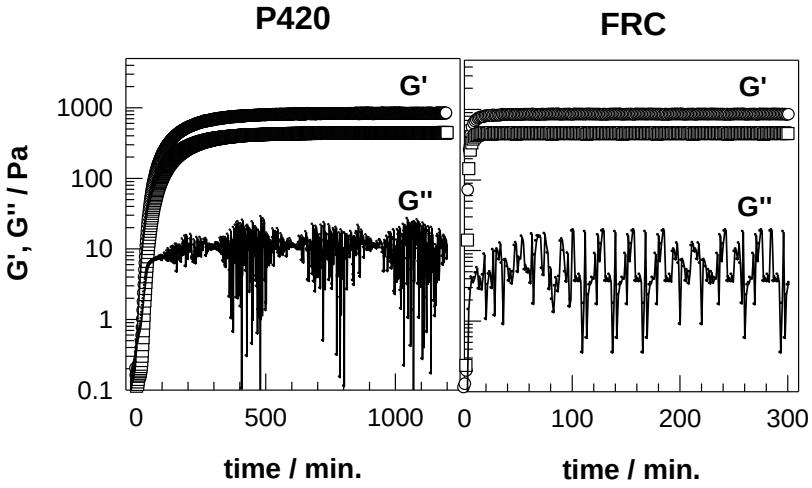

Figure 27 Elastic modulus, *G*', and viscous modulus, *G*'', are plotted versus time measured by rheometry. Left hand side: data for the photo cross-linking polymerization reaction; (□) P420-5, (○), (●) P420-6.5. Right hand side: data for to the free radical cross-linking copolymerization reaction; (□) FRC-5_4.41 mM MBA, (○), (●) FRC-6.5_3.5 mM MBA. $T_{obs.}$ = 25 °C, frequency: 1Hz.

It can be clearly seen that the elastic modulus increases while the reaction proceeds until a steady state value of *G*' is reached. This value corresponds to the elastic equilibrium modulus G_0' for $\omega \rightarrow 0$. In the case of free radical cross-linked hydrogels the steady state is already reached after 10 min whereas the elastic modulus of the photo cross-linked systems needs more than 9 hours to level off. FRC gels reach their final moduli significantly faster than PC gels. This is due to the different reaction mechanism of both types of gels and the intensity of the UV-lamp used during photo cross-linking reaction. The same behavior is obtained from P1120 gels and their analogous FRC gels. In the case of radically polymerized systems, cross-linking occurs fast and uncontrolled across the whole sample whereas polymers like the PNIPA-DMMI copolymer can only react if cross-linkable groups interact. So for the formation of hydrogels made by photo cross-linking the concentration of the preformed polymers has to exceed the overlap concentration which means that cross-linking through the whole sample just occurs in semi-dilute and concentrated regime. In dilute solutions only micro-gels can be formed. Hence the polymer concentration has also an influence on the cross-linking efficiency. In this case the overlap concentration, *c**, of the copolymer with

M_w = 420.000 g/mol is 0.016 g/ml which means the polymer concentration is more than 3 times higher than the critical value. This means, that in both cases the polymer coils overlap sufficiently and the polymer chains are sufficiently entangled to allow formation of macroscopic gels. The overlap concentration of the copolymer with M_w = 1.200.00 g/mol is c^*= 0.0065 g/ml so the polymer concentration is more than 7.5 times higher than the critical value which means excessive entanglements of the chains.

In Table 7 the elastic moduli of four different PC and FRC gel pairs are shown with their corresponding cross-linking efficiencies. Increasing the molecular weight and weight fraction of PNIPA-DMMI increases the elastic modulus and the cross-linking efficiency of the photo gels. Generally, the efficiency of cross-linking in the case of FRC gels is lower than that of PC gels. This is due to undesirable reactions during gelation of FRC gels such as formation of loops, dangling chains and living unreacted functional groups. On the other side, in the case of photo gelation, semi-dilute solutions of functionalized linear PNIPA molecules are cross-linked by selectively connecting the functional groups. It is the advantage of photo gelation that in this case cross-linking occurs in a random manner so cross-linking efficiency increases. Increasing the polymer concentration also leads to a higher cross-linking efficiency.

Table 7 Elastic modulus and cross-linking efficiency of photo cross-linking hydrogels and analogous free radical cross-linking hydrogels are given.

G' **(PC/FRC Pair) /Pa**	**PC gels and analogous FRC gels**	**Efficiency of cross-linking (v_{eff}/v_{th}) %**
400	P420 - 5	7.40
	FRC-5_4.41 mM MBA	3.70
800	P420 - 6.5	11.30
	FRC-6.5_3.5 mM MBA	9.20
600	P1120 - 5	11.0
	FRC-5_5.74 mM MBA	4.20
1100	P1120 - 6.5	15.60
	FRC-6.5_4.6 mM MBA	9.70

It was successful to find pairs of hydrogels synthesized by free radical cross-linking and photo cross-linking that show the same elastic modulus, meaning comparable macroscopic behavior. Now it is possible to analyze the hydrogels concerning their microstructure. In the following chapter the network inhomogeneities of these pairs of systems will be investigated.

5.2.3 Light Scattering Measurements

5.2.3.1 Dynamic Light Scattering

After obtaining the same macroscopic properties for both types of gels, their microstructure was analyzed. Dynamic light scattering is a suitable method to obtain information about homogeneity of gels. The non-ergodic method has been employed to analyze DLS data on 15 positions. From the measured intensity data, the time and ensemble-average scattering intensities are determined. The calculated autocorrelation function is then used to get information about the microstructure by applying suitable methods. Due to the non-ergodicity of gels, the fluctuating part and the frozen-in (static) part can be calculated from normalized intermediate ensemble-averaged scattering functions (eq. 35). The fluctuating part describes the sol fraction whereas the gel fraction is related to the frozen-in part of the autocorrelation function. By comparing the fluctuating and frozen-in parts of different measurements, statements in concern of the network inhomogeneity can be made. (Note that q is not given since the scattering angle that is used in all measurements is 90°.) Figure 28 shows the results of DLS measurements performed at $\theta = 90°$ on the P1120-6.5 gel and the analogous FRC-6.5 gel at different observation temperatures (10 °C $\leq T_{obs.} \leq$ 30 °C). As mentioned in the first part of this study, the solid horizontal line represents the ensemble-average of the scattering intensity, $\langle I \rangle_E$, obtained while the cuvette was steadily rotated and the dashed line indicates the fluctuating component of the scattered intensity, $\langle I_F \rangle_T$. It is clear that with decreasing observation temperature, spatial fluctuations of the time-average intensity, $\langle I \rangle_T$ (open circles), and ensemble-average intensity, $\langle I \rangle_E$, decrease significantly for both types of gels. The fluctuating component, $\langle I_F \rangle_T$, is also diminishing with decreasing temperature as expected. It is an important fact that the P1120-6.5 is formed by the copolymer with the highest molecular weight at the highest concentration investigated in this study. From these graphs in Figure 28 one can see that PC gels are not more homogeneous than FRC gels having the same mechanical properties. The ensemble-average scattering intensities, $\langle I \rangle_E$, and time-average intensities, $\langle I \rangle_T$, of P1120-6.5 gel are higher than those of the analogous FRC gel while

intensities of the fluctuating part, $\langle I_F \rangle_T$, are nearly same for both. This behavior becomes more obvious especially for the measurements below 30 °C. Additionally, intensities of the fluctuating values, $\langle I_F \rangle_T$, are given in Table 8 because it is difficult to see the exact values clearly from Figure 28 and Figure 29. Such a high inhomogeneous structure of P1120-6.5 gel is due to some reasons. First, the high molecular weight of the starting copolymer, PNIPA-DMMI, which is used for P1120 gels. Second, high polymer concentration which is 10 times higher than c^*. And the third one, the interactions between the DMMI units and solvent which show different interactions behavior than the PNIPA units and solvent. As a result of these facts even the solution of the corresponding P1120-6.5 gel was already quite viscous indicating an undesired amount of intermolecular interactions. Thus, an initial inhomogeneity of the sample seems to exist even before cross-linking occurred. This is probably due to the very high molecular weight of the starting copolymer that makes it difficult to homogeneously dissolve the polymer even after two days. The inhomogeneity of the solutions is discussed in more detailed in chapter 5.2.3.5. These facts could be the reason for the result that the P1120-6.5 gel is more inhomogeneous than analogous FRC-6.5 gel.

On the other hand, another parameter for the solubility of the polymer is the solvent quality which significantly changes with temperature for PNIPA. At higher temperatures the solvent water turns from a good solvent to a poor solvent for PNIPA as observed by LCST. Hence the PNIPA units of the copolymer, PNIPA-DMMI, have a lower tendency of attractive interactions with water. In contrast, the DMMI units prefer higher temperatures because these groups are dissolved easier at these conditions. There is an opposed tendency of both groups in the case of PC gels. As a result the change of the scattering intensity values of PC gels ($\langle I \rangle_E$, $\langle I \rangle_T$) with temperature is not as high as in the case of the FRC gels. For both, PC and FRC gels, the osmotic part of the swelling pressure gets smaller while the elastic part becomes more dominant as the temperature is increased. This is due to the fact that highly cross-linked regions of a gel lead to deswelling of these regions at the expense of the low cross-linked regions. As already explained earlier, the larger scattering with increasing temperature is due to a more pronounced scattering contrast whereas the characteristic length scales of the structure are not altered.

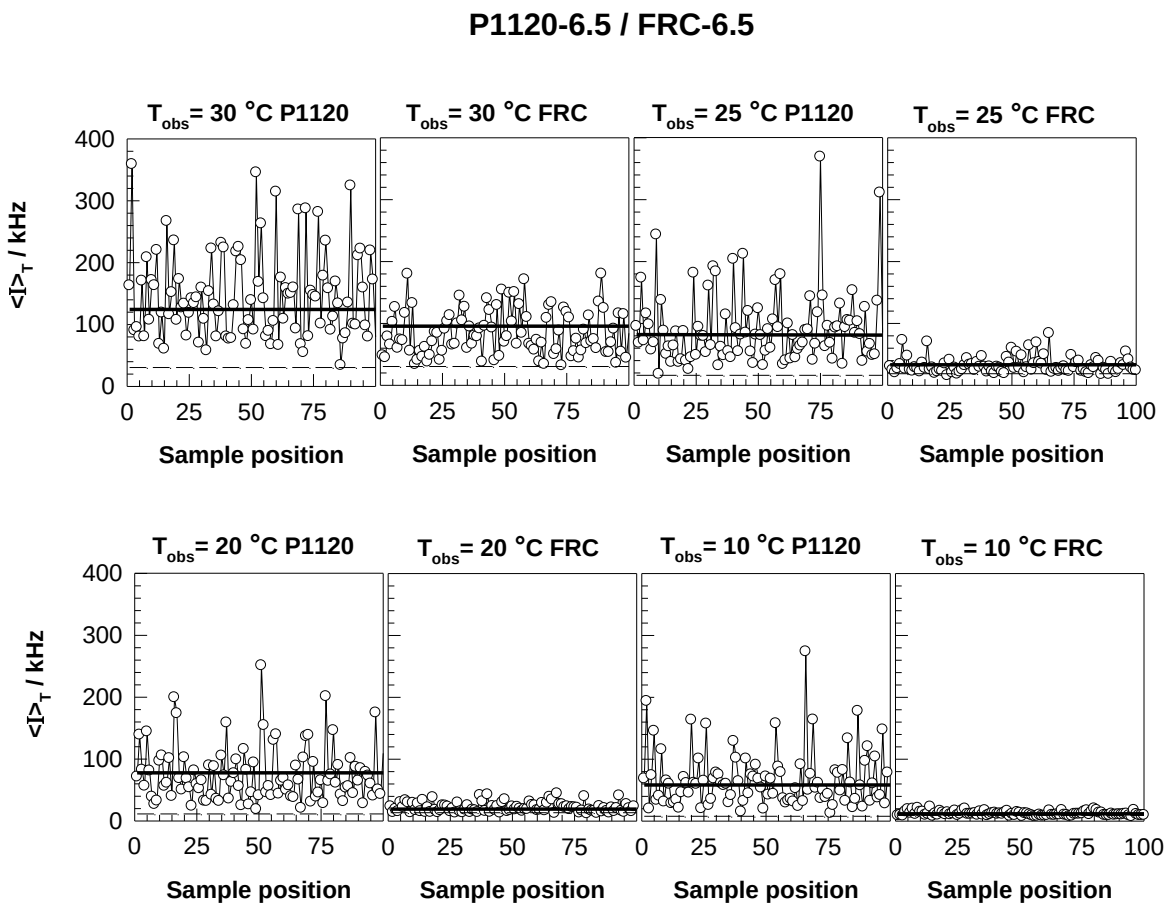

Figure 28 Variations of time-averaged scattering intensity, $\langle I \rangle_T$, with sample position at 4 different observation temperatures 30, 25, 20, 10 °C, for P1120-6.5 and analogous FRC-6.5 hydrogels. The solid line represents the ensemble-averaged scattered intensity, $\langle I \rangle_E$. The fluctuating component of the scattering intensity, $\langle I_F \rangle_T$, is represented by the dashed line, $\theta = 90°$.

Except P1120-6.5 gels, the ensemble-average scattered intensity, $\langle I \rangle_E$, and the fluctuating intensity, $\langle I_F \rangle_T$, are very close in the case of the other PC and FRC gel pairs. Figure 29 shows the DLS results of the P420-6.5 gel and its analogous FRC-6.5 gel at different $T_{obs.}$. There is a significant increase of all the intensity values for both types of gels when the temperature raises from 25 °C to 30 °C whereas the raise is smaller at temperatures between 10 to 25 °C. Since 34 °C is the LCST of NIPA, the inhomogeneity of the PNIPA gels increases drastically when the temperature approaches to this LCST. As can be seen from the graphs both type of gels show similar intensity values at different $T_{obs.}$.

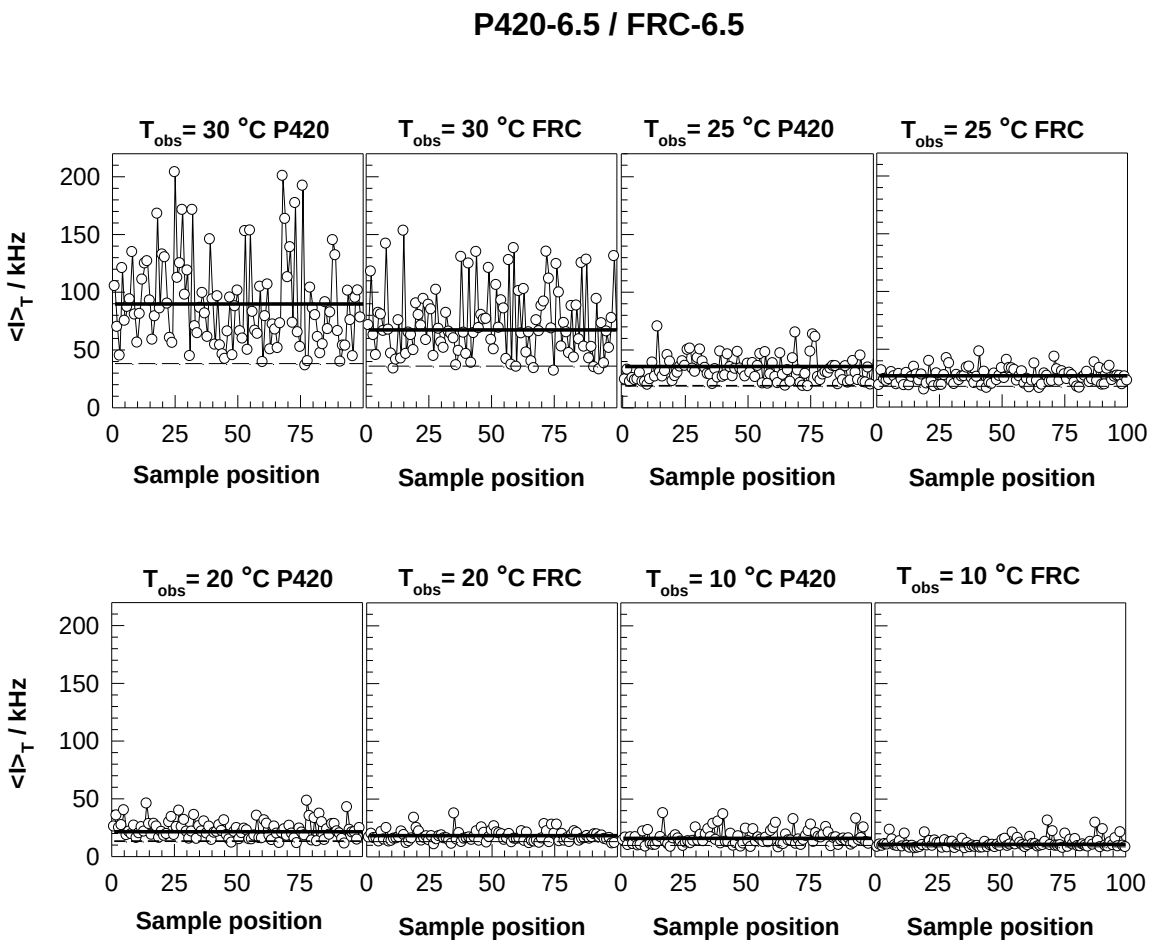

Figure 29 Variations of the time-averaged scattering intensity, $\langle I \rangle_T$, with sample position at 4 different observation temperatures 30, 25, 20, 10 °C, for P420-6.5 and analogous FRC-6.5 hydrogels. The solid line represents the ensemble-averaged scattered intensity, $\langle I \rangle_E$. The fluctuating component of the scattering intensity, $\langle I_F \rangle_T$, is represented by the dashed line, $\theta = 90°$.

The intensities of the fluctuating data, $\langle I_F \rangle_T$, from Figure 28 and Figure 29 are shown in the Table 8. As mentioned above, $\langle I_F \rangle_T$ values are nearly same for both PC and analogous FRC gels at all observation temperatures.

Table 8 Intensity values of the fluctuating, $\langle I_F \rangle_T$, part at different observation temperatures.

$T_{obs.}$	$\langle I_F \rangle_T$ (P420-6.5)	$\langle I_F \rangle_T$ (FRC-6.5) analogous to P420	$\langle I_F \rangle_T$ (P1120-6.5)	$\langle I_F \rangle_T$ (FRC-6.5) analogous to P1120
°C	kHz	kHz	kHz	kHz
30	38.25	36.07	30.50	30.35
25	18.94	17.91	16.07	18.62
20	13.36	13.11	11.40	13.44
15	9.88	8.62	7.66	9.03

Figure 30 presents the ensemble-average scattering intensities for all the PC and FRC gel pairs. Increasing the observation temperature increases the ensemble-average scattering intensities and the standard deviations of all gel samples. The standard deviation gives us information about the range of $\langle I \rangle_T$ values on the speckle pattern measured at 100 positions and hence about the structural inhomogenity. In Figure 30a, $\langle I \rangle_E$ and its standard deviation for P420-5 and analogous FRC-5 gel samples are given. FRC-5 is more inhomogeneous than P420-5, but only slightly. When the polymer concentration increases the inhomogeneity of the P420-6.5 gel becomes higher than the analogous FRC-6.5 gel as it can be seen in Figure 30b. The ensemble-average scattering intensity of the P420 gels remains nearly constant with increasing polymer concentration whereas the ensemble-average scattering intensity of FRC gels decreases i.e. FRC-5 gel has higher $\langle I \rangle_E$ than FRC-6.5. A critical polymer network concentration was found where the degree of inhomogeneity in PAAm gels formed by free radical reaction attains a maximum value [135]. This phenomenon was explained as a result of two opposite effects of the initial monomer concentration on the gel inhomogeneity. Increasing monomer concentration increases both effective cross-link density and polymer concentration of the hydrogels. While the inhomogeneity becomes more pronounced due to the first effect, the latter effect decreases the apparent gel inhomogeneity. The theory proposed by PANYUKOV and RABIN also predicts the appearance of a maximum degree of spatial gel inhomogenity at a critical polymer network concentration [10]. The intensity of the ensemble-average increases significantly for the case of PC gels formed by high molecular weight polymer. As can be seen from Figure 30c-d the photo gels P1120-5 and P1120-6.5 show significantly higher ensemble-average intensities and standard deviations than the photo

gels P420 due to the higher molecular weight of the starting copolymer, PNIPA-DMMI. This behavior is due to the fact that increasing the molecular weight of the copolymer while the relative amount of DMMI units stays constant (1%) results in a higher probability of intermolecular interactions between the DMMI units. Hence, cross-links are formed easier. This effect is also seen in the efficiency of cross-linking from the rheology results (Table 7). But these interactions can also cause agglomerations i.e. clusters, in the sol state which diminish the dissolution process of the copolymer. This can also be another reason of speckle pattern formation in the sol state for the P1120-6.5 sample. On the other side, as mentioned before, the polymer concentrations of the P1120-5 and P1120-6.5 gels are 7.5 and 10 times higher than the overlap concentration ($c^* = 0.016$ g/ml) which means excessive entanglements of the chains. The solutions of these gels have already quite high polymer concentration which results in rather high intensities of ensemble-averages and standard deviations for P1120 gels.

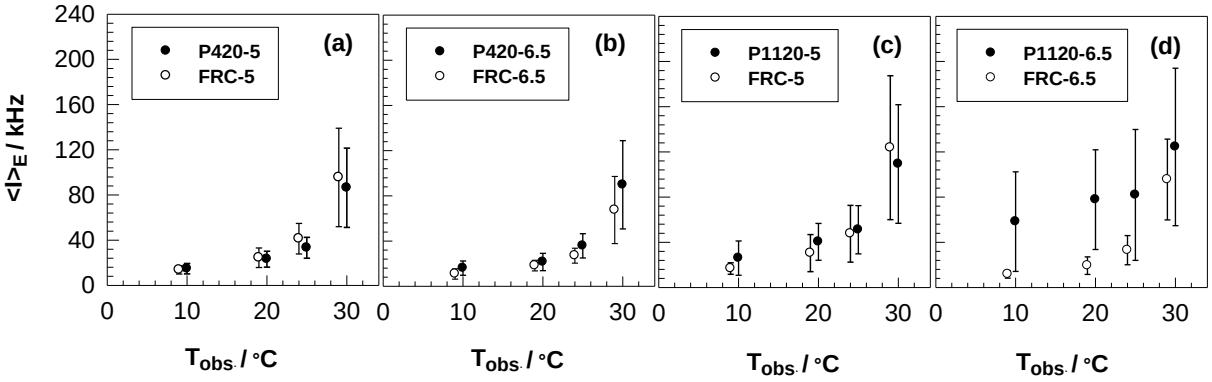

Figure 30 Ensemble-average intensity, $\langle I \rangle_E$, and standard deviations of all pairs of gels, plotted against the observation temperature 10°C ≤ $T_{obs.}$ ≤ 30°C. Note that the observation temperatures of the FRC gels are shifted 1 °C to see the results clearly.

The P1120-5 gel shows higher inhomogeneity than the analogous FRC-5 gel except at 30 °C. Increasing the polymer concentration from P1120-5 to P1120-6.5 raises the ensemble-average intensity and standard deviation significantly. Concerning P1120-6.5 and analogous FRC-6.5 gels, there is quite a big difference in the intensity of ensemble-averages and standard deviations between both types of gels. The P1120-6.5 gel is considerably more inhomogeneous than the analogous FRC-6.5 gel.

The copolymer shows easier dissolution if its molecular weight as well as the concentration is decreased. Hence, more homogenous solutions are obtained in general for lower M_w. Those solutions should give also more homogeneous gels after cross-linking. Since P420 gel samples are more homogenous than P1120 gel samples it is better to compare inhomogeneities of the free radical gels to those of P420 gels.

It is observed that the molecular weight of the copolymer plays an important role in determining the microstructure of the gel networks. The PC gels formed by the high molecular weight copolymer (P1120 gels) are significantly more inhomogeneous than their analogous FRC gels. However, the PC gels formed by the relatively low molecular weight copolymer (P420 gels) have nearly the same structural inhomogeneity as their analogous FRC gels. Actually, the results that are obtained from the dynamic light scattering experiments were not expected because photo cross-linking gels are predicted to be spatially more homogeneous than gels synthesized by free radical cross-linking mechanisms.

5.2.3.2 Static Light Scattering

SLS is also utilized to compare the homogeneity of both types of gels. To obtain correct spatial averaging across the sample, successive measurements at 5 different positions were made by turning the sample. Figure 31 demonstrates the total scattering intensity, $R(q)$, vs. the square of scattering vector, q^2, for the P1120 gels and their analogous FRC gels at observation temperatures between 10 °C ≤ $T_{obs.}$ ≤ 30 °C. Dynamic light scattering measurements showed that photo cross-linking gels are less homogenous than free radical cross-linking gels in the case of this study. As can be seen here, the same explanation holds true for the results obtained by static light scattering measurements. Since photo gels have DMMI units which make them less sensitive to the increasing temperature, the total scattering intensity, $R(q)$, of free radical gels increases more strongly with raising temperature. This behavior is also seen in DLS measurements when the data are analyzed thoroughly. DMMI becomes more soluble with increasing temperature unlike NIPA and two contrary behaviors occur in the photo gel state. This leads to less increase of $R(q)$ of photo gels (P1120) with raising temperature. From the graphs it is clearly seen that there is a strong angular dependency for the photo cross-linking gels which indicates inhomogeneity of the networks. The total scattering intensity of the FRC-5 sample is higher than that of the FRC-6.5 sample due to the critical value of initial monomer concentration [135] which is also observed from DLS results. Note that $R(q)$ reflects only the scattering intensity of gel, it doesn't give information about the change of

scattering upon gelation. The P1120-5 gel is more homogeneous than the P1120-6.5 gel as expected. It doesn't show strong angular dependence like the P1120-6.5 gel due to the low polymer concentration. The total scattering intensity of the P1120-5 gel is quite similar to its analogous FRC-5 gel except for $T_{obs.}$ = 10 °C. As mentioned above the temperature changes affect the P1120 gels less than FRC gels, so at low temperatures FRC gels are more homogeneous than PC gels but with increasing temperature the total intensity of FRC gels comes closer to that of the PC gels. The total scattering intensity of the P1120-6.5 gel has quite strong angular dependency when compared to the analogous FRC-6.5 gel. It is observed that the inhomogeneity of the P1120-6.5 gel is considerably higher than the analogous FRC-6.5 gel.

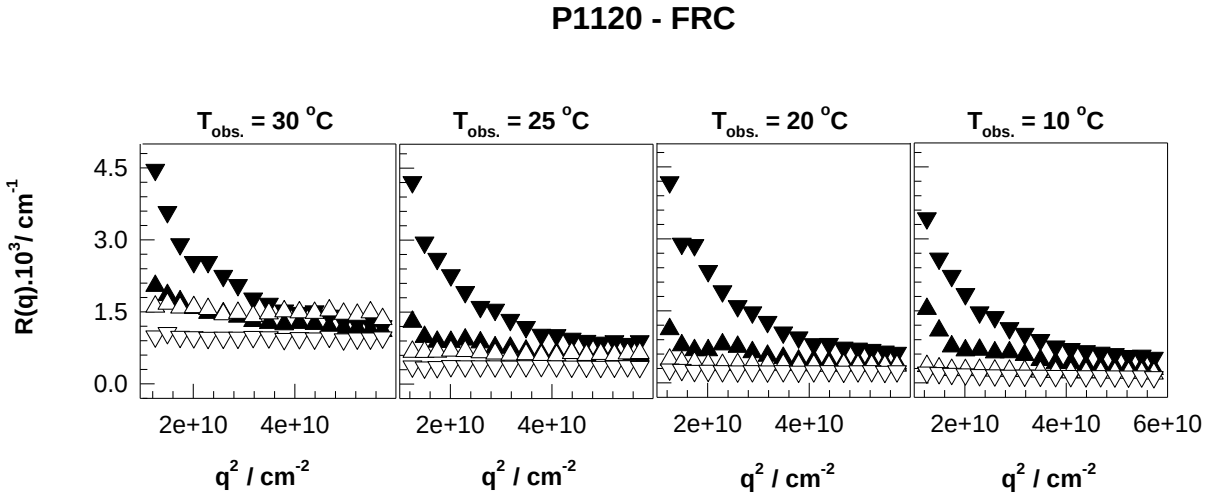

Figure 31 Total scattering intensities, $R(q)$, of P1120 and analogous FRC hydrogels are plotted versus square of the scattering vector, q^2, at different measurement temperatures $T_{obs.}$ (▲) P1120-5, (▼) P1120-6.5, (Δ) FRC-5, (▽) FRC-6.5.

The total scattering intensities of P420 gels and their analogous FRC gels are also plotted vs. the square of the scattering vector in Figure 32. The static light scattering results of these gels also fit quite well with those of the dynamic light scattering measurements. The angular dependency is less pronounced in the case of the P420 hydrogels and the intensity of the scattering light is quite similar for both PC and FRC gels at all the temperatures except $T_{obs.}$ = 30 °C. The scattering intensity of the FRC-5 gel is again higher than that of the FRC-6.5 gel due to the effect of the critical initial monomer concentration.

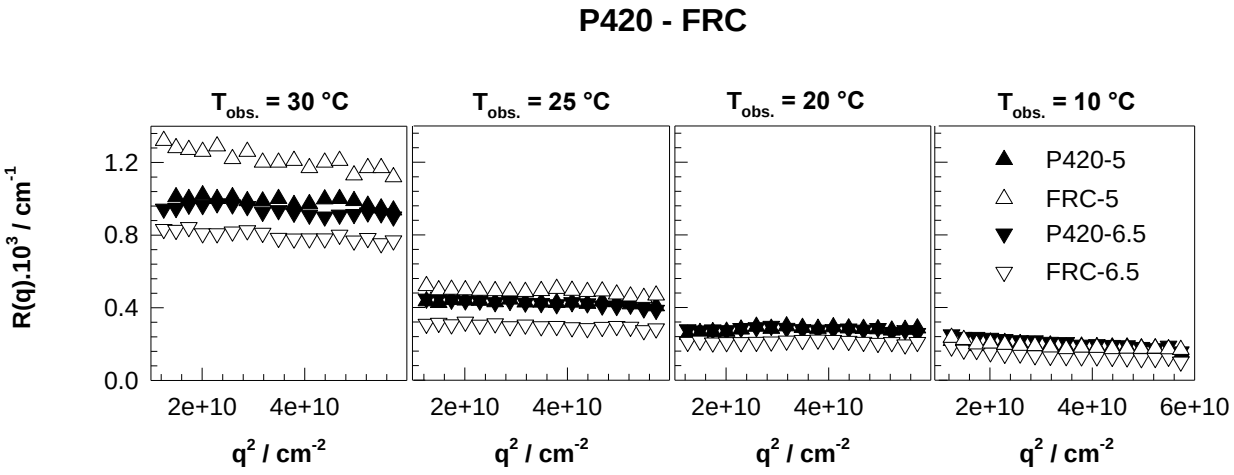

Figure 32 Total scattering intensities, $R(q)$, of P420 and analogous FRC hydrogels plotted versus the square of the scattering vector, q^2, at different measurement temperatures, $T_{obs.}$.

In the beginning it is assumed that photo cross-linking gels are more homogeneous than free radical cross-linking gels. Since photo gels are cross-linked from linear polymer and can react only from DMMI units, formation of more homogeneous gels are expected. However, this assumption is not supported by the results which are obtained from the static and dynamic light scattering experiments. This is because of the high molecular weight of the copolymers that were synthesized in the beginning. The solutions of these polymers were already dense and inhomogeneous so the PC gels that are obtained from these polymer solutions are not more homogeneous than FRC gels.

5.2.3.3 Data Evaluation

The absolute scattered intensities that are obtained from DLS and SLS alone are not sufficient to understand the spatial inhomogeneity of gels. Higher intensity cannot be exactly attributed to a more inhomogeneous network structure. Hence, relative terms are compared to gain a better understanding. As a measure of network inhomogeneity, the ratio of the fluctuating part of the network intensity, $\langle I_F \rangle_T$, and the corresponding ensemble-average intensity, $\langle I \rangle_E$, which are obtained from DLS measurements is used. (eq. 52)

$$0 \leq \frac{\langle I_F \rangle_T}{\langle I \rangle_E} \leq 1 \qquad (52)$$

The highest value, one, represents the fully fluctuating, ergodic system without any frozen-in components having an ideal homogeneous network structure that is not obtainable for real networks. The lowest value, zero, indicates networks being entirely frozen without any fluctuating component.

Figure 33 shows $\langle I_F \rangle_T / \langle I \rangle_E$ values from all the photo gels and analogous free radical gels versus observation temperatures. P420 samples and analogous FRC samples are given at the left hand side and P1120 samples and analogous FRC samples are given at the right hand side. Except for the P1120 gels, all other gels demonstrate a tendency of decreasing homogeneity ($\langle I_F \rangle_T / \langle I \rangle_E$) with increasing temperature as expected. P420 gels and analogous FRC gels exhibit quite homogenous network structure at $T_{obs.}$ = 10 °C. The ratio of $\langle I_F \rangle_T / \langle I \rangle_E$ is pretty close to one which corresponds to a nearly ideal homogeneous gel structure. One can also see that the homogeneity of P420 gels and their analogous FRC gels is similar at all temperatures. For the P1120-6.5 gel, the homogeneity seems to increase with increasing temperature from 10 to 30 °C. As mentioned in chapter 4.2.2.1, with increasing M_w and polymer concentration intermolecular hydrophobic interactions between DMMI units increase. Dissolution of DMMI increases with raising temperature contrary to PNIPA and this causes two contrary behaviors. Especially for the P1120-6.5 gel, the effect of DMMI units upon the temperature increase seems more dominant than the effect of deteriorating solvent quality of the PNIPA chains giving more homogenous gels at higher temperatures. In the right graph of Figure 33, it can be clearly seen that P1120 gels are more inhomogeneous than their analogous FRC gels except for $T_{obs.}$ = 30 °C.

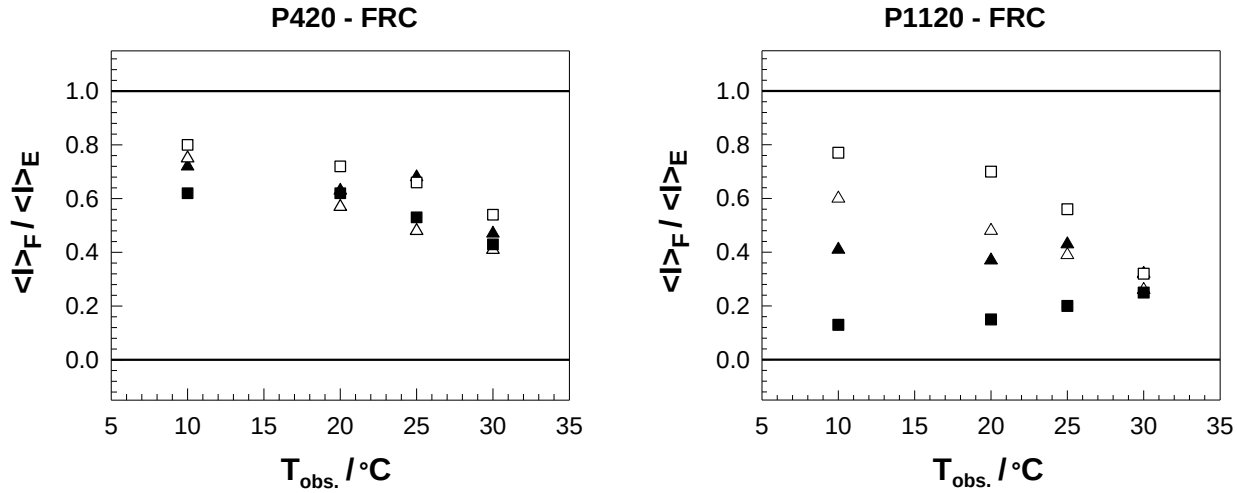

Figure 33 $\langle I_F \rangle_T$ / $\langle I \rangle_E$ of the all gel samples are plotted vs. observation temperature, $T_{obs.}$. Left hand side: comparison of P420 with analogous FRC gels; (■) P420-6.5, (□) FRC-6.5, (▲) P420-5, (Δ) FRC-5; right hand side: comparison of P1120 with analogous FRC gels; (■) P1120-6.5, (□) FRC-6.5, (▲) P1120-5, (Δ) FRC-5.

The results that are obtained from $\langle I_F \rangle_T$ / $\langle I \rangle_E$ values fit well with the DLS and SLS results. Homogeneity of P1120 gels dependence on the temperature seems clear from the relative results.

5.2.3.4 Comparison of DLS and SLS of the FRC and PC gels

In the first part of this study it is shown that SLS and DLS results agree well and two experimental approaches are equivalent for the free radical PNIPA gels. Intensity of static scattering values from SLS and DLS results were also compared in the case of PC and analogous FRC gels. Note that I_C corresponds to R_C which describes only the frozen part of the gel network; $I_C = \langle I \rangle_E - \langle I_F \rangle_T$. Equation 51 is applied in order to convert the values obtained by DLS in the same order of SLS values. The total scattering intensity values of the gels are already shown above. Figure 34 depicts a comparison of the temperature dependences of the scattering intensities (I_C, R_C) measured by SLS and DLS for the P420 gels and their analogous FRC gels at the angle 90°. In Figure 34a and 34b SLS and DLS values of the analogous FRC-5 gel seem fairly identical while for the P420-5 gel, SLS and DLS values do not seem similar. It is also shown that FRC-5 gel exhibits higher static intensity than P420-5 gel in both DLS and SLS measurements at 25 and 30 °C. (No data for P420-5 gel from SLS at 10 °C was obtained due to some experimental errors). In Figure 34c and 34d static intensity values of the analogous FRC-6.5 gel from SLS and DLS results seem nearly identical while

these intensity values do not seem similar in the case of P420-6.5 gel. Static intensities of the P420-6.5 gel from DLS results are higher than from SLS results. Furthermore frozen intensities of P420-6.5 gel are a bit higher than those of the analogous FRC-6.5 gel nearly at all temperatures.

In general the static intensities, I_C and R_C, of both type of gels from SLS and DLS show a similar behavior with increasing temperature.

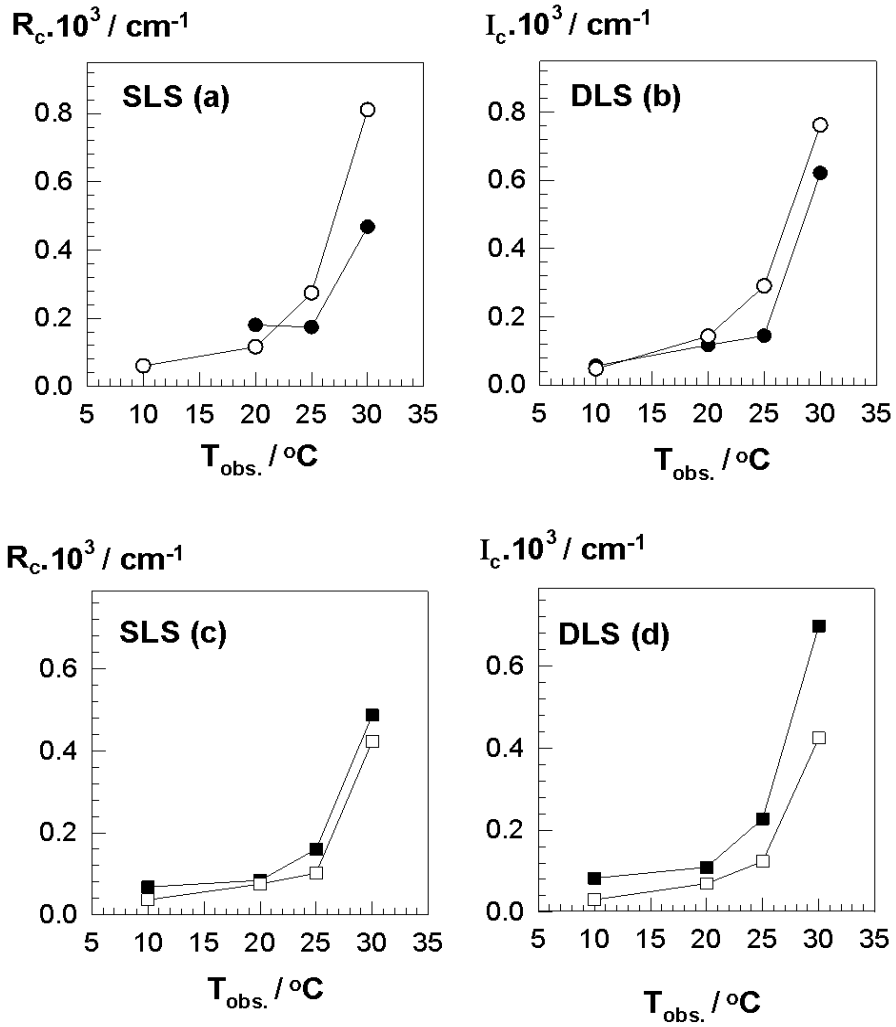

Figure 34 Comparison of the static scattering intensities measured at 90° by DLS (I_C) and SLS (R_C) as a function of observation temperature for P420-5 gel and analogous FRC-5 gel; (a), (b) and P420-6.5 gel, FRC420-6.5 gel; (c), (d). Open symbols represent the FRC gels while closed symbols show the P420 gels.

5.2.3.5 Inhomogeneity of Polymer Solutions

In order to understand the effect of molecular weight and DMMI content on the spatial inhomogeneity of the gels at different observation temperatures, polymer solutions were investigated by static light scattering. Beside PNIPA-DMMI copolymer, NIPA was also polymerized without any DMMI groups acquiring high molecular weight PNIPA (M_w = 1.100.000 g/mol) as an analogous solution. The polymer concentration was set to 5 wt-% for all the solutions. The solutions of P1120, P420 and high M_w PNIPA were analyzed by SLS. The polymer solutions were measured at 20, 25 and 30 °C. Between the temperature changes, the solutions were allowed to reach thermal equilibrium for one week. In Figure 35 the total scattering intensities of the solutions, $R(q)$, at the three observation temperatures are plotted.

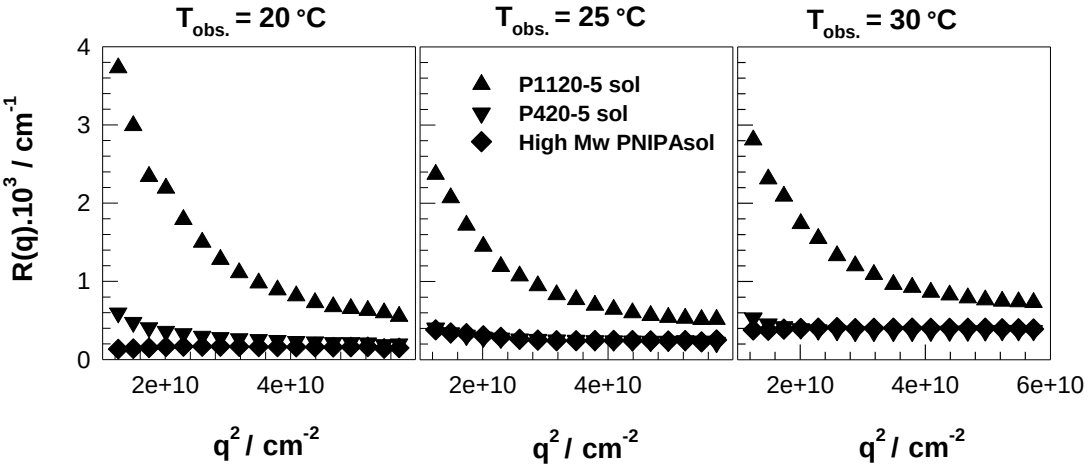

Figure 35 The total scattering intensity, $R(q)$, of polymer solutions measured by means of SLS at 20, 25 and 30 °C plotted against the square of the scattering vector, q^2.

The pure PNIPA solution shows a nearly horizontal course of the scattering intensity for every temperature indicating no inhomogeneous structures in the solution. However, it is seen that the scattering intensity increases when the temperature is raised from 20 to 30 °C. This is due to the temperature sensitive behavior of PNIPA. Since PNIPA has a LCST at around 34 °C, a temperature of 30 °C means a significant deterioration of the solvent quality in regard of this polymer. This leads to more and more pronounced density fluctuations because the polymer-polymer interactions are more and more favored. Hence, inhomogeneous areas can form resulting in a stronger scattering of the whole sample.

The P420-5 solution which has lower molecular weight than the other two polymers shows nearly the same behavior with the pure PNIPA solution. The total scattering intensity increases with increasing temperature as expected. But there is also slight angular dependence of the scattering intensity. In general, samples that show a distinct dependence of the scattering intensity on the measuring angle are known to possess a certain spatial inhomogeneity at a length scale $\geq \lambda/20$ nm. The solution of P1120-5 shows a strong angular dependence at all temperatures. This strong angular dependence indicates large inhomogeneous regimes in the polymer solution. The expected increase of the total scattering intensity on raising temperature is not observed clearly. It seems that this typical behavior of PNIPA is superimposed by another effect. Compared to the high molecular weight pure PNIPA solution, P1120-5 solution just differs in the incorporation of 1 mol-% DMMI units. It is obvious that different scattering behavior is due to the statistically introduced DMMI units. It can be assumed that the P1120-5 solution was not completely dissolved at all observation temperatures because of attractive interactions between the DMMI units which result in agglomerated regimes in the solution. These areas cause pronounced density fluctuations in the solution resulting in a higher scattering intensity compared to homogeneous solutions.

Thus it can be concluded that the results obtained from P1120 copolymer solutions and gels should be treated carefully. For more reliable comparisons it is better to use the P420 copolymer because it shows a similar scattering behavior as the pure PNIPA.

5.2.3.6 Influence of Observation Temperature on Correlation Length

Dynamic light scattering gives useful information about the dynamics of polymer solutions and gels. In diluted solutions, the self diffusion coefficient, D_s, can be determined. It describes the dynamic behavior of unperturbed molecules due to Brownian motion. After reaching the overlap concentration, no more individual information like the self diffusion coefficient can be obtained, but from this point on, a so called cooperative diffusion coefficient, D, can be determined by DLS. The dynamic correlation length is connected to the cooperative diffusion coefficient, D, as shown in eq. 36.

In the case of polymer gels this dynamic correlation length, ξ, can be related to the networks strands between junction points defining the whole mesh. Figure 36 shows the dependence of the cooperative diffusion coefficient, *D*, on observation temperature for the P1120 and P420 copolymer gels as well as for the analogous FRC gels.

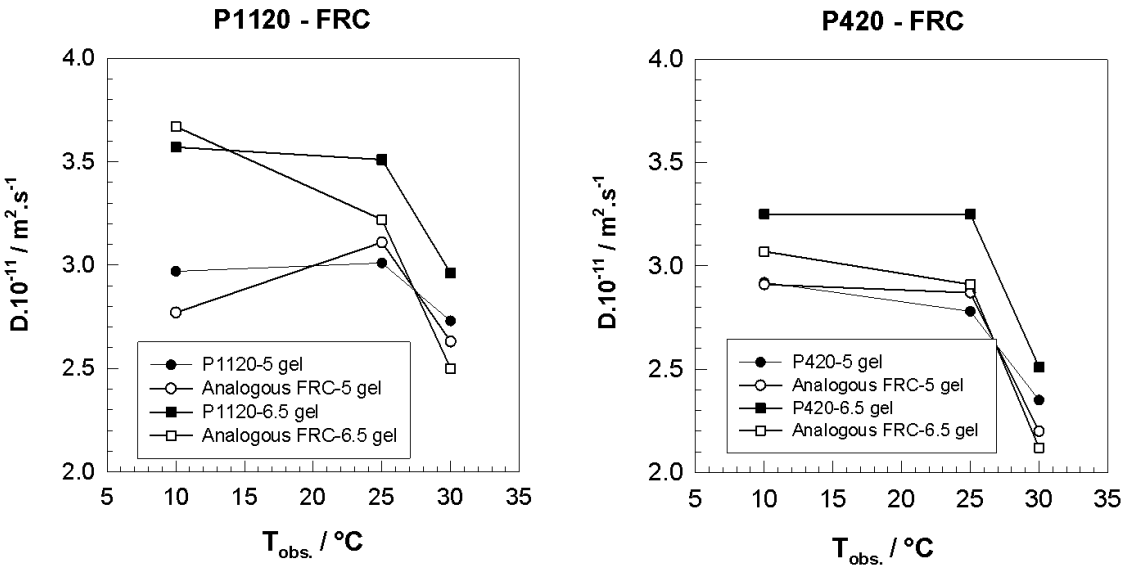

Figure 36 Cooperative diffusion coefficients, *D*, plotted against observation temperature, $T_{obs.}$. Left hand side; P1120 gels and their analogous FRC gels, right hand side; P420 gels and their analogous FRC gels.

In all cases, the gels formed at higher concentrations show higher diffusion coefficients, *D*, meaning smaller spacings between cross-links. Since the length scale is quite small, nearly no difference is observed by comparing the PC gels to the FRC gels. It can be seen clearly that all curves show a sharp decrease of the diffusion coefficient with increasing observation temperature from 25 to 30 °C. This decrease is related to the fact that all systems are approaching the critical temperature typical for PNIPA polymers. At this temperature the hydrodynamic screening length, ξ, diverges and so the cooperative diffusion coefficient, *D*, decreases drastically. It is important to understand that at temperatures close the LCST of a polymer, the hydrodynamic screening length, ξ, is no longer associated to the actual mesh size of the polymer gel but it rather reflects the spatial extent of concentration fluctuations of the network. Only at temperatures far below this critical temperature, the hydrodynamic screening length is related to the network strands.

6 Summary and Conclusion

This study is composed of two parts. In the first part variations of the static and dynamic components of the time-average and ensemble-average scattering intensities from PNIPA gels synthesized by conventional FRC were analyzed as a function of temperature. SLS and DLS results of the hydrogels were also compared and results fit perfectly together. All methods investigated yield consistent results and, in the first place, confirm the well-known fact that the static component raises strongly with increasing the cross-link density.

The results showed that contrary to the common assumption, the static component of the ensemble-average scattering intensity strongly depends on the observation temperature below the LCST. The increase of the thermal scattering is expected, of course, because thermal fluctuations become stronger when the LCST is approached. However, the static component of scattering intensity is affected by temperature to an even greater extent. This behavior is interpreted by assuming local swelling equilibrium in a gel whose cross-link density features some inhomogeneity. Equilibrium swelling is controlled by two competing factors, osmotic pressure and chain elasticity. The osmotic pressure of a semi-dilute polymer solution given by the FLORY–HUGGINS equation scales, to a first approximation, with excluded volume, or $(1-2\chi)$, where χ is the Flory interaction parameter. For PNIPA, χ increases with temperature and approaches 0.5 near the LCST. Hence, the osmotic pressure decreases with raising temperature, while the chain elasticity remains essentially constant. This means that upon raising the temperature, more densely cross-linked regions deswell at the expense of the less densely cross-linked ones. Accordingly, the scattering contrast is enhanced thus leading to a larger static scattering intensity, as first pointed out by TANAKA et al [13]. By following this argument it is supposed that both parts of the scattering intensity are governed by thermodynamic quantity, namely quality of the solvent. However, different dependencies apply thus leading to the fact that the static scattering seems to be slightly more sensitive to temperature than the fluctuating part of the scattering intensity. The interpretation based on local swelling equilibrium is in accordance with the view that polymer gels possess restricted ergodicity [10]. They have an inhomogeneous distribution of cross-links, but their density inhomogeneity is not fixed. Rather it is dependent on the establishment of local swelling equilibrium controlled by a distinct network topology.

In the second part of this study inhomogeneities of PNIPA gels prepared at T_{prep} = 25 °C via photo cross-linking reaction starting from linear PNIPA chains modified with DMMI functionalities and their analogous FRC gels starting from NIPA monomers were compared at different observation temperatures. The main difference between these two systems is the cross-linking process. The PC gels are formed by random cross-linking which is supposed to form homogeneous network structures. In contrast, FRC is generally assumed to yield more inhomogeneous networks due to the formation of highly cross-linked clusters in the beginning of the reaction. Two different linear polymers having different molecular weights, M_w, were used for the PC process. At first the macroscopic mechanical behavior of the hydrogels, i.e. the elastic modulus, was investigated. It was important to obtain the same elastic modulus for both PC and FRC gels before comparing their microscopic structure by means of light scattering methods. It was shown that FRC gels reach their steady state value of G' after 10 min while PC systems need more than 9 hours to level off. After finding the same elastic modulus, hydrogels were analyzed concerning their microstructure.

Dynamic light scattering experiments showed that increasing the observation temperature increases all the scattering values of both types of gels. Raising the molecular weight, M_w, of the initial copolymer leads to an increase in the scattering intensity of PC gels and shows a pronounced speckle pattern. In the first study, the non-ergodic method and partial heterodyne method were applied and they both showed the same results for PNIPA gels. In the second part of this study only the non-ergodic method was used to analyze the PC and FRC gels. It was found that the PC gel that is synthesized by using a high molecular weight and high polymer concentration (P1120-6.5) is more inhomogeneous than its analogous FRC gel. PC gels starting from relatively low molecular weight polymers (P420) generally show nearly the same scattering behavior as their analogous FRC gels. In general, static light scattering results fit well with dynamic light scattering results. In the case of PC gels starting from low molecular weight (P420) and their analogous FRC gels, the total scattering intensity, $R(q)$, increases significantly with increasing observation temperature. At low temperatures P420 gels and their analogous FRC gels show nearly same scattering intensity. A slight separation of the scattering intensities is observed at $T_{obs.}$ = 30 °C but it can still be concluded that PC gels are not more or less inhomogeneous than FRC gels. All the analogous FRC-5 gels showed higher scattering intensity than FRC-6.5 gels due to the critical polymer network concentration which leads to a decrease of the scattering intensities by increasing polymer concentrations. In addition SLS and DLS results of the PC and FRC gels were compared as a function of observation temperature. In the case of FRC gels SLS and DLS results fit well

together whereas PC gels show a slight difference. DLS values of PC gels are generally a bit higher than their SLS values.

A strong angular dependence is obtained in case of the P1120-6.5 gel indicating a remarkable inhomogeneity. In order to understand the scattering behavior thoroughly, corresponding polymer solutions of the gels were also examined by means of SLS. The high molecular weight polymer solution which belongs to the P1120-5 gel explicitly shows a strong angular dependency and a high scattering intensity at any observation temperature. The corresponding solutions of these P1120 gels were already inhomogeneous before the cross-linking process. The comparison of the PC gels that were formed from the low molecular weight copolymer to the FRC gels yielded more reliable results.

In the beginning of the study it was supposed that PC gels are more homogenous than FRC gels since PC gels are cross-linked randomly. In contrast to the general assumption the results of this study showed that the formed PC gels are not more homogenous than their analogous FRC gels. On the other hand the strong dependence of the inhomogeneity on the M_w of the linear polymer precursors is revealed. Increasing M_w of a polymer and solutions as well increases the inhomogeneity of the PC gels.

For the following studies it would be desirable to use copolymers carrying cross-linker groups with molecular weights below 1.000.000 g/mol. It is supposed that these preformed polymers form more homogeneous solutions before starting the cross-linking process.

7 References

[1] Funke, W.; Okay, O.; Joos-Muller, B. *Adv. Polym. Sci.*, **1998**, *136*, 139-234.

[2] Okay, O. *Progr. Polym. Sci.*, **2000**, *25*, 711-779.

[3] Bastide, J.; Candau, S.J. in: Cohen Addad, J.P; editor. *Physical Properties of Polymeric Gels*. Wiley: London, **1996**, p. 143.

[4] Debye, P.; Bueche, A. M. *J. Appl. Phys.*, **1949**, *20*, 518-525.

[5] Bueche, F. *J. Colloid Interface Sci.*, **1970**, *33*, 61-66.

[6] Soni, V. K.; Stein, R. S. *Macromolecules*, **1990**, *23*, 5257-5265.

[7] Bastide, J.; Leibler, L. *Macromolecules*, **1988**, *21*, 2647-2649.

[8] Panyukov, S.; Rabin, Y. *Phys. Rep.*, **1996**, *269*, 1-131.

[9] Horkay, F.; Hecht, A. M.; Geissler, E. *J. Chem. Phys.*, **1989**, *91*, 2706-2711.

[10] Panyukov, S.; Rabin, Y. *Macromolecules*, **1996**, *29*, 7960-7975.

[11] Rabin, Y.; Panyukov, S. *Macromolecules*, **1997**, *30*, 301-312.

[12] Ikkai, F.; Shibayama, M. *Phys. Rev. Lett.*, **1999**, *82*, 4946-4949.

[13] Matsuo, E.S.; Orkisz, M.; Sun, S.-T.; Li, Y.; Tanaka, T. *Macromolecules*, **1994**, *27*, 6791-6796.

[14] Shibayama, M.; Takata, S.-I.; Norisuye, T. *Physica A*, **1998**, *249*, 245-252.

[15] Joosten, J. G. H.; McCarthy, J. L.; Pusey, P.N. *Macromolecules*, **1991**, *24*, 6690-6699.

[16] Moussaid, A.; Candau, S. J.; Joosten, J. G. H. *Macromolecules*, **1994**, *27*, 2102-2110.

[17] Pusey, P. N.; van Megen, W. *Physica A*, **1989**, *157*, 705-741.

[18] Boutris, C.; Chatzi, E. G.; Kiparissides, C. P. *Polymer*, **1997**, *38*, 2567-2570.

[19] Okada, Y.; Tanaka, F. *Macromolecules*, **2005**, *38*, 4465-4471.

[20] Kawaguchi, T.; Kobayashi, K.; Osa, M.; Yoshizaki, T. *J. Phys. Chem. B*, **2009**, *113*, 5440-5447.

[21] Arndt, K. -F.; Schmidt, T.; Richter, A.; Kuckling, D. *Macromol. Symp.*, **2004**, *207*, 257-268.

[22] Richter, A.; Howitz, S.; Kuckling, D.; Arndt, K. -F. *Sensors Actuat. B*, **2004**, *99*, 451-458.

[23] Ballauf, M.; Lu, Y. *Polymer*, **2007**, *48*, 1815-1823.

[24] Takata, S.; Norisuye T.; Shibayama, M. *Macromolecules*, **2002**, *35*, 4779-4784.

[25] Shibayama, M.; Shirotani Y.; Shiwa, Y. *J. Chem. Phys.*, **2000**, *112*, 442-449.

[26] Shibayama, M. *Polymer J.*, **2011**, *43*, 18-34.

[27] Shibayama, M.; Takata, S.; Nakamoto, C. *Macromol. Symp.*, **2004**, *207*, 31-36.

[28] Shibayama, M.; Isono, K.; Okabe, S.; Karino, T.; Nagao, M. *Macromolecules*, **2004**, *37*, 2909-2918.

[29] Shibayama, M.; Kawakubo, K.; Norisuye, T. *Macromolecules*, **1998**, *31*, 1608-1614.

[30] Ikkai, F.; Shibayama, M. *J. Polym. Sci. B: Polym. Phys.*, **2005**, *43*, 617-628.

[31] Zhao, Y.; Zhang, G.; Wu, C. *Macromolecules*, **2001**, *34*, 7804-7808.

[32] Zhao, Y.; Yang, Y.; Wu, C. *Macromolecules*, **2003**, *36*, 855-859.

[33] Koizumi, S.; Monkenbusch, M.; Richter, D.; Schwahn, D.; Farago, B. *J. Chem. Phys.*, **2004**, *121*, 12721-12731.

[34] Joosten, J. G. H.; Gelade, E. T. F.; Pusey, P. N. *Phys. Rev. A*, **1990**, *42*, 2161-2173.

[35] Shibayama, M. *Macromol. Chem. Phys*., **1998**, *199*, 1-30.

[36] Fang, L.; Brown, W. *Macromolecules*, **1992**, *25*, 6897-6903.

[37] Tanaka, T.; Hocker, L. O.; Benedek, G. B. *J. Chem. Phys*., **1973**, *59*, 5151-5159.

[38] Rodd, A. B.; Dunstan, D. E.; Boger, D. V.; Schmidt, J.; Burchard, W. *Macromolecules*, **2001**, *34*, 3339-3352.

[39] Flory, P. J. *J. Chem. Phys.*, **1942**, *10*, 51.

[40] Flory, P. J. *Principles of Polymer Chemistry*; Cornell University Press: Ithaka, New York, **1953**.

[41] Hildebrand, J. H.; Scott, R.L. *The Solubility of Nonelectrolytes*, 3rd ed.; Van Nostrand Reinhold: New York, **1959**.

[42] De Gennes, P. G. *Scaling Concepts in Polymer Physics*; Cornell University Press: Ithaca and London, **1979**.

[43] Ying, Q.; Chu, B. *Macromolecules*, **1987**, *20*, 362.

[44] Des Cloizeaux, J.; Jannink, G. *Polymers in solution; Their modeling and structure*; Clarendon Press: Oxford, **1990**.

[45] Brandrup, J.; Immergut, E. H.; Grulke, E. A., editors. *Polymer Handbook*, 4th ed.; Wiley: New York, **1999**.

[46] M. Doi, M.; Edwards, S.F. *The theory of polymer dynamics,* Clarendon Press: *Oxford*, **1989**.

[47] Rubinstein, M.; Colby, R. *Polymer Physics*; Oxford University Press: New York, **2008**.

[48] Costa, R. O. R.; Freitas, R. F. S. *Polymer*, **2002**, *43*, 5879-5885.

[49] Gil, E. S.; Hudson, S. M. *Prog. Polym. Sci.*, **2004**, *29*, 1173-1222.

[50] Zhang, Y. J.; Furyk, S.; Bergbreiter, D. E.; Cremer, P. S. *J. Am. Chem. Soc.*, **2005**, *127*, 14505-14510.

[51] Zhang, Y.; Furyk, S.; Sagle, L. B.; Cho, Y.; Bergbreiter, D. E.; Cremer, P. S. *J. Phys. Chem. C*, **2007**, *111*, 8916-8924.

[52] Furyk, S.; Zhang, Y. J.; Ortiz-Acosta, D.; Cremer, P. S.; Bergbreiter, D. E. *J. Polym. Sci. Pol. Chem.*, **2006**, *44*, 1492-1501.

[53] Sagle, L. B.; Zhang, Y. J.; Litosh, V. A.; Chen, X.; Cho, Y.; Cremer, P. S. *J. Am. Chem. Soc.*, **2009**, *131*, 9304-9310.

[54] Gurau, M. C.; Lim, S. M.; Castellana, E. T.; Albertorio, F.; Kataoka, S.; Cremer, P. S. *J. Am. Chem. Soc.*, **2004**, *126*, 10522-10523.

[55] LunaBarcenas, G.; Gromov, D. G.; Meredith, J. C.; Sanchez, I. C.; dePablo, J. J.; Johnston, K. P. *Chem. Phys. Lett.*, **1997**, *278*, 302-306.

[56] Ahmed, Z.; Gooding, E. A.; Pimenov, K. V.; Wang, L. L.; Asher, S. A. *J. Phys. Chem. B*, **2009**, *113*, 4248-4256.

[57] Meersman, F.; Wang, J.; Wu, Y. Q.; Heremans, K. *Macromolecules*, **2005**, *38*, 8923-8928.

[58] ten Wolde, P. R.; Chandler, D. *Proceedings of the National Academy of Sciences of the United States of America (PNAS)*, **2002**, *99*, 6539-6543.

[59] Paricaud, P.; Galindo, A.; Jackson, G. *Mol. Phys.*, **2003**, *101*, 2575-2600.

[60] Smith, G. D.; Bedrov, D. *J. Phys. Chem. B*, **2003**, *107*, 3095-3097.

[61] Esteve, A.; Bail, A.; Landa, G.; Dkhissi, A.; Brut, M.; Rouhani, M. D.; Sudor, J.; Gue, A. M. *Chem. Phys.*, **2007**, *340*, 12-16.

[62] Jones, R. A. L. *Soft Condensed Matter*; Oxford University Press: Oxford, **2002**.

[63] Lin, Y.G.; Mallin, D. T.; Chien, J. C. W.; Winter, H. H. *Macromolecules*, **1991**, *24*, 850-854.

[64] Gilbert, M. *J. M.S-Rev. Macromol. Chem. Phys.*, **1994**, *C34*, 77-135.

[65] Kleppinger, R.; van Es, M.; Mischenko, N.; Koch, M. H. J.; Reynaers, H. *Macromolecules*, **1998**, *31*, 5805-5809.

[66] Sato, T.; Watanabe, H.; Osaki, K. *Macromolecules*, **2000**, *33*, 1686-1691.

[67] Crne, M.; Park, J. O.; Srinivasarao, M. *Macromolecules*, **2009**, *42*, 4353-4355.

[68] Itagaki, H.; Takahashi, I. *Macromolecules*, **1995**, *28*, 5477-5486.

[69] Shibayama, M. *Macromol. Chem. Phys.*, **1998**, *199*, 1-30.

[70] Orakdogen, N.; Kizilay, M. Y.; Okay, O. *Polymer*, **2005**, *46*, 11407-11415.

[71] Stein, R. S. *J. Polym. Sci.: Polym. Lett.*, **1969**, *7*, 657-660.

[72] Jong, L.; Stein, R. S. *Macromolecules*, **1991**, *24*, 2323-2329.

[73] Oppermann, W.; Lindemann, B.; Vögerl, B. *Polym. Preprints*, **2000**, *41*, 700.

[74] Schröder, U.P.; Oppermann, W. *Makromol. Chemie, Macromol. Symp*., **1993**, *76*, 63.

[75] Okay, O.; Kurz, M.; Lutz, K.; Funke, W. *Macromolecules*, **1995**, *28*, 2728.

[76] Okay, O. Nagash, H. J.; Capek, I. *Polymer*, **1995**, *36*, 2413.

[77] Cerid, H.; Okay, O. *Eu. Polym. J*., **2004**, *40*, 579-587.

[78] Keskinel, M.; Okay, O. *Polym. Bull*., **1998**, *40*, 491-498.

[79] Dusek, K.; Duskova-Smrckova, M. *Prog. Polym. Sci*., **2000**, *25*, 1215-1260.

[80] Dusek, K. In *Polymer Networks*; Stepto, R. F. T., Ed.; Blackie Academic & Professional: London, **1998**, p 64.

[81] Liu, R. G.; Oppermann, W. *Macromolecules*, **2006**, *39*, 4159-4167.

[82] Shibayama, M. *Bull. Chem. Soc. Jpn.*, **2006**, *79*, 1799-1819.

[83] Proctor, A. D.; Gilbert, A.; Mitchell, G. R. *Makromolekulare Chemie – Macromol. Chem. Phys.*, **1992**, *193*, 1499-1508.

[84] Jones, J. R.; Liotta, C. L.; Collard, D. M.; Schiraldi, D. A. *Macromolecules*, **2000**, *33(5)*, 1640-1645.

[85] Schinner, R.; Wolff, T.; Kuckling, D. *Berichte der Bunsen-Gesellschaft-Phys. Chem. Chem. Phys.*, **1998**, *102*, 1710-1714.

[86] Schinner, R.; Wolff, T. *Colloid. Polym. Sci*., **2001**, *279*, 1225-1230.

[87] Hoffmann, F.; Wolff, T. *J. Colloid Interface Sci.*, **2008**, *322*, 434-447.

[88] Kuznetsova, N. A.; Kaliya, O. L. *Uspekhi Khimii*, **1992**, *61*, 1243-1267.

[89] Ngai, T.; Wu, C. *Macromolecules*, **2003**, *36*, 848-854.

[90] Susoff, M.; Oppermann, W. *Macromolecules*, **2009**, *42*, 9195-9198.

[91] Seiffert, S.; Oppermann, W. *Polymer*, **2008**, *49*, 4115-4126.

[92] Zweifel, H. *Photog. Sci. Eng.*, **1983**, *27*, 114-118.

[93] Finter, J.; Widmer, E.; Zweifel, H. *Angew. Makromol. Chem.*, **1984**, *128*, 71-97.

[94] Berger, J.; Zweifel, H. *Angew. Makromol. Chem.*, **1983**, *115*, 163-181.

[95] Gansel, J. *Untersuchungen zur Dynamik in Polyacrylmid-Lösungen und –Gelen mittels Fluoreszenzkorrelationsspektroskopie*, Dissertation: Clausthal, **2009**.

[96] Kuckling, D.; Vo, C. D.; Adler, H. J. P.; Volkel, A.; Colfen, H. *Macromolecules*, **2006**, *39*, 1585-1591.

[97] Seiffert, S.; Weitz, D. A. *Soft Matter*, **2010**, *6*, 3184-3190.

[98] Seiffert, S. *Structure and Tracer Dynamics in Polyacrylamide Hydrogels*, Dissertation: Clausthal, **2007**.

[99] Farnum, D. G.; Mostashari, A. J. *Org Photochem Synth*., **1971**, *1*, 103.

[100] Minsk, L. M.; Smith, I. G.; Wright, J. F. *J. Appl. Polym. Sci.*, **1959**, *2*, 302.

[101] Rennert, J.; Ruggiero, E. M.; Rapp, J. *Photochem. Photobiol.*, **1967**, *6*, 29.

[102] Tsuda, M. *J. Chem. Soc. Jpn.*, **1969**, *42*, 905.

[103] Egerton, P. L.; Pitts, E.; Reiser, A. *Macromolecules*, **1981**, *14*, 95.

[104] Nakayama, Y.; Matsuda, T. *J. Polym. Sci. A*, **1992**, *30*, 2451.

[105] Coqueret, X. *Macromol. Chem. Phys.*, **1999**, *200*, 1567.

[106] Schenck; G:O.; von Wilucki; I.; Krauch, C. H. *Chem. Ber.*, **1962**, *95*, 1409.

[107] Hammond, G. S.; Stout, C. A.; Lamola, A. A. *J. Am. Chem. Soc.*, **1964**, *86*, 3103.

[108] Chujo, Y.; Sada, K.; Saegusa, T. *Macromolecules*, **1990**, *23*, 2693.

[109] Ngai, T.; Wu, C. *Macromolecules*, **2003**, *36*, 848.

[110] De Schryver, F. C.; Feast, W. J.; Smets, G. *J. Polym. Sci. A-1*, **1970**, *8*, 1939.

[111] Zweifel, H. *Photogr. Sci. Eng.*, **1983**, *27*, 114.

[112] Berger, J.; Zweifel, H. *Angew. Makromol. Chem*., **1983**, *115*, 163.

[113] Finter, J.; Haniotis, Z.; Lohse, F.; Meier, K.; Zweifel, H. *Angew. Makromol. Chem*., **1985**, *133*, 147.

[114] Kuckling, D.; Adler, H. J. P.; Ling, L.; Habicher, W. D.; Arndt, K. F. *Polym. Bull*., **2000**, *44*, 268.

[115] Kuckling, D.; Duan Vo, C.; Wohlrab, S. E. *Langmuir*, **2002**, *18*, 4263.

[116] Steinmetz, R. *Fortschr. Chem. Forsch.*, **1967**, *7*, 445.

[117] Herkstroeter, W. G.; Lamola, A. A.; Hammond, G. S. *J. Am. Chem. Soc*., **1964**, *86*, 4537.

[118] Hammond, G. S.; Turro, N. J.; Leermakers, P. A. *J. Phys. Chem.*, **1962**, *66*, 1144.

[119] Wilkinson, F. *J. Phys. Chem.*, **1962**, *66*, 2569.

[120] Scharf, H. D. *Fortschr. Chem. Forsch.*, **1969**, *11*, 216.

[121] Murov, S. L. *Handbook of photochemistry*, New York: Marcel Dekker Inc., **1973**.

[122] Engel, P. S.; Monroe, B. M. *Adv. Photochem.*, **1972**, *8*, 245.

[123] Lathioor, E. C.; Leigh, W. J. *Photochem. Photobiol*., **2006**, *82*, 291.

[124] Kronfeld, K. P.; Timpe, H. J. *J. Prakt. Chem*., **1988**, *330*, 571.

[125] Ferreira, G. C., Schmitt, C. C.; Neumann, M. G. *J. Braz. Chem. Soc.*, **2006**, *17*, 905.

[126] Fouassier, J. P. *Photoinitiation, photopolymerization and photocuring*. Cincinnati: Hanser Gardner, **1995**.

[127] Allonas, X.; Ley, C.; Bibaut, C.; Jacques, P.; Fouassier, J. P. *Chem. Phys. Lett*., **2000**, *322*, 483.

[128] Lewis, F. D.; Saunders, W. H. *J. Am. Chem. Soc*., **1968**, *90*, 7033.

[129] Meier, K.; Zweifel, H. *J. Photochem.*, **1986**, *35*, 353.

[130] Chu, B. *Laser Light Scattering; Basic Principles and Practice*, 2nd ed.: Academic Press: San Diego, **1991**.

[131] Berne, B. J.; Pecora, R. *Dynamic light scattering;* Wiley: New York, **1976**.

[132] Nie, J.; Du, B.; Oppermann, W. *Macromolecules*, **2004**, *37*, 6558-6564.

[133] Shibayama, M.; Ikkai, F.; Shiwa, Y.; Rabin, Y. *J. Chem. Phys.*, **1997**, *107*, 5227-5235.

[134] Kuru, E. A.; Orakdogen, N.; Okay, O. *Eu. Polym. J.*, **2007**, *43*, 2913-2921.

[135] Kizilay, M. Y.; Okay, O. *Macromolecules*, **2003**, *36*, 6856-6862.

[136] Abdurrahmanoglu, S.; Okay, O. *J. Macromol. Sci. A. Pure Appl. Chem.*, **2008**, *45*, 769-775.

[137] Berne, B. J.; Pecora, R. *Dynamic Light Scattering*, Dover Publ.; Mineola, New York, **2000**, pp. 44-46.

[138] Hecht, A. -M.; Horkay, F.; Schleger, P.; Geissler, E. *Macromolecules*, **2002**, *35*, 8552-8555.

[139] Geissler, E. in *Dynamic Light Scattering*; ed. W. Brown: Oxford University Press, **1993**, pp. 471-511.

[140] Geissler, E.; Horkay, F.; Hecht A. -M. *Phys. Rev. Lett.*, **1993**, *71*, 645-648.

[141] Orakdogen, N.; Okay, O. *Polym. Bull.*, **2006**, *57*, 631-641.

[142] Ricka, J. *Appl. Opt.*, **1993**, *32*, 2860-2875.

[143] Gisler, T.; Rüger, H.; Egelhaaf, S. U.; Tschumi, J.; Schurtenberger, P.; Ricka, J. *Appl. Opt.*, **1995**, *34*, 3546-3553.

[144] Norisuye, T.; Tran-Cong-Miyata, Q.;Shibayama, M. *Macromolecules*, **2004**, *37*, 2944-2953.

[145] Schätzel, K. *Appl. Opt*., **1993**, *32*, 3880-3885.

[146] Mezger, T. G. *Das Rheologie-Handbuch*; Vol. 2, Vincentz Network: Hannover, **2007**.

[147] Macosko, C. W. *Rheology - Prinicples, Measurements, and Applications*; VCH Publishers: New York, **1994**.

[148] Barnes, H. A. *An Introduction to Rheology*; Elsevier: New York, **1989**.

[149] Winter, H. H. *Polym Eng. Sci.*, **1987**, *27*, 1698-1702.

[150] Scanlan, J. C.; Winter, H. H. *Macromolecules*, **1991**, *24*, 47-54.

[151] Richter, S. *Macromolecular Chemistry and Physics*, **2007**, *208*, 1495-1502.

[152] Winter, H. H.; Mours, M. *Neutron Spin Echo Spectroscopy Viscoelasticity Rheology*, **1997**, *134*, 165-234.

[153] Ling, L.; Habicher, W. D.; Kuckling, D.; Adler, H. J. P. *Des. Monom. Polym.*, **1999**, *2*, 351.

[154] Duan Vo, C.; Kuckling, D.; Adler, H. J. P.; Schönhoff, M. *Colloid Polym. Sci*., **2002**, *280*, 400.

[155] Pabon, M.; Selb, J.; Candau, F.; Gilbert, R. G. *Polymer*, **1999**, *40*, 3101.

[156] Fevola, M. J.; Hester, R. D.; McCormick, C. L. *J. Polym. Sci.: Part A*, **2003**, *41*, 560.

[157] Gupta, A.; Mukhtar, R.; Seltzer, S. *J. Phys. Chem*., **1990**, *84*, 2356.

[158] McCarthy, K. J.; Burkhardt, C. W.; Parazak, D. P. *J. Appl. Polym. Sci*., **1987**, *33*, 1699.

[159] Seiffert, S.; Oppermann, W.; Saalwächter, K. *Polymer*, **2007**, *48*, 5599-5611.

[160] Treloar, L. R. G. *The Physics of Rubber Elasticity*, 3rd ed., Clarendon Press: Oxford, UK, **1975**.

[161] Naghash, H. J.; Okay, O. *J. Appl. Polym. Sci.*, **1996**, *60*, 971.

[162] Patras, G.; Qiao, G. G.; Solomon, D. H. *Macromolecules*, **2001**, *34*, 6369.

[163] Susoff, M. *Dynamik polymerer Sonden in halbverdünnten Polystyrol-Lösungen und Gelen*, Dissertation: Clausthal, **2009**.

Curriculum Vitae

Name:	**Saadet Dogu**
Address:	August-Hölscher Str. 104
	49080-Osnabrück
Mobile:	0049 176 38 95 1687
E-mail:	dsaadet@gmail.com
Date, Place of Birth:	27.02.1984, Üsküdar / Istanbul
Nationality:	Turkish

Education

June 2013	PhD student at the Institute of Physical Chemistry, Clausthal University of Technology (advisor: Prof. W. Oppermann)
	Doctoral Thesis: *„Influence of Temperature on Light Scattering of Poly-N-isopropylacrylamide Hydrogels Synthesized by Two Different Cross-Linking Methods*"
January 2009	M.Sc. in Polymer Science and Technology, Istanbul Technical University, Faculty of Science Istanbul, (advisor: Prof.O.Okay, grade: "very good")
	Master Thesis: *„Organogels based* on *butyl rubber: effect of preparation conditions"*
June 2006	B.Sc. in Chemistry, Kocaeli University, Departement of Science and Literature, Kocaeli , Turkey (grade: "good")

Research Projects

2006 – 2007	Design of nano and micro – sized regions in polymeric gels
2007 – 2009	Synthesis and application of new sorbents for removal of oil spill from sea ecosystem
2009 – 2012	Investigation of inhomogeneities in free-radical and photo-crosslinked gels at different conditions

Publications

- Dogu, S.; Okay, O. Tough organogels based on polyisobutylene with aligned porous structures. *Polymer*, **2008**, *49*, 4626-4634.
- Dogu, S.; Kilic, M.; Okay, O. Collapse of acrylamide-based polyampholyte hydrogels in water. *J. Appl. Polym. Sci.*, **2009**, *113*, 1375-1382.
- Ceylan, D.; Dogu, S.; Karacik, B.; Yakan, S. D.; Okay, O. S.; Okay, O. Evaluation of butyl rubber as sorbent material for the removal of oil and polycyclic aromatic hydrocarbons from seawater. *Environ. Sci. Technol.*, **2009**, *43 (10)*, 3846-3852.
- Dogu, S.; Oppermann, W. Influence of observation temperature on light scattering of poly-*N*-isopropylacrylamide hydrogels. *Soft Matter*, **2012**, *8*, 2705-2713.